

พลวัตและกลไกปฏิกิริยาการถ่ายโอนโปรตอนในวัสดุ  
แอโรแมติกเฮเทอโรไซคลิกเชื่อมกับกรดฟอสฟอริก



นางสาวจิตติมา ทิสสุวรรณ

วิทยานิพนธ์นี้เป็นส่วนหนึ่งของการศึกษาตามหลักสูตรปริญญาวิทยาศาสตรดุษฎีบัณฑิต  
สาขาวิชาเคมี  
มหาวิทยาลัยเทคโนโลยีสุรนารี  
ปีการศึกษา 2558

**DYNAMICS AND MECHANISMS OF PROTON  
TRANSFER IN AROMATIC HETEROCYCLIC  
MATERIALS DOPED WITH  
PHOSPHORIC ACID**

**Jittima Thisuwan**

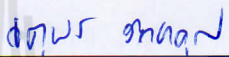


**A Thesis Submitted in Partial Fulfillment of the Requirements for the  
Degree of Doctor of Philosophy in School of Chemistry  
Suranaree University of Technology  
Academic Year 2015**

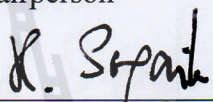
**DYNAMICS AND MECHANISMS OF PROTON TRANSFER IN  
AROMATIC HETEROCYCLIC MATERIALS DOPED  
WITH PHOSPHORIC ACID**

Suranaree University of Technology has approved this thesis submitted in partial fulfillment of the requirements for the Degree of Doctor of Philosophy.

Thesis Examining Committee

  
\_\_\_\_\_  
(Assoc. Prof. Dr. Jatuporn Wittayakun)

Chairperson

  
\_\_\_\_\_  
(Prof. Dr. Katsana Sagarik)

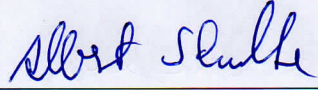
Member (Thesis Advisor)

  
\_\_\_\_\_  
(Prof. Dr. Supot Hannongbua)

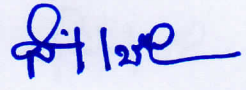
Member

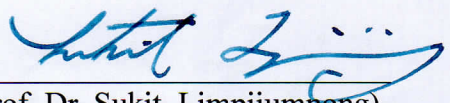
  
\_\_\_\_\_  
(Assoc. Prof. Dr. Anan Tongraar)

Member

  
\_\_\_\_\_  
(Assoc. Prof. Dr. Albert Schulte)

Member

  
\_\_\_\_\_  
(Prof. Dr. Santi Maensiri)

  
\_\_\_\_\_  
(Prof. Dr. Sukit Limpijumnong)

Vice Rector for Academic Affairs  
and Innovation

Dean of Institute of Science

จิตติมา ทิสสุวรรณ : พลวัตและกลไกปฏิกิริยาการถ่ายโอนโปรตอนในวัสดุแอโรแมติก  
เฮเทอโรไซคลิกเจือกับกรดฟอสฟอริก (DYNAMICS AND MECHANISMS OF  
PROTON TRANSFER IN AROMATIC HETEROCYCLIC MATERIALS DOPED  
WITH PHOSPHORIC ACID) อาจารย์ที่ปรึกษา : ศาสตราจารย์ ดร.กฤษณะ ศาคริก,  
115 หน้า

วิทยานิพนธ์เรื่องนี้ศึกษาพลวัตและกลไกปฏิกิริยาการแลกเปลี่ยนและถ่ายโอนโปรตอนในระบบอิมิดาโซล (imidazole, Im) เจือกรดฟอสฟอริก (doped phosphoric acid,  $H_3PO_4$ ) โดยวิธีทางเคมีควอนตัมที่ระดับ B3LYP/TZVP และวิธีการจำลองพลวัตเชิงโมเลกุลบอร์น-ออปเพนไฮเมอร์ (Born-Oppenheimer molecular dynamics (BOMD) simulations) การศึกษาเชิงทฤษฎีเริ่มด้วยการเลือกแบบจำลองการละลายล่วงหน้า (presolvation model) ที่เหมาะสมสำหรับปฏิกิริยาการแตกตัว (proton dissociation) และการถ่ายโอนโปรตอน (proton transfer) โดยใช้โครงสร้างพันธะไฮโดรเจนแบบ “ฝังตื้น” (embedded structure) และแบบ “ปลายทาง” (terminal structure) ของระบบ  $H^+(H_3PO_4)(Im)_n$  ( $n = 1-4$ ) เป็นตัวแทนตามลำดับ การคำนวณด้วยวิธี B3LYP/TZVP ยืนยันว่าเงื่อนไขการมีโปรตอนส่วนเกิน (excess proton condition) มีความจำเป็นในการสนับสนุนให้เกิดปฏิกิริยาการแลกเปลี่ยนโปรตอน โดยสารเชิงซ้อนระหว่างกลาง (intermediate complex) เกิดได้ดีในสถานะแวดล้อมไดอิเล็กทริกเฉพาะที่ต่ำ (low local-dielectric environment) ในทางตรงข้ามสถานะไดอิเล็กทริกเฉพาะที่สูงมีส่วนสำคัญในการทำให้ประจุบวกในพันธะไฮโดรเจนมีเสถียรภาพมากขึ้น และช่วยป้องกันมิให้โปรตอนเคลื่อนที่กลับไปยังโมเลกุลอิมิดาโซลเดิม ผลการคำนวณเชิงสถิต (static results) แสดงว่าโครงสร้างพันธะไฮโดรเจนแบบฝังตื้นที่มี  $n = 2$  เป็นสารเชิงซ้อนระหว่างกลางที่เล็กที่สุดสำหรับปฏิกิริยาการแตกตัว ในขณะที่โครงสร้างพันธะไฮโดรเจนแบบปลายทางที่มี  $n = 3$  มีประสิทธิภาพการถ่ายโอนโปรตอนในโซ่โมเลกุลอิมิดาโซลสูงสุด ผลการจำลองพลวัตเชิงโมเลกุลบอร์น-ออปเพนไฮเมอร์ ยืนยันผลการคำนวณเชิงสถิตและเสนอต่อไปว่าการกระเพื่อม (fluctuation) ของความยาวโซ่พันธะไฮโดรเจน และการกระเพื่อมของสถานะแวดล้อมไดอิเล็กทริกเฉพาะที่ต้องนำมาพิจารณา โดยเป็นส่วนหนึ่งของกลไกปฏิกิริยาการแตกตัวและถ่ายโอนโปรตอน ผลการวิเคราะห์ความเปลี่ยนแปลงมุมของการบิด (torsional angle) ในโซ่พันธะไฮโดรเจนแสดงลักษณะเฉพาะของการจัดเรียงตัวที่เรียกว่า “การเคลื่อนที่หมุนแบบเกลียว” (helical rotational motion) ซึ่งขับเคลื่อนโปรตอนให้ออกห่างจากสารเจือกรดฟอสฟอริก ผลการศึกษาทางทฤษฎียังแสดงในรายละเอียดเป็นครั้งแรก ถึงพื้นฐานการมีปฏิกิริยาต่อกันและกัน

ของการเคลื่อนที่หลัก ซึ่งมีส่วนสำคัญในการกำหนดพลวัตและกลไกปฏิกิริยาการแลกเปลี่ยนและถ่ายโอนโปรตอนในระบบอิมิดาโซลเจือกรดฟอสฟอริก



สาขาวิชาเคมี  
ปีการศึกษา 2558

ลายมือชื่อนักศึกษา Jithima Thisuwan  
ลายมือชื่ออาจารย์ที่ปรึกษา R. S. S. S.

JITTIMA THISUWAN : DYNAMICS AND MECHANISMS OF PROTON  
TRANSFER IN AROMATIC HETEROCYCLIC MATERIALS DOPED  
WITH PHOSPHORIC ACID. THESIS ADVISOR : PROF. KRITSANA  
SAGARIK, Ph.D. 115 PP.

LINEAR H-BOND/IMIDAZOLE/PHOSPHORIC ACID/PROTON DISSOCIATION  
AND TRANSFER/BOMD SIMULATIONS/VIBRATIONAL SPECTRA

In this thesis, the dynamics and mechanisms of proton exchange and transfer in a phosphoric acid ( $\text{H}_3\text{PO}_4$ ) doped imidazole (Im) system were studied using a quantum chemical method at the B3LYP/TZVP level and Born-Oppenheimer molecular dynamics (BOMD) simulations. The theoretical studies began with selecting the appropriate presolvation models for proton dissociation and transfer, which were represented by embedded and terminal hydrogen bond (H-bond) structures of  $\text{H}^+(\text{H}_3\text{PO}_4)(\text{Im})_n$  ( $n = 1-4$ ), respectively. B3LYP/TZVP calculations confirmed that an excess proton condition is required to promote proton exchange, and the intermediate complexes are preferentially formed in a low local-dielectric environment. In contrast, a high local-dielectric environment is required to stabilize the positive charge and prevent the proton from returning to the original Im molecule. The static results also revealed that the embedded structure with  $n = 2$  represents the smallest, most active intermediate complex for proton dissociation, whereas the terminal structure with  $n = 3$  favors proton transfer in the Im H-bond chain. BOMD simulations confirmed the static results and further suggested that the fluctuations of the H-bond chain lengths and the local-dielectric environment must be included in the proton dissociation and transfer

mechanisms. Analyses of the time evolutions of torsional angles in the Im H-bond chain showed characteristic solvent structure reorganization, regarded as helical-rotational motion, which drives the proton away from the  $\text{H}_3\text{PO}_4$  dopant. The current theoretical results showed in detail for the first time the interplay among the “key molecular motions” that fundamentally underlie the dynamics and mechanisms of proton exchange in the  $\text{H}_3\text{PO}_4$  doped Im H-bond system.



School of Chemistry

Academic Year 2015

Student's Signature Jittima Thirawan

Advisor's Signature H. S. Paul

## ACKNOWLEDGEMENTS

First, I would like to gratefully thank my thesis advisor, Prof. Dr. Kritsana Sagarik for the opportunity to accomplish a Ph.D. degree, valuable advices, guidance, suggestions on the research work and kindness, patience throughout the years of my studies, and for offering several precious opportunities for my future academic career.

The members of the thesis committee, Prof. Dr. Supot Hannongbua, Assoc. Prof. Dr. Jatuporn Wittayakun (chairperson), Assoc. Prof. Dr. Anan Tongraar, Assoc. Prof. Dr. Albert Schulte have received my sincere appreciation for their valuable comments, suggestions, and time. I would also like to acknowledge all the lecturers of School of Chemistry, Suranaree University of Technology for their positive attitudes, useful advices, and constructive suggestions.

Special thanks should also go to Suranaree University of Technology through SUT-Ph.D. program (SUT-Ph.D./05/2554) for financial support and overseas research opportunity at Ruđer Bošković Institute, Zagreb, Croatia, with Dr. Nađa Došlić. I am thankful to all of the staff at the School of Chemistry, Suranaree University of Technology for their assistance and supports.

Most importantly, I am deeply indebted to my parents, brother, and sister for their supports, inspiration, patience, believe, and encouragement throughout the long years of my studies, and without those love and understanding this work would not have been possible.

Jittima Thisuwan

# CONTENTS

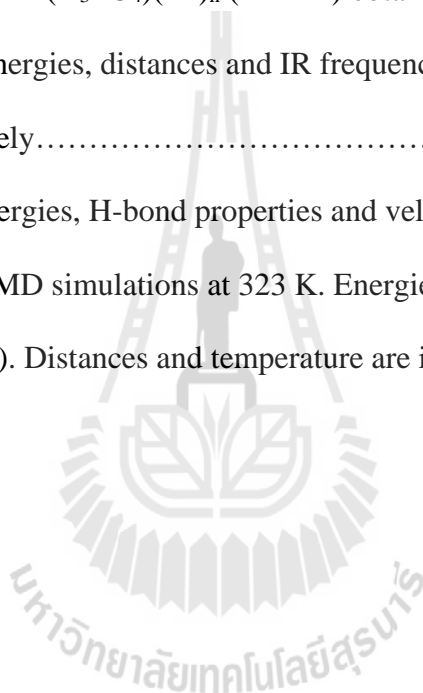
	<b>Page</b>
ABSTRACT IN THAI.....	I
ABSTRACT IN ENGLISH.....	III
ACKNOWLEDGEMENTS.....	V
CONTENTS.....	VI
LIST OF TABLES.....	VIII
LIST OF FIGURES.....	IX
LIST OF ABBREVIATIONS.....	XV
<b>CHAPTER</b>	
<b>I INTRODUCTION.....</b>	<b>1</b>
1.1 Introduction.....	1
1.2 References.....	17
<b>II COMPUTATIONAL METHODOLOGY.....</b>	<b>18</b>
2.1 Presolvation models.....	18
2.2 Quantum chemical calculations.....	28
2.3 Static calculations.....	34
2.4 Dynamic calculations.....	36
2.5 References.....	44
<b>III RESULTS AND DISCUSSION.....</b>	<b>48</b>
3.1 Static results.....	48

## CONTENTS (Continued)

	<b>Page</b>
3.1.1 Excess proton conditions and tendencies of proton dissociation and transfer.....	49
3.1.2 Two-dimensional potential energy surfaces and solvent effects.....	51
3.1.3 Mechanisms of proton transfer in the Im H-bond chains.....	55
3.1.4 Effects of Im H-bond chain structure reorganization.....	59
3.2 Dynamic results.....	63
3.2.1 Dynamics of proton dissociation.....	63
3.2.2 The effects of doping on the dynamics of proton transfer.....	77
3.2.3 Dynamics of the Im H-bond chain structure reorganization.....	84
3.3 References.....	89
<b>IV CONCLUSION.....</b>	<b>92</b>
APPENDICES.....	95
APPENDIX A PUBLICATIONS.....	96
APPENDIX B LIST OF ABSTRACTS.....	114
CURRICULUM VITAE.....	115

## LIST OF TABLES

Table	Page
1.1 Fuel cells categorized by applied electrolytes.....	3
2.1 Static results of $\text{H}^+(\text{H}_3\text{PO}_4)(\text{Im})_n$ ( $n = 1-4$ ) obtained from B3LYP/TZVP calculations. Energies, distances and IR frequencies are in kJ/mol, Å and $\text{cm}^{-1}$ , respectively.....	26
2.2 Drifts in the energies, H-bond properties and velocity of proton obtained from NVT BOMD simulations at 323 K. Energies and velocity are in atomic unit (au). Distances and temperature are in Å and K, respectively.....	40



## LIST OF FIGURES

Figure	Page
1.1 Basic operation of the fuel cell.....	2
1.2 Symmetric and asymmetric O–H stretching bands of the transferring proton in the shared-proton structures, together with the O–O vibration band, obtained from BOMD simulations at 350 K. a) In the gas phase ( $\epsilon = 1$ ). b) In continuum aqueous solution ( $\epsilon = 78$ ).....	7
1.3 Characteristic proton transfer profiles for the Zundel complex obtained from BOMD simulations at 350 K. a) Large-amplitude vibrations. b) Small-amplitude vibrations. c) Snapshots of H-bond structures.....	8
1.4 Elementary reactions consisting of quasi-dynamic equilibriums for the interconversion between the formation and cleavage of the H-bonds linking the transition state complex and water molecules in the second hydration shells. a) The excess proton transferring in a linear H-bond structure. b) The excess proton transferring in a fully hydrated transition state complex.....	10
1.5 Elementary steps of the structural diffusion process in the H-bond chain. Quasi-dynamic equilibriums between the shared-proton ( $n = 3$ ) and close-contact structures ( $n \geq 4$ ) are labelled with <b>(I)</b> , <b>(II)</b> , and <b>(III)</b> .....	13

## LIST OF FIGURES (Continued)

Figure	Page
2.1	a) - b) Embedded and terminal presolvation models employed in the studies of proton dissociation and transfer in $\text{H}^+(\text{H}_3\text{PO}_4)(\text{Im})_n$ ( $n = 1-4$ ), respectively. <b>1<sup>st</sup></b> = first solvation shell; <b>2<sup>nd</sup></b> = part of second solvation shell; <b>(1) - (7)</b> = labels of H-bonds; <b>(I) - (VII)</b> = labels of Im molecules.....23
2.2	Correlations between the results obtained from the RIMP2/TZVP and B3LYP/TZVP calculations. a) - b) Asymmetric stretching coordinates ( $\Delta d_{\text{DA}}$ ) in the N–H···O and N–H···N H-bonds, respectively. c) - d) The $R_{\text{N-O}}$ and $R_{\text{N-N}}$ H-bond distances, respectively. e) - f) Asymmetric N–H stretching frequencies in the N–H <sup>+</sup> ···O and N–H···N H-bonds, respectively. g) Interaction ( $\Delta E$ ) and solvation ( $\Delta E^{\text{sol}}$ ) energies.....30
2.3	a) Energy conservation and velocity plots obtained from NVT BOMD simulations on structure <b>G2-[1]<sup>(I,II)</sup></b> at 323 K. b) Plot of MSD and BOMD simulation time (t) for proton in H-bond <b>(1)</b> of structure <b>G2-[1]<sup>(I,II)</sup></b> at 323 K.....39
2.4	Definitions of the velocity vectors used in the calculations of the symmetric and asymmetric O–H stretching modes, as well as the O–O vibration (Sagarik <i>et al.</i> , 2010)-Reproduced by permission of the PCCP Owner Societies.....42

## LIST OF FIGURES (Continued)

Figure	Page
2.5	a) VACF of the proton in the Zundel complex obtained from BOMD simulations at 350 K. b) The exponential relaxation behavior of the envelope of the VACF. c) Plot of the natural log of the first-order rate constant ( $\ln(k)$ ) and $1000/T$ . (Lao-ngam <i>et al.</i> , 2013)-Reproduced by permission of the Elsevier B.V.....43
3.1	Plots of asymmetric N–H stretching frequencies ( $\nu^{\text{NH}}$ ) as a function of asymmetric stretching coordinates ( $\Delta d_{\text{DA}}$ ), obtained from B3LYP/TZVP calculations. The dashed lines separate the protons that are susceptible and not susceptible to exchange. a) N–H $\cdots$ O H-bonds in the first solvation shell. b) N–H $\cdots$ N H-bonds in Im H-bond chains.....51
3.2	Two-dimensional potential energy surfaces (2D-PES) of proton dissociation in the gas phase and continuum solvent. a) Proton dissociation in H-bond ( <b>1</b> ) of the embedded structure <b>G2-[1]<sup>(I,II)</sup></b> . b) Proton dissociation in H-bond ( <b>1</b> ) of the embedded structure <b>C2-[1]<sup>(I,II)</sup></b> . (a), (b) and (c) are the cross-sectional plots of the single- and double-well potentials, respectively.....53
3.3	a) The effects of Im H-bond chain extension in low local-dielectric environment. b) Examples of elementary steps of proton transfer in Im H-bond chains. <b>step 1</b> = Terminal structure formation. <b>step 2</b> = Proton transfer in Im H-bond chains.....57

## LIST OF FIGURES (Continued)

Figure	Page
3.4 Effects of Im H-bond chain structure reorganization on the energetics of proton transfer. Potential energy curves of proton displacement in H-bonds <b>(3)</b> and <b>(5)</b> are included. a) Proton displacement in $\text{H}^+(\text{H}_3\text{PO}_4)(\text{Im})_4$ in low local-dielectric environment ( $\epsilon = 1$ ). b) Proton displacement in $\text{H}^+(\text{H}_3\text{PO}_4)(\text{Im})_4$ in high local-dielectric environment (COSMO, $\epsilon = 23$ ).....61	61
3.5 a) - b) Variations of the $R_{\text{N-O}}$ and $R_{\text{N-H}}$ distances in H-bond <b>(1)</b> of structure <b>G2-[1]<sup>(I,II)</sup></b> , obtained from BOMD simulations at 353 K. c) Characteristic vibrational spectra of proton dissociation in H-bond <b>(1)</b> of structure <b>G2-[1]<sup>(I,II)</sup></b> , obtained from BOMD simulations at 353 K. d) Arrhenius plot of proton dissociation in H-bond <b>(1)</b> of structure <b>G2-[1]<sup>(I,II)</sup></b> , obtained from BOMD simulations over the temperature range of 298 to 423 K. <b>S</b> and <b>L</b> = small- and large-amplitude N–O vibrations, respectively. $\Delta E^{\ddagger, \text{Arr}}$ = Arrhenius activation energy of proton dissociation.....64	64
3.6 Distributions of the N–H covalent bond distances ( $R_{\text{N-H}}$ ) in H-bonds of the intermediate complexes, obtained from BOMD simulations. a) Distribution of $R_{\text{N-H}}$ in H-bond <b>(1)</b> of structure <b>G2-[1]<sup>(I,II)</sup></b> at 353 K. b) - c) Distributions of $R_{\text{N-H}}$ in H-bonds <b>(1)</b> and <b>(2)</b> of structure <b>G3-[1]<sup>(I,II)</sup></b> at 353 K, respectively. d) Distribution of $R_{\text{N-H}}$ in H-bond <b>(3)</b> of structure <b>G3-[2]<sup>(III)</sup></b> at 298 K.....68	68

## LIST OF FIGURES (Continued)

Figure	Page
3.7 a) - b) Variations of the $R_{N-O}$ and $R_{N-H}$ distances in H-bond (1) of structure <b>G3-[1]<sup>(I,II)</sup></b> , obtained from BOMD simulations at 353 K. c) Characteristic vibrational spectra of proton dissociation in H-bond (1) of structure <b>G3-[1]<sup>(I,II)</sup></b> , obtained from BOMD simulations at 353 K. d) Arrhenius plot of proton dissociation in H-bond (1) of structure <b>G3-[1]<sup>(I,II)</sup></b> , obtained from BOMD simulations over the temperature range of 298 to 423 K. e) - f) Variations of the $R_{N-O}$ and $R_{N-H}$ distances in H-bond (2) of structure <b>G3-[1]<sup>(I,II)</sup></b> , obtained from BOMD simulations at 353 K. g) Characteristic vibrational spectra of H-bond (2) of structure <b>G3-[1]<sup>(I,II)</sup></b> , obtained from BOMD simulations at 353 K. <b>S</b> and <b>L</b> = small- and large-amplitude N–O vibrations, respectively. $\Delta E^{+Arr}$ = Arrhenius activation energy of proton dissociation.....	71
3.8 a) - b) Variations of the $R_{N-N}$ and $R_{N-H}$ distances in H-bond (3) of structure <b>G3-[2]<sup>(III)</sup></b> , obtained from BOMD simulations at 353 K. c) Characteristic vibrational spectra of proton transfer in H-bond (3) of structure <b>G3-[2]<sup>(III)</sup></b> , obtained from BOMD simulations at 353 K. d) Arrhenius plot of proton transfer in H-bond (3) of structure <b>G3-[2]<sup>(III)</sup></b> , obtained from BOMD simulations over the temperature range of 298 to 423 K. $\Delta E^{+Arr}$ = Arrhenius activation energy of proton transfer.....	79

## LIST OF FIGURES (Continued)

Figure	Page
3.9 a) - b) Variations of the $R_{N-N}$ and $R_{N-H}$ distances in H-bond of $H^+(Im)_4$ , obtained from BOMD simulations at 350 K. c) Characteristic vibrational spectra of proton transfer in H-bond of $H^+(Im)_4$ , obtained from BOMD simulations at 350 K. d) Arrhenius plot of proton transfer in H-bond of $H^+(Im)_4$ , obtained from BOMD simulations over the temperature range of 298 to 423 K. e) Distribution of $R_{N-H}$ in H-bond of $H^+(Im)_4$ , obtained from BOMD simulations at 350 K. $\Delta E^{+Arr}$ = Arrhenius activation energy of proton transfer (Buagern <i>et al.</i> ).....	81
3.10 Proton transfer profiles of H-bonds <b>(3)</b> and <b>(5)</b> , and time evolutions of $\omega_3$ and $\omega_5$ in the terminal structure <b>G3-[2]<sup>(III)</sup></b> , obtained from BOMD simulations at 298 K. (a) - (c) = H-bond <b>(3)</b> ; (d) - (f) = H-bond <b>(5)</b> .....	85
3.11 Conformations of structure <b>G3-[2]<sup>(III)</sup></b> sampled from panel <b>P1</b> to <b>P4</b> and projections of the reference vectors ( $v^{ref}$ ), obtained from the analyses of the time evolutions of $\omega_3$ and $\omega_5$ in Figure 3.10. Angles in degree; <b>(III)</b> = $v^{ref}$ of Im <b>(III)</b> ; <b>(V)</b> = $v^{ref}$ of Im <b>(V)</b> .....	86
3.12 Distributions of the N-H covalent bond distances ( $R_{N-H}$ ) in H-bond <b>(3)</b> of structure <b>G3-[2]<sup>(III)</sup></b> , obtained from BOMD simulations at 298 K. a) - d) Distributions in panel <b>P1</b> to <b>P4</b> in Figure 3.10, respectively .....	87

## LIST OF ABBREVIATIONS

$\Delta d_{DA}$	Asymmetric stretching coordinate
$\Delta E$	Interaction energy
$\Delta E^{Sol}$	Solvation energy
$\Delta E^{+,Arr}$	Activation energy of proton dissociation and transfer obtained from the Arrhenius plot
$\epsilon$	Relative permittivity or dielectric constant
$\nu^{NH}$	Asymmetric N–H stretching frequency
$\nu^{NH*}$	Threshold asymmetric N–H stretching frequency
$\nu^{NH,MD}$	Asymmetric N–H stretching frequency obtained from BOMD simulations
$\nu^{NN,MD}$	N–N vibrational frequency obtained from BOMD simulations
$\nu^{NO,MD}$	N–O vibrational frequency obtained from BOMD simulations
$\nu^{OH,MD}$	Asymmetric O–H stretching frequency obtained from BOMD simulations
$\nu^{ref}$	Reference vector
$\omega_3$	Dihedral angle of H-bond (3)
$\omega_5$	Dihedral angle of H-bond (5)
$\tau_{1/2}$	Half-life to the exponential decay function
$\delta_A$	Drift in property A
2D-PES	Two-dimensional potential energy surface

**LIST OF ABBREVIATIONS (Continued)**

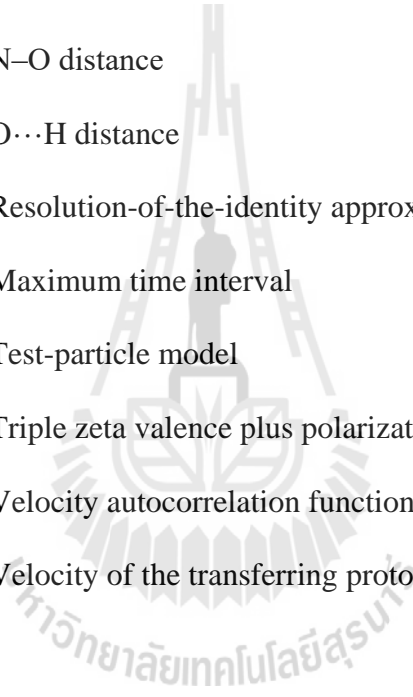
AIMD	<i>ab initio</i> molecular dynamics
au	Atomic unit
B3LYP	Becke three-parameters hybrid functional combined with Lee-Yang-Parr correlation function
BI	Benzimidazole
BOMD	Born-Oppenheimer molecular dynamics
COSMO	Conductor-like screening model
CPMD	Car-Parrinello molecular dynamics
DFT	Density functional theory
$E^{\circ}_{\text{Cell}}$	Standard reduction potential
$E^{\text{Kin}}$	Kinetic energy
$E^{\text{Pot}}$	Potential energy
$E^{\text{Tot}}$	Total energy
fs	Femtosecond
H-bond	Hydrogen bond
HClO <sub>4</sub>	Perchloric acid
H <sub>2</sub> PO <sub>4</sub> <sup>-</sup>	Dihydrogen phosphate anion
H <sub>3</sub> PO <sub>4</sub>	Phosphoric acid
H <sub>4</sub> PO <sub>4</sub> <sup>+</sup>	Protonated phosphoric acid
H <sub>2</sub> SO <sub>4</sub>	Sulfuric acid
Im	Imidazole

**LIST OF ABBREVIATIONS (Continued)**

ImH <sup>+</sup>	Protonated imidazole
kJ/mol	Kilo Joule per mole
k	First-order rate constant
K	Kelvin
LCS	Localized charge solvent
NMR	Nuclear magnetic resonance spectroscopy
MD	Molecular dynamics
MP2	Second order Møller-Plesset perturbation theory
MSD	Mean-square displacement
MS-EVB	Multiscale empirical valence bond model
NH <sub>3</sub>	Ammonia
NVE	Microcanonical ensemble
NVT	Canonical ensemble
P <sub>1</sub> , P <sub>2</sub> , P <sub>3</sub> , ..., P <sub>n</sub>	Panels on the proton transfer profiles
P <sub>A··H··B</sub>	Probability of finding the intermediate complex with the shared-proton A··H··B H-bond
P <sub>BA</sub>	Probability of finding a proton transfer from atom B to A
PBI	Poly(benzimidazole)
PD	Parallel-displaced
PEMFCs	Polymer electrolyte membrane fuel cells
POD	Poly(oxodiazole)

**LIST OF ABBREVIATIONS (Continued)**

ps	Picosecond
Pz	Pyrazole
$R^2$	Correlation coefficient
$R_{N-H}$	N–H distance
$R_{N-O}$	N–O distance
$R_{O\cdots H}$	O $\cdots$ H distance
RI	Resolution-of-the-identity approximation
$t_{\max}$	Maximum time interval
T-model	Test-particle model
TZVP	Triple zeta valence plus polarization function
VACF	Velocity autocorrelation function
$v^{H^+}$	Velocity of the transferring proton



# CHAPTER I

## INTRODUCTION

### 1.1 Introduction

The increasing demands of energy and clean environment have provided strong motivation for scientists and engineers to develop alternative energy sources and effective energy conversion technologies (Larminie and Dicks, 2001; Vincent and Scrosati, 1997; Koppel, 1999). Fuel cell is one of the most environmental friendly energy technologies which has been continuously developed in the past decades. It is an electrochemical device that converts chemical energy of fuels into electrical energy without combustion. Specifically, in fuel cell, the spontaneous reaction between the oxygen and hydrogen gases (fuels) generates water, electricity and heat as the products. The redox reactions taking place in fuel cell are shown in equation (1) - (3). The basic operation of fuel cell is illustrated in Figure 1.1.

In Figure 1.1, the hydrogen gas is passed through the anode, ionized into protons and electrons (equation (1)). Electrons are conducted through the external circuit to the cathode, whereas protons transfer through liquid electrolyte or polymer electrolyte membrane to the cathode and react with the oxygen gas and electron, producing water and heat (equation (2)).

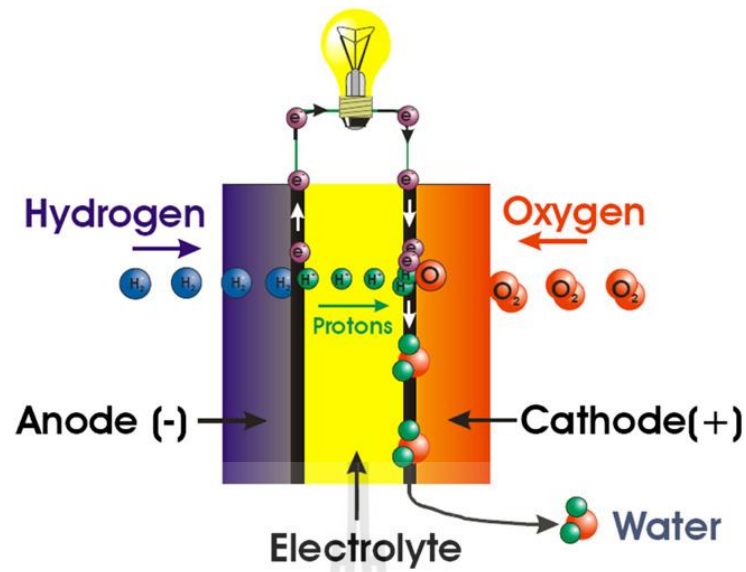


**Figure 1.1** Basic operation of the fuel cell (Peighambardoust, Rowshanzamir, and Amjadi, 2010).



$$E^\circ_{\text{Cell}} = 1.23\text{V}; \Delta H^\circ_{\text{f}} = -241.8 \text{ kJ/mol}$$

Fuel cells are generally categorized based on the electrolytes used. Table 1.1 summarizes types of fuel cells, their operating temperatures and applications (Peighambardoust *et al.*, 2010).

**Table 1.1** Fuel cells categorized by applied electrolytes.

Type	Electrolyte	Temp. (°C)	Applications
Alkaline (AFC)	Alkaline solution	60-90	Space, mobile
Phosphoric acid (PAFC)	Acidic solution	160-220	Distributed power
Polymer electrolyte membrane (PEMFC)	Solid polymer membrane	50-80	Portable, mobile, stationary
Molten carbonate (MCFC)	Molten carbonate salt	600-700	Distributed power generation
Solid oxide (SOFC)	Ceramic ion	800-1000	Baseload power generation

Because the transferring of protons plays important roles in determining the efficiency and operating conditions of fuel cells, attempts have been made in the past decades to develop new types of electrolyte membranes which can efficiently transport protons from the anode to the cathode. Polymer electrolyte membrane fuel cells (PEMFCs) have received considerable attention due to their potential as effective power generators (Koppel, 1999; Larminie *et al.*, 2001; Narayanan, Yen, Liu, and Greenbaum, 2006). Commercially available PEMFCs employ Nafion<sup>®</sup> as a polymer electrolyte membrane. Nafion<sup>®</sup> consists of Teflon<sup>®</sup> backbone and randomly attached hydrophilic side chains. Because the backbone and side chains of Nafion<sup>®</sup> are terminated by trifluoromethane sulfonic (triflic) acid groups which are preferentially hydrated, proton transfer takes place mainly in the interconnected hydrophilic domains. Therefore, this type of fuel cell has serious limitations on the operating temperature as Nafion<sup>®</sup> based fuel cells cannot be operated above the boiling point of water.

Aromatic heterocyclic compounds such as benzimidazole (BI), pyrazole (Pz) and imidazole (Im), as well as polymers containing amide functional groups such as

poly(oxodiazole) (POD) and poly(benzimidazole) (PBI), have shown high potential as alternative proton solvents (Schuster and Meyer, 2003). Due to the autoprotolysis property, a high amphotericity and being a good proton solvent, as well as the ability to form extensive hydrogen bond (H-bond) network, these aromatic heterocyclic materials possess high proton conductivities in the condensed phase (Schuster *et al.*, 2003).

PBI is an aromatic heterocyclic polymer that exhibits excellent thermal, mechanical and chemical stabilities (Schuster *et al.*, 2003). Although PBI is an intrinsic proton conductor, experiments have revealed that blank PBI is a proton insulator (Glipa, Bonnet, Mula, Jones, and RozieÁre, 1999; Pohl and Chartoff, 1964; Xing and Savadogo, 1999), and a sample preparation in which the PBI membrane is dipped into an acid solution represents an essential step for the conductivity measurements (He, Li, Xiao, and Bjerrum, 2003; Xing *et al.*, 1999). Doping a PBI membrane with acids such as H<sub>2</sub>SO<sub>4</sub>, H<sub>3</sub>PO<sub>4</sub> and HClO<sub>4</sub> can considerably increase the proton conductivity, among which PBI doped with H<sub>3</sub>PO<sub>4</sub> yields the highest proton conductivity (Xing *et al.*, 1999).

In the pure state, because all hydrogen atoms are capable of forming extensive H-bonds, H<sub>3</sub>PO<sub>4</sub> shows the highest intrinsic proton conductivity (Chin and Chang, 1989). However, it was demonstrated that the proton conductivity of H<sub>3</sub>PO<sub>4</sub> decreases considerably when strong electrolytes such as H<sub>2</sub>SO<sub>4</sub> were added (Munson and Lazarus, 1967). In contrast, the conductivity was found to increase significantly with water content. The latter is attributed to the promotion of self-ionization and an increase in the number of protons (He *et al.*, 2003).

Given the high proton conductivity with respect to the *c* crystallographic direction (Hickman, Mascal, Titman, and Wood, 1999; Kawada, McGhie, and Labes, 1970) and properties as an excellent proton solvent, Im has been frequently employed

as a prototypical molecule in the study of proton transfer in aromatic heterocyclic materials (Fischbach, Spiess, Saalwächter, and Goward, 2004; Hickman *et al.*, 1999; Iannuzzi and Parrinello, 2004; Kawada *et al.*, 1970; Kreuer, Fuchs, Ise, Spaeth, and Maier, 1998; Münch, Kreuer, Silvestri, Maier, and Seifert, 2001). Experiments have shown that Im can form extensive H-bond chains in the condensed phase, along which protons can be conducted by the Grotthuss mechanism (Hickman *et al.*, 1999; Kawada *et al.*, 1970). It was suggested that to complete the proton transfer process, the Grotthuss mechanism must be followed by a cooperative ring reorientation (ring-flip) as an important rate-determining step (Münch *et al.*, 2001). However, solid-state  $^{15}\text{N}$  NMR experiments demonstrated that for pure Im, the Grotthuss mechanism need not involve the reorientation of the Im ring (Hickman *et al.*, 1999).

The influence of Im and 1-methyl Im on the conductivity of 99 wt.%  $\text{H}_3\text{PO}_4$  solutions and  $\text{H}_3\text{PO}_4$  doped PBI membranes was studied over the temperature range of 350 to 473 K under various humidity conditions (Schechter and Savinell, 2002). It appeared that the conductivity of the solutions decreased with an increasing amount of Im and increased with temperature. The former is attributed to a reduction in the number of proton charge carriers as a consequence of the acid-base reaction, and the viscosity of the solutions was suggested to play an important role in the proton conduction, especially at temperatures below 373 K. Because proton conduction in pure  $\text{H}_3\text{PO}_4$  is perturbed by the addition of Im (Schechter *et al.*, 2002), to investigate the mechanism underlying this effect, *ab initio* molecular dynamics (AIMD) simulations on a  $\text{H}_3\text{PO}_4$ -Im 2:1 system (36  $\text{H}_3\text{PO}_4$  and 18 Im molecules) were performed at 400 K (Vilčiauskas, Tuckerman, Melchior, Bester, and Kreuer, 2013). Due to the acid-base reaction, stable ion-pair complexes between  $\text{H}_2\text{PO}_4^-$  and  $\text{ImH}^+$  and Zundel-like ions, characterized by

proton shuttling between two Im molecules ( $\text{H}^+(\text{Im})_2$ ), were observed in AIMD simulations. Analyses of the local structures and energetic and dynamic results suggested that, due to the proton transfer from  $\text{H}_3\text{PO}_4$  to Im, the proton density in the  $\text{H}_3\text{PO}_4$  phase is reduced and the formation of the ion-pair complexes leads to significantly shorter H-bond chains compared to those in the pure state. These reduce the cooperative effects of the proton transport mechanism and the effectiveness of proton transfer in the Im H-bond chain (Vilčiauskas *et al.*, 2013).

The dynamics and mechanisms of proton transfer in aqueous solution were theoretically studied using the H-bond complexes formed from  $\text{H}_3\text{O}^+$  and  $n\text{H}_2\text{O}$ ,  $n = 1-4$ , as model systems and quantum chemical methods as model calculations (Lao-ngam, Asawakun, Wannarat, and Sagarik, 2011). The investigations began with searching for intermediate complexes in the proton transfer pathways and the characteristics of the transferring protons in the gas phase ( $\epsilon = 1$ ) and continuum aqueous solution ( $\epsilon = 78$ ) using density functional theory (DFT) method at the B3LYP/TZVP level, followed by Born–Oppenheimer molecular dynamics (BOMD) simulations at 350 K. The B3LYP/TZVP results revealed the threshold asymmetric O–H stretching frequencies ( $\nu^{\text{OH}*}$ ) for the proton transfers in the smallest, most active intermediate complex (the Zundel complex ( $\text{H}_5\text{O}_2^+$ )) in the gas phase and continuum aqueous solution at 1984 and 1881  $\text{cm}^{-1}$ , respectively. BOMD simulations suggested slightly lower threshold frequencies ( $\nu^{\text{OH,MD}*} = 1917$  and 1736  $\text{cm}^{-1}$ , respectively) with two characteristic  $\nu^{\text{OH,MD}}$  being the vibrational spectral signatures of the transferring protons; the low-frequency bands ( $\nu^{\text{OH,MD}}$ ) in Figures 1.2 are associated with the “oscillatory shuttling motion” (Figure 1.3b) and the high-frequency band with the “structural diffusion motion” (Figure 1.3a).

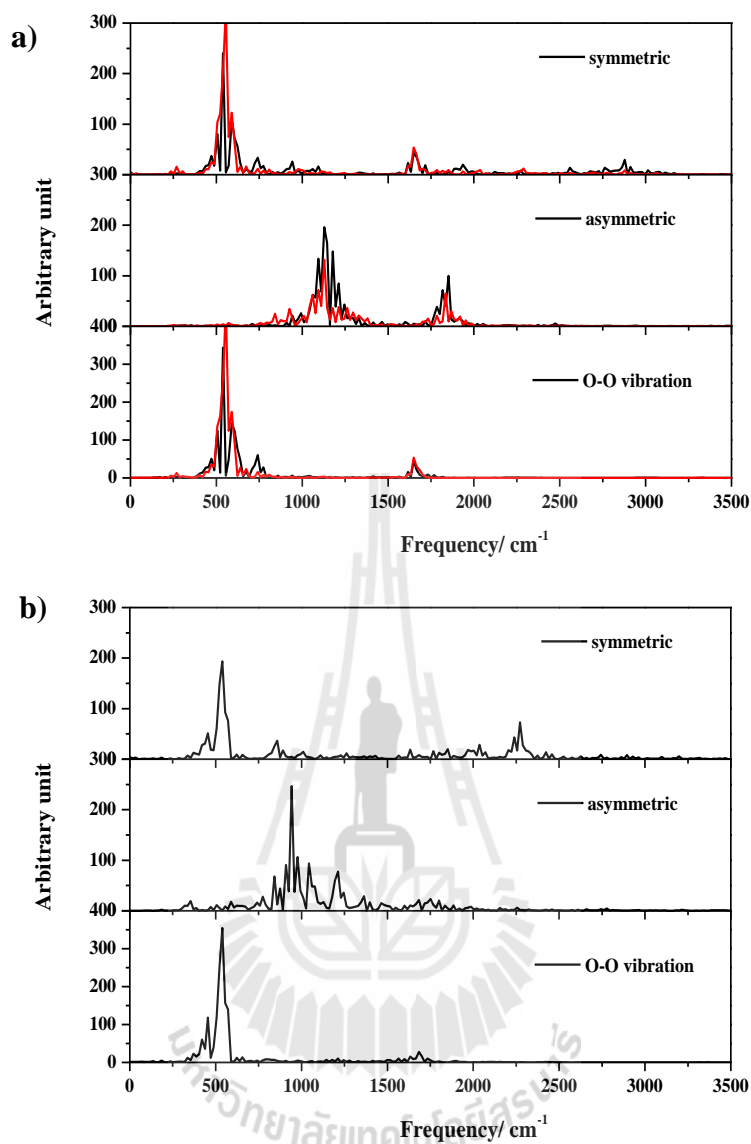


**Figure 1.2** Symmetric and asymmetric O–H stretching bands of the transferring proton in the shared-proton structures, together with the O–O vibration band, obtained from BOMD simulations at 350 K. a) In the gas phase ( $\epsilon = 1$ ). b) In continuum aqueous solution ( $\epsilon = 78$ ). (Lao-ngam *et al.*, 2011)-Reproduced by permission of the PCCP Owner Societies.

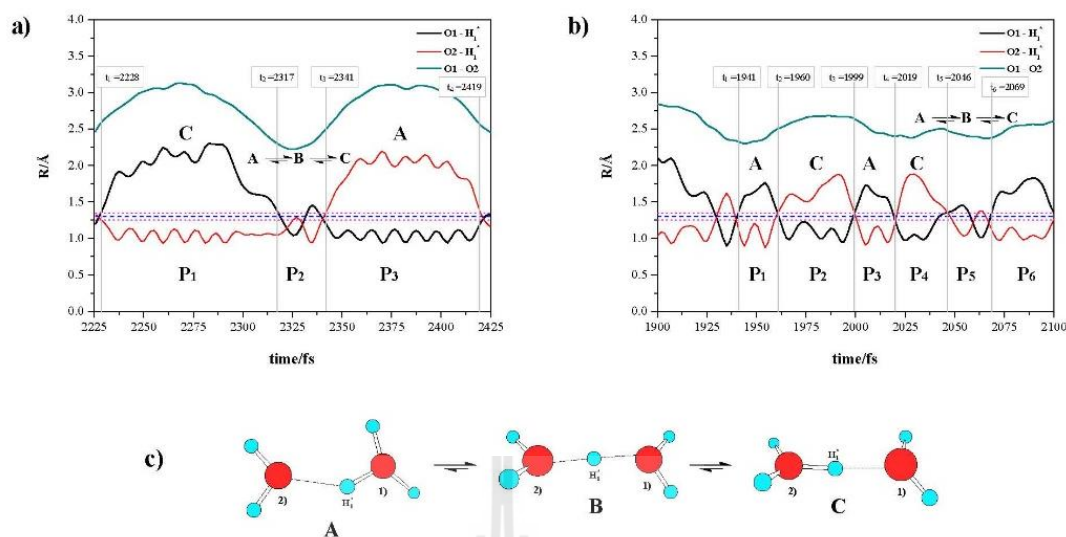


**Figure 1.3** Characteristic proton transfer profiles for the Zundel complex obtained from BOMD simulations at 350 K. a) Large-amplitude vibrations. b) Small-amplitude vibrations. c) Snapshots of H-bond structures. (Sagarik *et al.*, 2008)-Reproduced by permission of the PCCP Owner Societies.

These can be regarded as the spectroscopic evidences of the formations of the shared-proton structure ( $O\cdots H^+\cdots O$ ) and the  $H_3O^+-H_2O$  contact structure ( $O-H^+\cdots O$ ), respectively. The theoretical results also showed that, because the quasi-dynamic equilibrium between the Zundel and Eigen complexes was suggested to be the rate-determining step, to achieve an “ideal” maximum efficiency of proton transfer, a concerted reaction pathway should be taken and the most effective interconversion between the two proton states, the shared-proton structure and the  $H_3O^+-H_2O$  contact structure, can be reflected from comparable intensities of the oscillatory shuttling and structural diffusion peaks. The results iterated the previous conclusions that static proton transfer potentials cannot provide complete description of the structural diffusion process and it is essential to incorporate thermal energy fluctuations and

dynamics in the model calculations (Sagarik, Chaiwongwattana, Vchirawongkwin, and Prueksaaron, 2010).

Due to significant roles played by the methyloxonium ion ( $\text{CH}_3\text{OH}_2^+$ ), the proton transfer reactions in hydrated complexes formed from  $\text{CH}_3\text{OH}$ ,  $\text{H}_3\text{O}^+$  and  $\text{H}_2\text{O}$  were studied using theoretical methods (Sagarik *et al.*, 2010). In this work, the investigations started with searching for equilibrium structures at low hydration levels using the DFT method, from which active H-bonds in the gas phase ( $\epsilon = 1$ ) and continuum aqueous solution ( $\epsilon = 78$ ) were characterized and analyzed. Based on the asymmetric stretching coordinates ( $\Delta d_{\text{DA}}$ ), four H-bond complexes were identified as potential intermediate complexes, in which the most active unit is characterized by an excess proton nearly equally shared between  $\text{CH}_3\text{OH}$  and  $\text{H}_2\text{O}$ . BOMD simulations revealed that, when the thermal energy fluctuations and dynamics were included in the model calculations, the spectral signatures at  $\nu^{\text{OH,MD}} \approx 1000 \text{ cm}^{-1}$  appeared. In continuum aqueous solution, the H-bond complex with incomplete water coordination at charged species are to be the only active intermediate complex. Because the thermal energy fluctuations and dynamics could temporarily break the H-bonds linking the intermediate complex and water molecules in the second hydration shell, elementary reactions of proton transfer were proposed as shown in Figure 1.4.

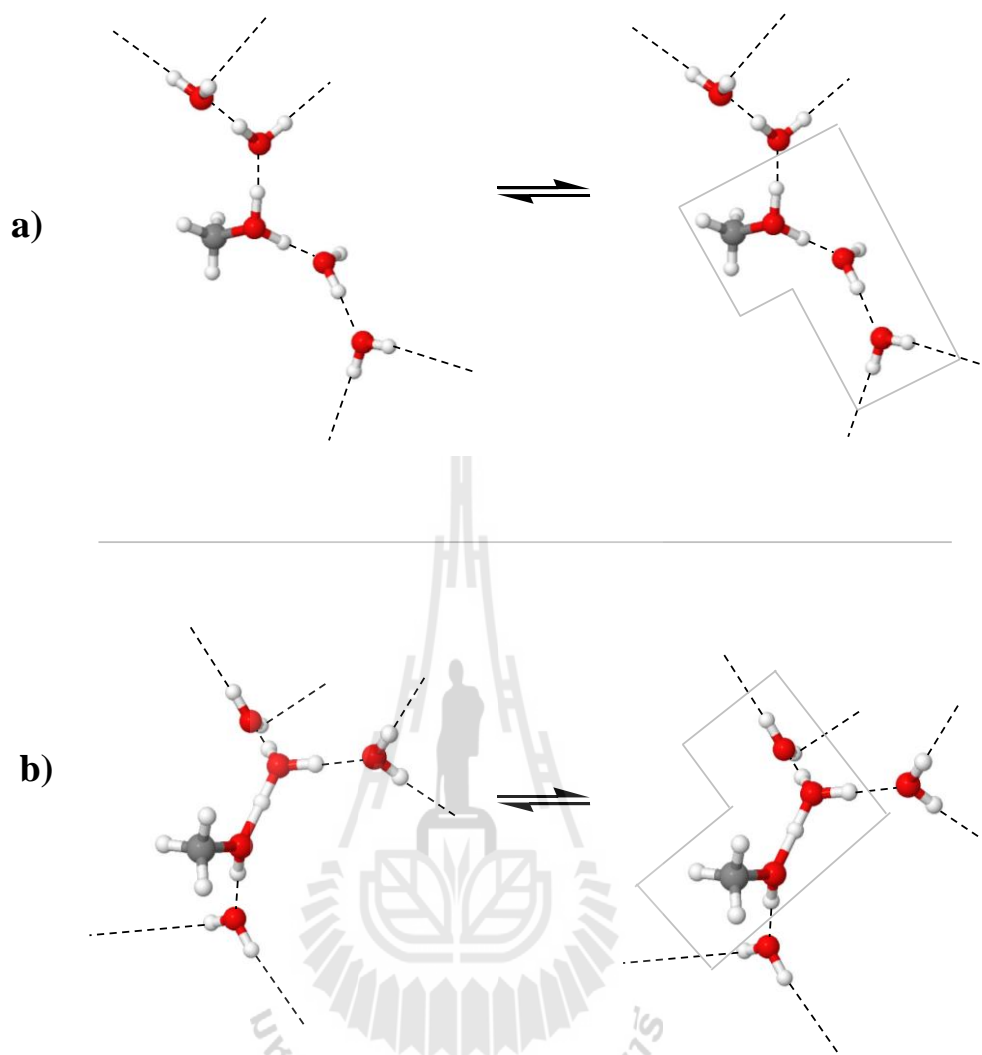


**Figure 1.4** Elementary reactions consisting of quasi-dynamic equilibriums for the interconversion between the formation and cleavage of the H-bonds linking the transition state complex and water molecules in the second hydration shells. a) The excess proton transferring in a linear H-bond structure. b) The excess proton transferring in a fully hydrated transition state complex. (Sagarik *et al.*, 2010)-Reproduced by permission of the PCCP Owner Societies.

This study showed that, due to the coupling among various modes of vibrations, proton transfer reactions cannot be discussed based only on static proton transfer

potentials and inclusion of thermal energy fluctuations and dynamics in the model calculations, as in the case of BOMD simulations, together with systematic vibrational spectral analyses, have been proved to be the most effective theoretical approaches.

Based on the same approaches (Chaiwongwattana, Phonyiem, Vchirawongkwin, Prueksaaron, and Sagarik, 2012), dynamics and mechanism of proton transfer in a protonated H-bond chain were studied using the  $\text{CH}_3\text{OH}_2^+(\text{CH}_3\text{OH})_n$  complexes,  $n = 1-4$ , as model systems. This theoretical investigation used B3LYP/TZVP calculations and BOMD simulations to obtain characteristic H-bond structures, energetic and vibrational spectra of the transferring protons in the gas phase ( $\epsilon = 1$ ) and continuum liquid ( $\epsilon = 32$ ). The static and dynamic results were compared with the  $\text{H}_3\text{O}^+(\text{H}_2\text{O})_n$  (Lao-ngam *et al.*, 2011) and  $\text{CH}_3\text{OH}_2^+(\text{H}_2\text{O})_n$  complexes,  $n = 1-4$  (Sagarik *et al.*, 2010). It was confirmed that the H-bond chains with  $n = 1$  and 3 represent the most active intermediates and the  $\text{CH}_3\text{OH}_2^+(\text{CH}_3\text{OH})_n$  complexes possess the lowest threshold frequency of proton transfer. The vibrational spectra obtained from BOMD simulations revealed that the thermal energy fluctuation and dynamics help promote proton transfer in the shared-proton structure with  $n = 3$  by lowering the vibrational energy for the interconversion between the oscillatory shuttling and structural diffusion motions, leading to a higher population of the structural diffusion motion than in the shared-proton structure with  $n = 1$ . Additional explanation on the previously proposed mechanisms was introduced in Figure 1.5, with the emphases on the energetic of the transferring proton, the fluctuation of the number of the  $\text{CH}_3\text{OH}$  molecules in the H-bond chain, and the quasi-dynamic equilibriums between the shared-proton structure ( $n = 3$ ) and the close-contact structures ( $n \geq 4$ ). The latter prohibits proton transfer reaction in the H-bond chain from

being concerted, since the rate of the structural diffusion depends upon the lifetime of the shared-proton intermediate state.



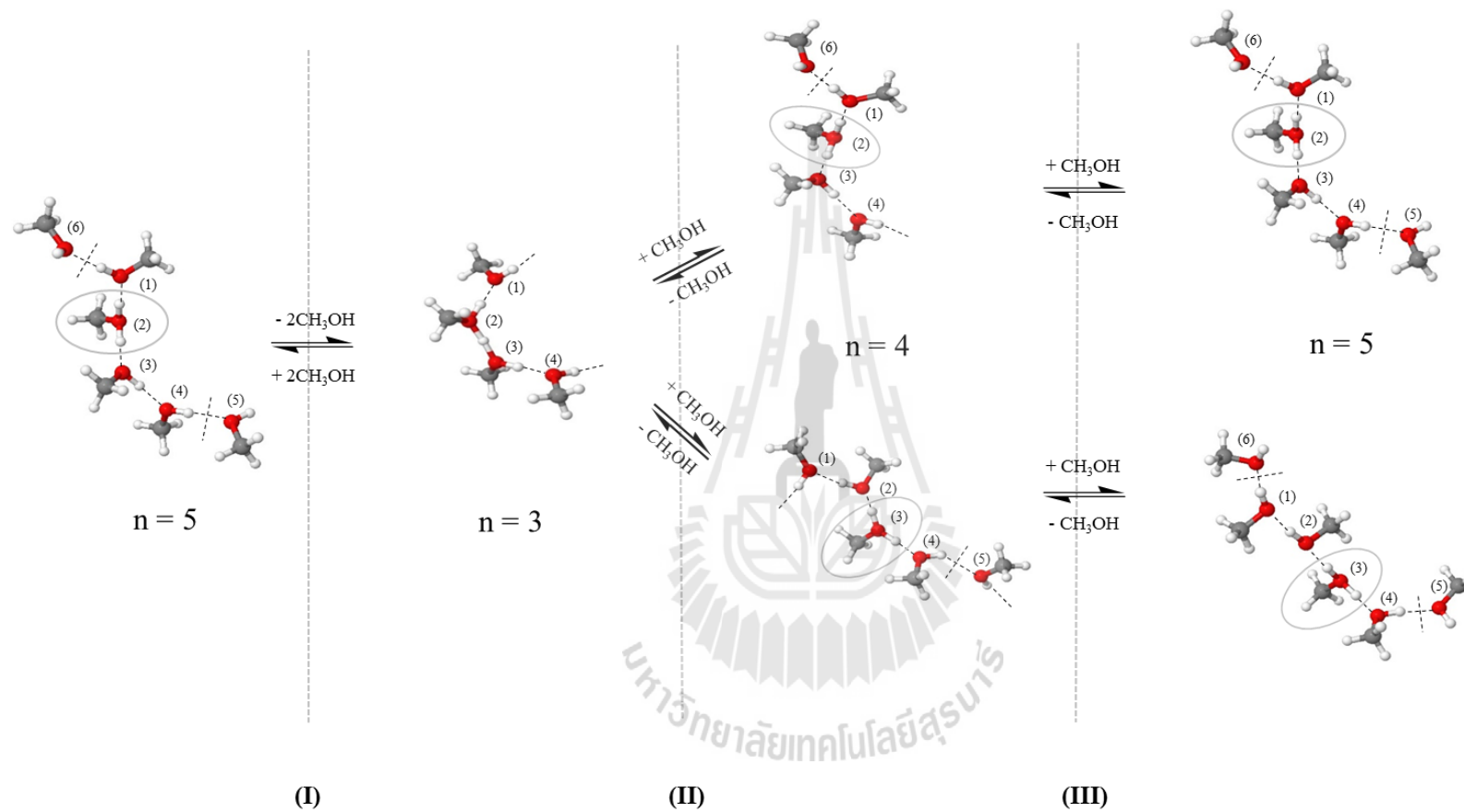


**Figure 1.5** Elementary steps of the structural diffusion process in the H-bond chain. Quasi-dynamic equilibria between the shared-proton ( $n = 3$ ) and close-contact structures ( $n \geq 4$ ) are labelled with **(I)**, **(II)**, and **(III)**. (Chaiwongwattana *et al.*, 2011)-  
 Reproduced by permission of Wiley Periodicals, Inc.

Based on the theoretical information accumulated in the previous work (Sagarik, Phonyiem, Lao-ngam, and Chaiwongwattana, 2008), to study proton transfer in the hydrophilic domains of Nafion<sup>®</sup>, structures, energetics and dynamics of proton transfer reactions at the sulfonic acid groups in Nafion<sup>®</sup> were theoretically studied, using complexes formed from the triflic acid (CF<sub>3</sub>SO<sub>3</sub>H), H<sub>3</sub>O<sup>+</sup> and H<sub>2</sub>O, as model systems. The potential precursors and transition states at low hydration levels were primarily determined using the test-particle model (T-model), DFT and *ab initio* calculations. They were employed as starting configurations in BOMD simulations at 298 K, from which elementary reactions were analyzed and categorized. For the H<sub>3</sub>O<sup>+</sup>-H<sub>2</sub>O complexes, BOMD simulations suggested that a quasi-dynamic equilibrium could be established between the Eigen and Zundel complexes, and that was considered to be one of the most important elementary reactions in the proton transfer process. The average lifetime of H<sub>3</sub>O<sup>+</sup> obtained from BOMD simulations is close to the lowest limit, estimated from low-frequency vibrational spectroscopy. It was demonstrated that proton transfer reactions at -SO<sub>3</sub>H are not concerted, due to the thermal energy fluctuation and the existence of various quasi-dynamic equilibria, and -SO<sub>3</sub>H could directly and indirectly mediate proton transfer reactions through the formation of proton defects, as well as the -SO<sub>3</sub><sup>-</sup> and -SO<sub>3</sub>H<sub>2</sub><sup>+</sup> transition state.

In addition, proton transfer reactions and dynamics of the hydrophilic group (-SO<sub>3</sub>H) in Nafion<sup>®</sup> were studied at low hydration levels using the complexes formed from CF<sub>3</sub>SO<sub>3</sub>H, H<sub>3</sub>O<sup>+</sup> and *n*H<sub>2</sub>O, 1 ≤ *n* ≤ 3, as model systems (Phonyiem, Chaiwongwattana, Lao-ngam, and Sagarik, 2011). The equilibrium structures obtained from DFT calculations suggested at least two structural diffusion pathways at the -SO<sub>3</sub>H group namely, the “pass-through” and “pass-by” mechanisms. The former

involves the protonation and deprotonation at the  $-\text{SO}_3\text{H}$  group, whereas the latter the proton transfer in the adjacent Zundel complex. Analyses of the asymmetric O–H stretching frequencies ( $\nu^{\text{OH}}$ ) of the H-bond protons showed the threshold frequencies ( $\nu^{\text{OH}*}$ ) of proton transfer in the range of 1700 to 2200  $\text{cm}^{-1}$ . BOMD simulations at 350 K anticipated slightly lower threshold frequencies ( $\nu_{\text{A}}^{\text{OH}*,\text{MD}}$ ) with two characteristic asymmetric O–H stretching frequencies being the spectral signatures of proton transfer in the H-bond complexes. The lower frequency ( $\nu_{\text{A}}^{\text{OH},\text{MD}}$ ) is associated with the oscillatory shuttling motion and the higher frequency ( $\nu_{\text{B}}^{\text{OH}*,\text{MD}}$ ) the structural diffusion motion. Comparison of the present results with BOMD simulations on protonated water clusters indicated that the  $-\text{SO}_3\text{H}$  group facilitates proton transfer by reducing the vibrational energy for the interconversion between the two dynamic states ( $\Delta\nu_{\text{BA}}^{\text{OH},\text{MD}}$ ), resulting in a higher population of the H-bonds with the structural diffusion motion. One could therefore conclude that the  $-\text{SO}_3\text{H}$  groups in Nafion<sup>®</sup> act as active binding sites which provide appropriate structural, energetic and dynamic conditions for effective structural diffusion processes in PEMFC. These results suggested for the first time a possibility to discuss the tendency of proton transfer in H-bond using  $\Delta\nu_{\text{BA}}^{\text{OH},\text{MD}}$  and provided theoretical bases and guidelines for the investigations of proton transfer reactions in theory and experiment.

Insights into proton dissociation and transfer in an aqueous solution were additionally obtained by Suwannakham *et al.*, in which the dynamics and mechanisms of proton exchange in hydrated  $\text{H}_3\text{PO}_4$  under excess proton conditions were studied using  $\text{H}^+(\text{H}_3\text{PO}_4)(\text{H}_2\text{O})_n$  ( $n = 1-4$ ) as the model system with *ab initio* calculations and BOMD simulations at the RIMP2/TZVP level as the model calculations. Based on the static results in the gas phase ( $\epsilon = 1$ ) and continuum aqueous

solvent ( $\epsilon = 78$ ), mechanisms of proton dissociation and transfer that involve fluctuations of the number of water molecules in the H-bond chain and the local-dielectric environment were proposed. It was concluded that the smallest, most active intermediate complex for proton dissociation ( $n = 1$ ) is formed in a low local-dielectric environment (*e.g.*,  $\epsilon = 1$ ) and that the proton transfer from the first hydration shell is driven by fluctuations in the number of water molecules in a high local-dielectric environment (*e.g.*,  $\epsilon = 78$ ) through the Zundel complex, which connects the first and second hydration shells. BOMD simulations over a temperature range of 298 to 430 K confirmed that only the H-bond chains with asymmetric hydration at  $\text{H}_4\text{PO}_4^+$  are involved in the proton dissociation and transfer. This finding validated the proposed mechanisms by showing that an agreement between the theoretical and experimental activation energies can be achieved based on the proposed rate-determining processes (Suwannakham, Chaiwongwattana, and Sagarik, 2015).

In this thesis, the dynamics and mechanisms of proton dissociation and transfer in a  $\text{H}_3\text{PO}_4$  doped Im H-bond system were studied using the quantum chemical method at the B3LYP/TZVP level and BOMD simulations. Based on the concept of presolvation (Berkelbach, Lee, and Tuckerman, 2009; Marx, Chandra, and Tuckerman, 2010) and the observation that a unit cell of the Im crystal structure is monoclinic with four molecules forming a linear H-bond chain along the  $c$  crystallographic axis,  $\text{H}^+(\text{H}_3\text{PO}_4)(\text{Im})_n$  ( $n = 1-4$ ) were selected as model systems. The characteristic properties of the exchange protons in the intermediate complexes in low and high local-dielectric environments were investigated and analyzed in detail. The elementary steps of proton dissociation and transfer were proposed based on the static results and confirmed by BOMD simulations in the temperature range between 298 and 423 K. The interplay

among the key molecular motions that fundamentally underlie the dynamics and mechanisms of proton exchange in the H<sub>3</sub>PO<sub>4</sub> doped Im H-bond system were analyzed and discussed.

## 1.2 References

- Berkelbach, T. C., Lee, H.-S., and Tuckerman, M. E. (2009). Concerted hydrogen-bond dynamics in the transport mechanism of the hydrated proton: A first-principles molecular dynamics study. **Physical Review Letters**. 103: 238302.
- Chaiwongwattana, S., Phonyiem, M., Vchirawongkwin, V., Prueksaaron, S., and Sagarik, K. (2012). Dynamics and mechanism of structural diffusion in linear hydrogen bond. **Journal of Computational Chemistry**. 33: 175-188.
- Chin, D. T. and Chang, H. H. (1989). On the conductivity of phosphoric acid electrolyte. **Journal of Applied Electrochemistry**. 19: 95-99.
- Fischbach, I., Spiess, H. W., Saalwächter, K., and Goward, G. R. (2004). Solid state NMR spectroscopic investigations of model compounds for imidazole-based Proton Conductors. **The Journal of Physical Chemistry B**. 108: 18500-18508.
- Glipa, X., Bonnet, B., Mula, B., Jones, D. J., and RozieÁre, J. (1999). Investigation of the conduction properties of phosphoric and sulfuric acid doped polybenzimidazole. **Journal of Materials Chemistry**. 9: 3045-3049.
- He, R., Li, Q., Xiao, G., and Bjerrum, N. J. (2003). Proton conductivity of phosphoric acid doped polybenzimidazole and its composites with inorganic proton conductors. **Journal of Membrane Science**. 226: 169-184.

- Hickman, B. S., Mascal, M., Titman, J. J., and Wood, I. G. (1999). Protonic conduction in imidazole: A solid-state  $^{15}\text{N}$  NMR study. **Journal of the American Chemical Society.** 121: 11486-11490.
- Iannuzzi, M. and Parrinello, M. (2004). Proton transfer in heterocycle crystals. **Physical Review Letters.** 93: 025901.
- Kawada, A., McGhie, A. R., and Labes, M. M. (1970). Protonic conductivity in imidazole single crystal. **The Journal of Chemical Physics.** 52: 3121-3125.
- Koppel, T. (1999). **Powering the future: The ballard fuel cell and the race to change the world.** New York: John Wiley & Sons Ltd.
- Kreuer, K. D., Fuchs, A., Ise, M., Spaeth, M., and Maier, J. (1998). Imidazole and pyrazole-based proton conducting polymers and liquids. **Electrochimica Acta,** 43: 1281-1288.
- Lao-ngam, C., Asawakun, P., Wannarat, S., and Sagarik, K. (2011). Proton transfer reactions and dynamics in protonated water clusters. **Physical Chemistry Chemical Physics.** 13: 4562-4575.
- Larminie, J. and Dicks, A. (2001). **Fuel Cell Systems.** Chichester: John Wiley & Sons Ltd.
- Marx, D., Chandra, A., and Tuckerman, M. E. (2010). Aqueous basic solutions: Hydroxide solvation, structural diffusion, and comparison to the hydrated proton. **Chemical Reviews.** 110: 2174-2216.
- Münch, W., Kreuer, K. D., Silvestri, W., Maier, J., and Seifert, G. (2001). The diffusion mechanism of an excess proton in imidazole molecule chains: First results of an ab initio molecular dynamics study. **Solid State Ionics.** 145: 437-443.

- Munson, R. A. and Lazarus, M. E. (1967). The influence of ionic solutes upon the conductivity of molten phosphoric acid. **The Journal of Physical Chemistry**. 71: 3245-3248.
- Narayanan, S. R., Yen, S. P., Liu, L., and Greenbaum, S. G. (2006). Anhydrous proton-conducting polymeric electrolytes for fuel cells. **Journal of Physical Chemistry B**. 110: 3942-3948.
- Peighambardoust, S. J., Rowshanzamir, S., and Amjadi, M. (2010). Review of the proton exchange membranes for fuel cell applications. **International Journal of Hydrogen Energy**. 35: 9349-9384.
- Phonyiem, M., Chaiwongwattana, S., Lao-ngam, C., and Sagarik, K. (2011). Proton transfer reactions and dynamics of sulfonic acid groups of Nafion<sup>®</sup>. **Physical Chemistry Chemical Physics**. 13: 10923.
- Pohl, H. A. and Chartoff, R. P. (1964). Carriers and unpaired spins in some organic semiconductors. **Journal of Polymer Science Part A: Polymer Chemistry**. 2: 2787-2806.
- Sagarik, K., Phonyiem, M., Lao-Ngam, C., and Chaiwongwattana. S. (2008). Mechanisms of proton transfer in Nafion<sup>®</sup>: Elementary reactions at the sulfonic acid groups. **Physical Chemistry Chemical Physics**. 10: 2098-2112.
- Sagarik, K., Chaiwongwattana, S., Vchirawongkwin, V., and Prueksaaron, S. (2010). Proton transfer reactions and dynamics in CH<sub>3</sub>OH-H<sub>3</sub>O<sup>+</sup>-H<sub>2</sub>O complexes. **Physical Chemistry Chemical Physics**. 12: 918-929.
- Schechter, A. and Savinell, R. F. (2002). Imidazole and 1-methyl imidazole in phosphoric acid doped polybenzimidazole, electrolyte for fuel cells. **Solid State Ionics**. 147: 181-187.

Schuster, M. F. H. and Meyer, W. (2003). Anhydrous proton-conducting polymer.

**Annual Review of Materials Research.** 33: 233-261.

Suwannakham, P., Chaiwongwattana, S., and Sagarik, K. (2015). Proton dissociation and transfer in hydrated phosphoric acid clusters. **International Journal of**

**Quantum Chemistry.** 115: 486-501.

Vilčiauskas, L., Tuckerman, M. E., Melchior, J. P., Bester, G., and Kreuer, K.-D.

(2013). First principles molecular dynamics study of proton dynamics and transport in phosphoric acid/imidazole (2:1) system. **Solid State Ionics.** 252: 34-39.

Vincent, C. A. and Scrosati, B. (1997) **Modern Batteries: An introduction to electrochemical power sources.** New York: John Wiley & Sons Ltd.

Xing, B. and Savadogo, O. (1999). The effect of acid doping on the conductivity of polybenzimidazole (PBI). **Journal of New Materials for Electrochemical**

**Systems.** 2: 95-101.



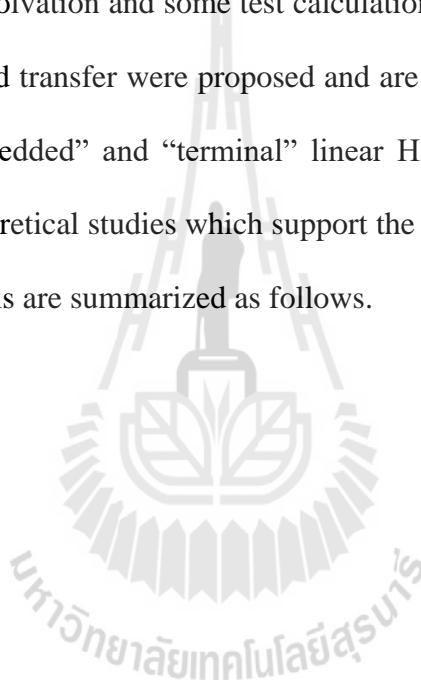
## CHAPTER II

# COMPUTATIONAL METHODOLOGY

### 2.1 Presolvation models

Because the proton exchange processes in H-bonds are complicated, care must be exercised in selecting the model systems. In the present case, the model systems for proton dissociation and transfer were chosen based on the concept of presolvation (Lao-ngam *et al.*, 2011; Marx *et al.*, 2010); the local energy fluctuations and dynamics in solution lead to the weakening or breaking of some H-bonds in the first and second solvation shells, resulting in a reduction in the solvent coordination number such that the proton-accepting species possesses a solvation structure corresponding to the species into which it will be transformed to complete the structural diffusion process. It was shown in the previous work that the dynamics of the transferring protons can be studied reasonably well because the moderate sizes of the presolvation models help reduce the complexity in the H-bond systems and allow theoretical calculations to be made using quantum chemical methods at higher level of accuracy, provided that an appropriate presolvation model is selected and that all of the important rate-determining processes are included in the model calculations (Lao-ngam *et al.*, 2011; Lao-ngam, Phonyiem, Chaiwongwattana, Kawazoe, and Sagarik, 2013; Phonyiem *et al.*, 2011; Chaiwongwattana *et al.*, 2012; Sagarik *et al.*, 2010)

In the present work, because a unit cell of the Im crystal structure is monoclinic with four Im molecules forming a linear H-bond chain along the *c* crystallographic axis,  $\text{H}^+(\text{H}_3\text{PO}_4)(\text{Im})_n$  ( $n = 1-4$ ) were selected as model systems. The cluster size ( $n = 4$ ) is consistent with the average number of Im molecules obtained from molecular dynamics (MD) simulations with excess proton solvated in liquid Im, using a reactive multistate empirical valence bond (MS-EVB) model (Li, Cao, Li, Yan, and Shen, 2012). Based on the concept of presolvation and some test calculations, the presolvation models for proton dissociation and transfer were proposed and are shown in Figure 2.1, regarded hereafter as the “embedded” and “terminal” linear H-bond structures, respectively. Experimental and theoretical studies which support the linear H-bond arrangements in the presolvation models are summarized as follows.



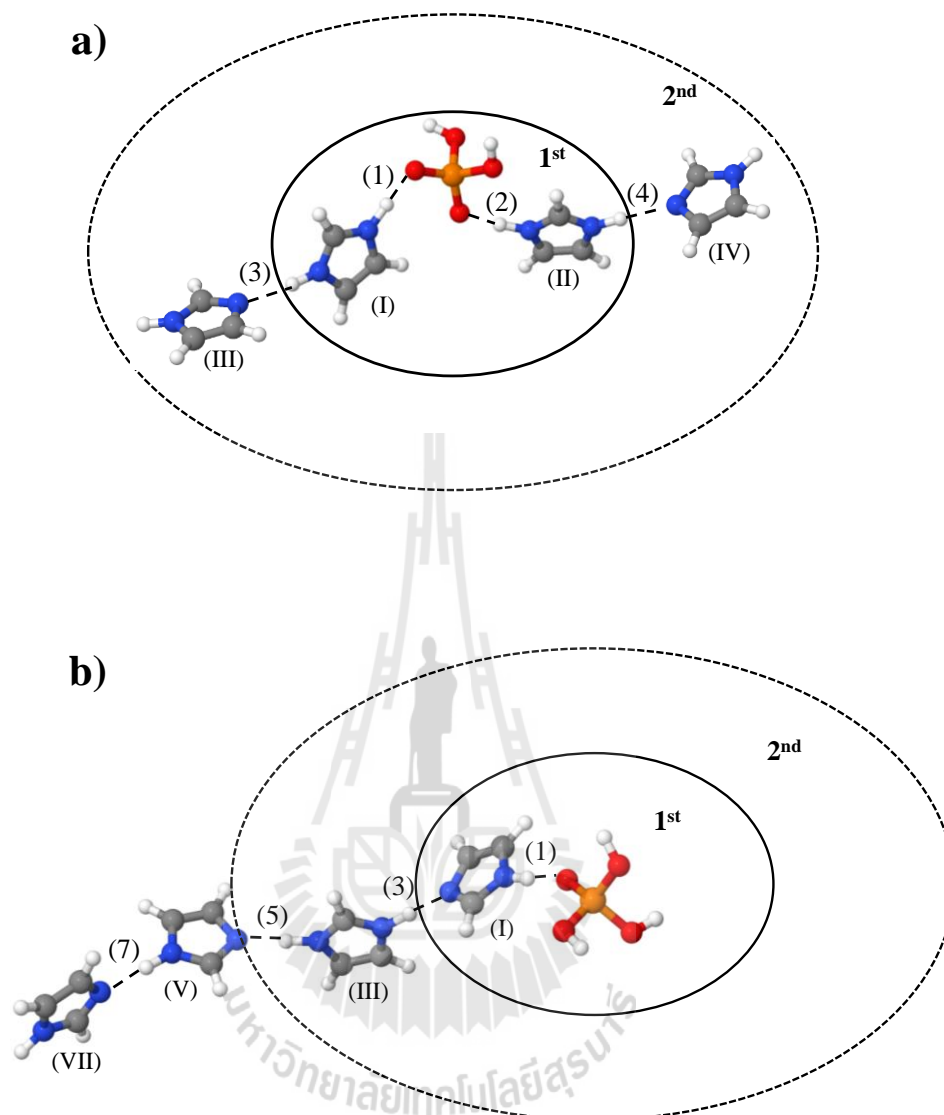


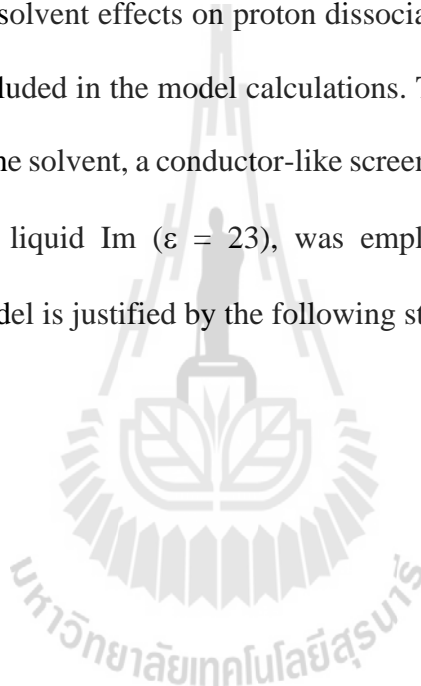
**Figure 2.1** a) - b) Embedded and terminal presolvation models employed in the studies of proton dissociation and transfer in  $\text{H}^+(\text{H}_3\text{PO}_4)(\text{Im})_n$  ( $n = 1-4$ ), respectively. **1<sup>st</sup>** = first solvation shell; **2<sup>nd</sup>** = part of second solvation shell; **(1) - (7)** = labels of H-bonds; **(I) - (VII)** = labels of Im molecules.

In condensed phase, due to the amphoteric character, computer simulations (Iannuzzi, 2006) and experiments (Kawada *et al.*, 1970) showed that Im molecules form polymeric chains, along which excess proton can be relayed between two Im molecules through the Grotthuss shuttling mechanism. Possessing only one proton donor (N–H) and one proton acceptor (N) in the same molecule, the linear H-bond chains in liquid Im are not as extensive as the H-bond networks in water (two proton donors and two proton acceptors in the same molecule). Because the proton donor and acceptor are used in the H-bond chain formation, the interactions between parallel chains could be the C–H $\cdots\pi$  H-bond and  $\pi\cdots\pi$  interactions, which are considerably weaker than the interactions in the protonated Im H-bond chains; for the benzene dimers, the interaction energies for the C–H $\cdots\pi$  H-bond in the T-shaped structure, and the  $\pi\cdots\pi$  interaction in the sandwich structure, computed at the second-order Møller-Plesset perturbation theory (MP2) level, are only -8.8 and -3.6 kJ/mol (Hobza, Selzle, and Schlag, 1994), respectively, compared to the interaction energy of the protonated Im dimer of -116 kJ/mol (Buagern and Sagarik).

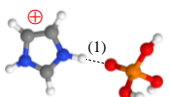
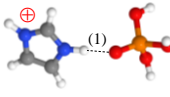
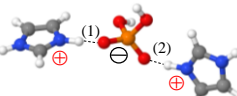
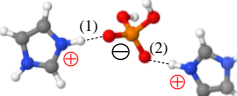
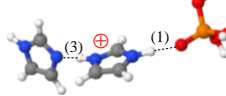
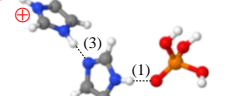
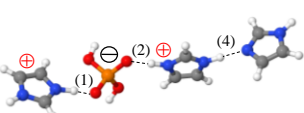
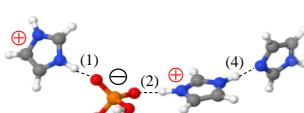
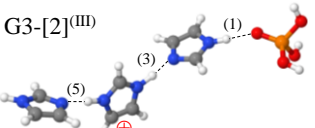
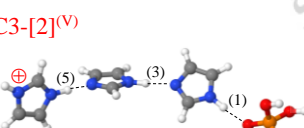
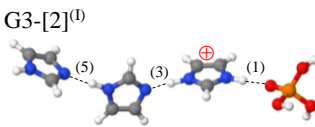
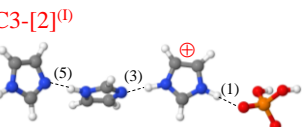
The theoretical study on proton transfer in protonated Im H-bond clusters (Buagern *et al.*) revealed that the intermediate complexes (the H-bond structure with a shared-proton) exist only in the linear H-bond chains (see Table 2.1), which is in accordance with the protonic-chain conduction mechanism (Greenwood and Thompson, 1959; Munson *et al.*, 1967); B3LYP/TZVP geometry optimizations suggested that the linear H-bond arrangements are the global and local minimum energy geometries in the protonated pure (Buagern *et al.*), and doped Im systems. It should be noted that, although the globular H-bond structures could possess larger contact area and smaller free energy, based on the characteristic properties of the transferring proton

(*e.g.*, asymmetric stretching coordinates ( $\Delta_{\text{DA}}$ ) and vibrational frequencies, the H-bonds in the globular structures are not susceptible to proton transfer (Buagern *et al.*). Because this work focuses on the dynamics of the transferring protons in the intermediate complexes, linear 1m H-bond chains were selected as the presolvation models; the lifetime of the intermediate complex has been shown in many H-bond systems to represent the rate-determining processes in proton transfer mechanisms.

To investigate solvent effects on proton dissociation and transfer, a continuum solvent model was included in the model calculations. To account for the electrostatic effects introduced by the solvent, a conductor-like screening model (COSMO), with the dielectric constant of liquid 1m ( $\epsilon = 23$ ), was employed. The application of the continuum solvent model is justified by the following studies.



**Table 2.1** Static results of  $\text{H}^+(\text{H}_3\text{PO}_4)(\text{Im})_n$  ( $n = 1-4$ ) obtained from B3LYP/TZVP calculations. Energies, distances and IR frequencies are in kJ/mol, Å and  $\text{cm}^{-1}$ , respectively.

Gas	COSMO	$\Delta E$	$\Delta E^{\text{sol}}$	H-bond	$R_{\text{N-N}}$	$R_{\text{N-O}}$	$\Delta d_{\text{DA}}$	$\nu^{\text{NH}}$
G1-[1] 	C1-[1] 	-101.75 (-19.67)	-242.68	(1)	-	2.66 (2.72)	0.56 (0.62)	2811 (2806)
G2-[1] <sup>(d,II)</sup> 	C2-[1] <sup>(d,II)</sup> 	-218.61 (-97.94)	-244.76	(1) (2)	- -	2.54 (2.65) 2.55 (2.67)	0.33 (0.54) 0.36 (0.56)	2033 (2645) 2158 (2687)
G2-[2] <sup>(I)</sup> 	C2-[2] <sup>(III)</sup> 	-199.64 (-40.65)	-206.44	(1) (3)	- 2.74 (2.73)	2.72 (2.85) -	0.60 (0.58) 0.64 (0.81)	3011 (3216) 2411 (2348)
G3-[1] <sup>(d,II)</sup> 	C3-[1] <sup>(d,II)</sup> 	-300.95 (-126.50)	-231.66	(1) (2) (4)	- - 2.79 (2.77)	2.52 (2.65) 2.61 (2.68) -	0.26 (0.65) 0.46 (0.58) 0.67 (0.65)	1799 (2633) 2472 (2751) 2652 (2564)
G3-[2] <sup>(III)</sup> 	C3-[2] <sup>(V)</sup> 	-271.51 (-61.79)	-196.39	(1) (3) (5)	- 2.77 (2.72) 2.69 (2.86)	2.81 (2.86) - -	0.75 (0.81) 0.49 (0.78) 0.65 (0.56)	3201 (3233) 2092 (2863) 2575 (2274)
G3-[2] <sup>(I)</sup> 	C3-[2] <sup>(I)</sup> 	-269.14 (-67.36)	-204.33	(1) (3) (5)	- 2.85 (2.87) 2.67 (2.74)	2.74 (2.77) - -	0.66 (0.71) 0.45 (0.60) 0.77 (0.79)	3055 (3079) 1949 (2391) 2880 (2893)

$\Delta E$  = interaction energy;  $\Delta E^{\text{sol}}$  = solvation energy;  $R_{\text{N-O}}$  and  $R_{\text{N-N}}$  = H-bond distances;  $\Delta d_{\text{DA}}$  = asymmetric stretching coordinate; COSMO = continuum solvent;  $\nu^{\text{NH}}$  = asymmetric N-H stretching frequency; (..) = continuum solvent.

**Table 2.1** (Continued) Static results of  $\text{H}^+(\text{H}_3\text{PO}_4)(\text{Im})_n$  ( $n = 1-4$ ) obtained from B3LYP/TZVP calculations. Energies, distances and IR frequencies are in kJ/mol, Å and  $\text{cm}^{-1}$ , respectively.

Gas	COSMO	$\Delta E$	$\Delta E^{\text{sol}}$	H-bond	$R_{\text{N-N}}$	$R_{\text{N-O}}$	$\Delta d_{\text{DA}}$	$\nu^{\text{NH}}$
G4-[1] <sup>(I,II)</sup> 	C4-[1] <sup>(I,IV)</sup> 	-379.20 (-144.69)	-212.28	(1) (2) (3) (4)	- - 2.80 (2.72) 2.80 (2.78)	2.59 (2.66) 2.60 (2.76) - -	0.43 (0.56) 0.45 (0.68) 0.68 (0.56) 0.68 (0.65)	2351 (2705) 2427 (2991) 2694 (2277) 2698 (2565)
G4-[2] <sup>(I,II)</sup> 	C4-[2] <sup>(I,II)</sup> 	-364.65 (-147.62)	-229.75	(1) (2) (4) (6)	- - 2.73 (2.76) 2.88 (2.87)	2.50 (2.67) 2.62 (2.69) - -	0.23 (0.55) 0.50 (0.59) 0.57 (0.62) 0.80 (0.79)	1684 (2658) 2588 (2771) 2355 (2477) 2943 (2900)
G4-[3] <sup>(III)</sup> 	C4-[3] <sup>(III)</sup> 	-337.18 (-96.12)	-205.04	(1) (3) (5) (7)	- 2.71 (2.77) 2.71 (2.76) 2.87 (2.87)	2.82 (2.86) - - -	0.77 (0.81) 0.55 (0.65) 0.53 (0.62) 0.79 (0.79)	3223 (3211) 2309 (2543) 2180 (2449) 2920 (2907)
G4-[3] <sup>(V)</sup> 	C4-[3] <sup>(V)</sup> 	-331.13 (-94.02)	-209.68	(1) (3) (5) (7)	- 2.80 (2.86) 2.66 (2.75) 2.78 (2.78)	2.85 (2.89) - - -	0.80 (0.86) 0.70 (0.78) 0.42 (0.61) 0.66 (0.66)	3254 (3245) 2717 (2873) 1852 (2442) 2625 (2585)
-	C4-[3] <sup>(VII)</sup> 	- (-85.39)	-201.04	(1) (3) (5) (7)	- - (2.87) - (2.85) - (2.72)	- (2.89) - - -	- (0.86) - (0.79) - (0.75) - (0.56)	- (3247) - (2906) - (2823) - (2266)
G4-[3] <sup>(I)</sup> 	C4-[3] <sup>(I)</sup> 	-328.83 (-86.97)	-204.92	(1) (3) (5) (7)	- 2.64 (2.74) 2.80 (2.86) 2.89 (2.88)	2.75 (2.77) - - -	0.64 (0.71) 0.38 (0.60) 0.68 (0.77) 0.82 (0.80)	3083 (3082) 1714 (2393) 2680 (2854) 2990 (2930)

In liquid phase, analyses of a MS-EVB model revealed that the first solvation shell of the  $\text{ImH}^+$  ion is highly ordered due to the formation of the strong protonated H-bond ( $\text{ImH}^+\cdots\text{Im}$ ), whereas the second solvation shell is highly disordered (Chen, Yan, and Voth, 2009). These suggest that the interactions connecting the Im molecules in the first and second solvation shells are weak. As the first and second solvation shells are loosely connected, mechanical and chemical interactions between the two solvation shells could be approximately neglected in the model systems, and it is reasonable to incorporate the electrostatic effects introduced by the weak-polar organic solvent by a continuum solvent model.

MD simulations also suggested that the proton transfer in liquid Im can be considered as a “local event” (Li *et al.*, 2012; Münch *et al.*, 2001), with very short spatial/temporal correlation (Li *et al.*, 2012) (involving only Im molecules close to  $\text{ImH}^+$ ) and driven by local rather than long-range cooperative motions (reorientations) of the Im molecules (Münch *et al.*, 2001). Based on Car-Parrinello molecular dynamics (CPMD) simulations (Münch *et al.*, 2001), the time scale for the long-range cooperative reorientation process is about 30 ps, which is considerably longer than the proton transfer step of about 0.3 ps. Therefore, the effects of the fluctuations of bulk solvent structures on the conformations of the solute ( $\text{ImH}^+\cdots\text{Im}$ ) could be neglected, and the approximation of the electrostatic effects of the local-dielectric environment by a continuum solvent model is reasonable and justifiable.

## 2.2 Quantum chemical calculations

Three basic steps used in the previous work (Lao-ngam *et al.*, 2011; Lao-ngam *et al.*, 2013; Phonyiem *et al.*, 2011; Chaiwongwattana *et al.*, 2012; Sagarik *et al.*, 2010)

were employed: (1) searching for equilibrium structures and intermediate complexes in the proton dissociation and transfer pathways using the Test-particle model (T-model) potentials (Sagarik and Ahlrichs, 1987; Sagarik and Asawakun, 1997; Sagarik, Chaiwongwattana, and Sisot, 2004; Sagarik and Dokmaisrijan, 2005; Sagarik, Pongpituk, Chiyapongs, and Sisot, 1991); (2) refining the T-model optimized structures using the quantum chemical method; and (3) performing BOMD simulations on the candidate intermediate complexes using the refined structures as the starting configurations.

It is worth remarking on the quantum chemical method employed in this study. As discussed in the previous work (Phonyiem *et al.*, 2011), because of the ability to approximate the effects of electron correlation with reasonable accuracy and computational resources, DFT methods have been used extensively in studies of interacting systems. However, the accuracy of the DFT methods depends on the chemical systems under investigation; the DFT methods tend to underestimate the interaction energy ( $\Delta E$ ) for the systems with strong effects of the electron correlation. The T-shaped and parallel-displaced (PD) structures of a phenol-benzene dimer are a typical example in which the interplay between the electrostatic and dispersion interactions was examined in detail (Kwac, Lee, Jung, and Han, 2006); the stability of the former is dominated by the electrostatic interaction and the latter by the dispersion interaction. However, B3LYP/6-311++G(d,p) calculations predicted the PD structure to be unstable, with positive  $\Delta E$ , whereas  $\Delta E$  of the T-shaped structure with the O-H $\cdots\pi$  interaction is considerably higher than the experimental value, -8.4 kJ/mol and -16.7 kJ/mol (Knee, Knundkar, and Zewail, 1985), respectively. Because the effects of the electron correlation could play an important role in the present model systems, the

applicability and performance of the B3LYP/TZVP calculations were examined by benchmarking with MP2 method, with the resolution of the identity (RI) approximation and the TZVP basis set, with abbreviated RIMP2/TZVP calculations. The correlations between the key properties, *e.g.*, the H-bond structures, interaction energies and vibrational frequencies, are illustrated in Figure 2.2. The methods were in agreement and obtained maximum correlation coefficient ( $R^2$ ) for  $\Delta d_{DA}$  of only 0.97. Therefore, to ensure reasonable computational efforts, the B3LYP/TZVP calculations were employed in both the static and dynamic calculations. All of the quantum chemical calculations and BOMD simulations were performed using the TURBOMOLE 6.5 software package (Ahlrichs, Baer, Haeser, Horn, and Koelmel, 1989; Treutler and Ahlrichs, 1995).

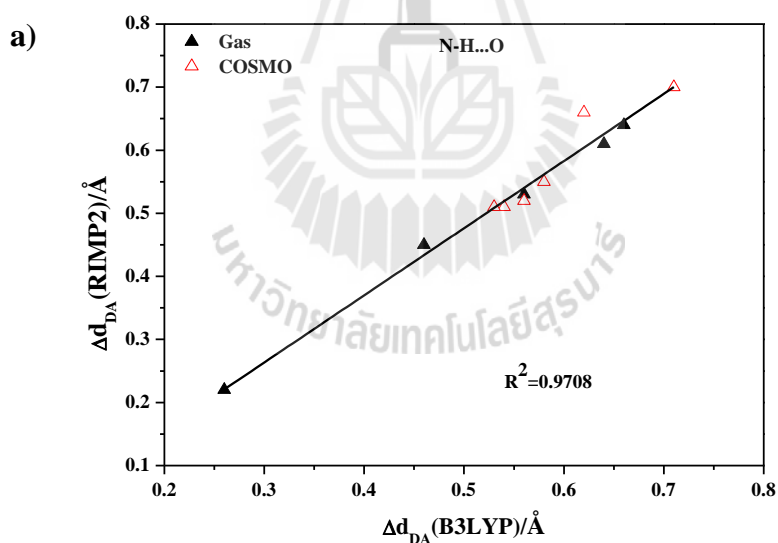


**Figure 2.2** Correlations between the results obtained from the RIMP2/TZVP and B3LYP/TZVP calculations. a) - b) Asymmetric stretching coordinates ( $\Delta d_{DA}$ ) in the N-H...O and N-H...N H-bonds, respectively. c) - d) The  $R_{N-O}$  and  $R_{N-N}$  H-bond distances, respectively. e) - f) Asymmetric N-H stretching frequencies in the N-H<sup>+</sup>...O and N-H...N H-bonds, respectively. g) Interaction ( $\Delta E$ ) and solvation ( $\Delta E^{\text{sol}}$ ) energies.

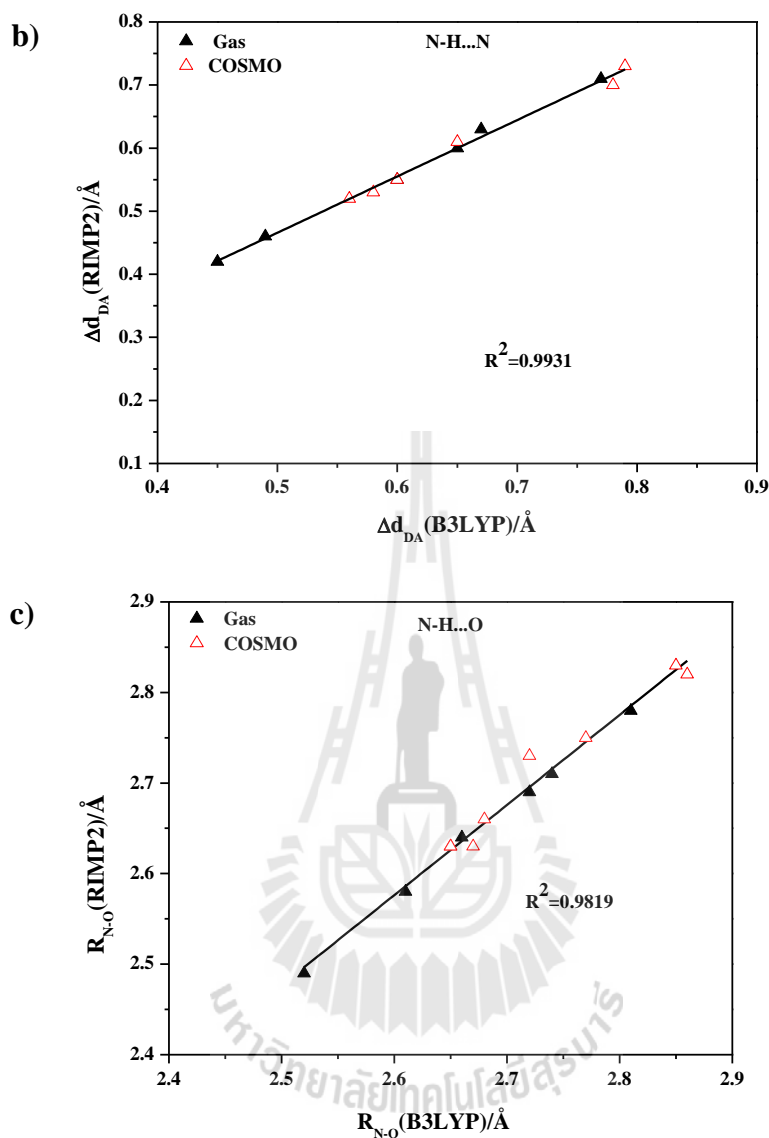


**Figure 2.2** (Continued) Correlations between the results obtained from the RIMP2/TZVP and B3LYP/TZVP calculations. a) - b) Asymmetric stretching coordinates ( $\Delta d_{DA}$ ) in the N-H...O and N-H...N H-bonds, respectively. c) - d) The  $R_{N-O}$  and  $R_{N-N}$  H-bond distances, respectively. e) - f) Asymmetric N-H stretching frequencies in the N-H<sup>+</sup>...O and N-H...N H-bonds, respectively. g) Interaction ( $\Delta E$ ) and solvation ( $\Delta E^{\text{sol}}$ ) energies.

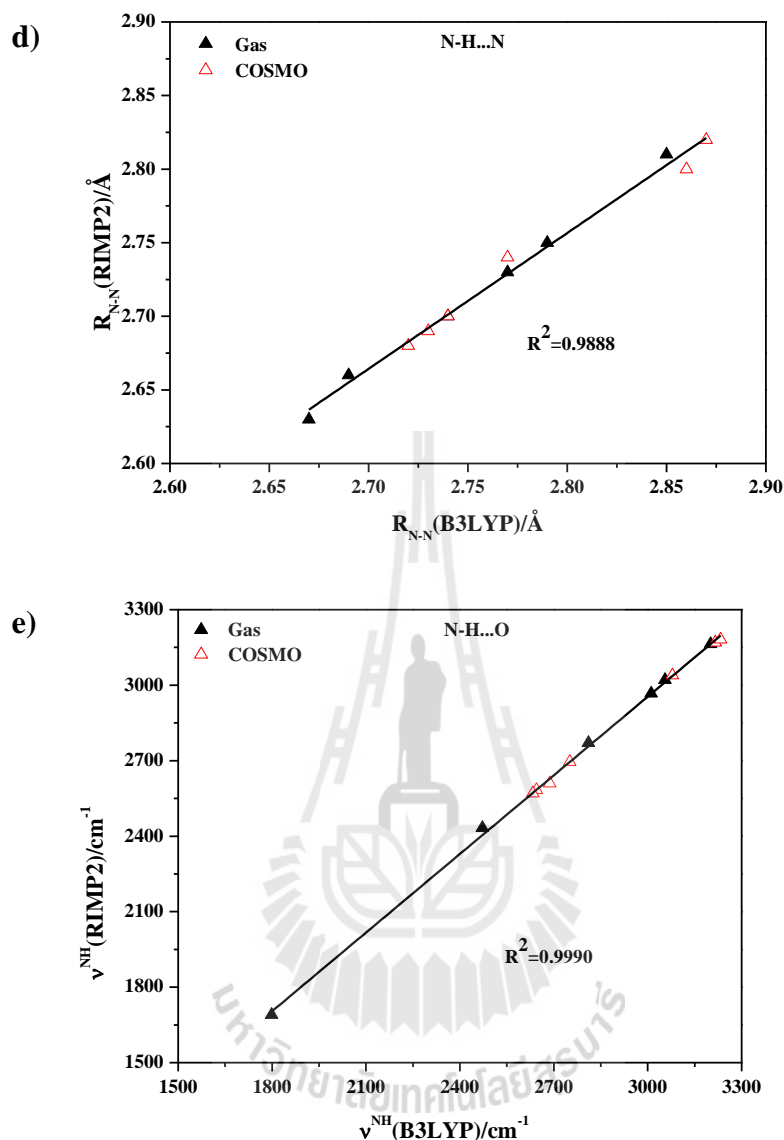


**Figure 2.2** (Continued) Correlations between the results obtained from the RIMP2/TZVP and B3LYP/TZVP calculations. a) - b) Asymmetric stretching coordinates ( $\Delta d_{DA}$ ) in the N-H $\cdots$ O and N-H $\cdots$ N H-bonds, respectively. c) - d) The  $R_{N-O}$  and  $R_{N-N}$  H-bond distances, respectively. e) - f) Asymmetric N-H stretching frequencies in the N-H $\cdots$ O and N-H $\cdots$ N H-bonds, respectively. g) Interaction ( $\Delta E$ ) and solvation ( $\Delta E^{sol}$ ) energies.

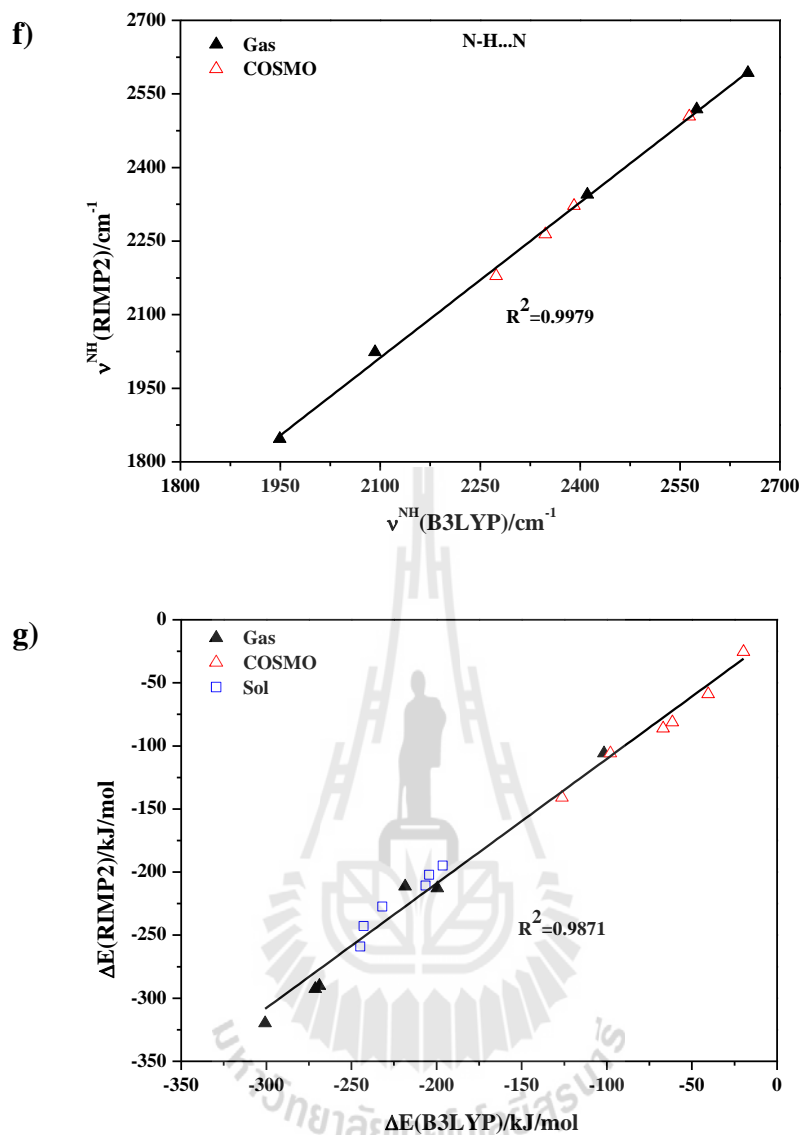


**Figure 2.2** (Continued) Correlations between the results obtained from the RIMP2/TZVP and B3LYP/TZVP calculations. a) - b) Asymmetric stretching coordinates ( $\Delta d_{DA}$ ) in the N-H $\cdots$ O and N-H $\cdots$ N H-bonds, respectively. c) - d) The  $R_{N-O}$  and  $R_{N-N}$  H-bond distances, respectively. e) - f) Asymmetric N-H stretching frequencies in the N-H $^+\cdots$ O and N-H $\cdots$ N H-bonds, respectively. g) Interaction ( $\Delta E$ ) and solvation ( $\Delta E^{sol}$ ) energies.

## 2.3 Static calculations

To obtain the fundamental information for the discussion of the dynamics and mechanisms of proton dissociation and transfer in the  $\text{H}_3\text{PO}_4$  doped Im system under an excess proton condition, the structural, energetic and spectroscopic properties of  $\text{H}^+(\text{H}_3\text{PO}_4)(\text{Im})_n$  ( $n = 1-4$ ) were computed using B3LYP/TZVP calculations, both in the gas phase ( $\epsilon = 1$ ) and the continuum solvent (COSMO,  $\epsilon = 23$ ). The interaction energies ( $\Delta E$ ) of the H-bond complexes were computed from  $\Delta E = E(\text{H}^+(\text{H}_3\text{PO}_4)(\text{Im})_n) - [E(\text{H}_4\text{PO}_4^+) + nE(\text{Im})]$ ;  $E(\text{H}^+(\text{H}_3\text{PO}_4)(\text{Im})_n)$  is the total energy of the equilibrium structure of  $\text{H}^+(\text{H}_3\text{PO}_4)(\text{Im})_n$ ;  $E(\text{H}_4\text{PO}_4^+)$  and  $E(\text{Im})$  are the total energies of the isolated species at their equilibrium structures. The solvation energies ( $\Delta E^{\text{sol}}$ ) were approximated from  $\Delta E^{\text{sol}} = E(\text{H}^+(\text{H}_3\text{PO}_4)(\text{Im})_n)^{\text{COSMO}} - E(\text{H}^+(\text{H}_3\text{PO}_4)(\text{Im})_n)$ ;  $E(\text{H}^+(\text{H}_3\text{PO}_4)(\text{Im})_n)^{\text{COSMO}}$  and  $E(\text{H}^+(\text{H}_3\text{PO}_4)(\text{Im})_n)$  are the total energies of the equilibrium structures obtained with and without COSMO, respectively.

The behaviors of proton dissociation and transfer were primarily evaluated from the asymmetric stretching coordinate ( $\Delta d_{\text{DA}}$ ), computed from  $\Delta d_{\text{DA}} = |d_{\text{A-H}} - d_{\text{B}\cdots\text{H}}|$ , where  $d_{\text{A-H}}$  and  $d_{\text{B}\cdots\text{H}}$  are the A-H and B $\cdots$ H distances in the A-H $\cdots$ B H-bond, respectively. The H-bond that is susceptible to proton transfer is represented by a  $\Delta d_{\text{DA}}$  value that is close to zero as for a proton located near or at the center of the H-bond. As an effective probe for the dynamics of proton transfer in the H-bond, this study employed vibrational spectroscopy. The vibrational frequencies of protons in  $\text{H}^+(\text{H}_3\text{PO}_4)(\text{Im})_n$  ( $n = 1-4$ ) were computed using the B3LYP/TZVP method with the harmonic approximation. They were used as guidelines to assign the vibrational modes predicted by the BOMD simulations. As the anharmonicity is neglected, the vibrational

frequencies obtained from quantum chemical methods are generally overestimated. A scaling factor of 0.9614 proved to be appropriate for the B3LYP/TZVP calculations (Scott and Radom, 1996) and was therefore employed in this work. The dynamics of the proton dissociation and transfer were discussed based on the asymmetric O–H and N–H stretching frequencies,  $\nu^{\text{OH}}$  and  $\nu^{\text{NH}}$ , respectively (Chaiwongwattana *et al.*, 2011; Lao-ngam *et al.*, 2011; Phonyiem *et al.*, 2011; Sagarik *et al.*, 2010). Additionally, because the motions of protons moving in single- and double-well potentials are different, H-bonds that are susceptible and not susceptible to transfer were distinguished by the threshold asymmetric N–H stretching frequencies ( $\nu^{\text{NH}^*}$ ) that were calculated from the plots of  $\nu^{\text{NH}}$  and  $\Delta d_{\text{DA}}$  (Lao-ngam *et al.*, 2011). The relationship between  $\nu^{\text{NH}}$  and  $\Delta d_{\text{DA}}$  is described by a reflected normal distribution function, for which the second derivative is equal to zero at  $\nu^{\text{NH}} = \nu^{\text{NH}^*}$ . The H-bond proton is considered to be susceptible to transfer when  $\nu^{\text{NH}} < \nu^{\text{NH}^*}$  (Lao-ngam *et al.*, 2011). To provide energetic information for the discussion of the solvent effects, two-dimensional potential energy surfaces (2D-PES) of the transferring protons in the smallest, most active intermediate complexes were constructed in both the gas phase and the continuum solvent by calculating  $\Delta E$  at various  $R_{\text{N-O}}$  and  $R_{\text{N-H}}$  distances. As in the previous studies (Lao-ngam *et al.*, 2013), equally spaced grid points were generated from  $\Delta E$  and the 2D-PES were plotted as a function of  $R_{\text{N-O}}$  and  $\Delta d_{\text{DA}}$  using the SURFER program (“SURFER for Window”, 1997). The interaction energy paths connecting the single- and double-well potentials, as well as the path with the highest energy barriers, were identified and discussed in detail.

## 2.4 Dynamic calculations

The dynamics and mechanisms of proton transfer in H-bonds were successfully studied in the previous work by performing NVT BOMD simulations on the smallest, most active intermediate complexes in the presolvation models (Lao-ngam *et al.*, 2013; Phonyiem *et al.*, 2011; Chaiwongwattana *et al.*, 2012; Sagarik *et al.*, 2010; Suwannakum *et al.*, 2015). The present study focuses the dynamics of the transferring protons (*e.g.*, the oscillatory shuttling and structural diffusion motions) in the intermediate complexes, which occur locally in a very short time scale; according to the MS-EVB MD simulations (Li *et al.*, 2012), these involve linear H-bond chains with few Im molecules. As the intermediate complexes with the shared-proton structures are repeatedly formed and relaxed, and BOMD simulations involve only limited number of Im molecules, the periodic boundary conditions are not necessary in this case; the periodic boundary conditions are generally employed in computer simulations of condensed phase to solve the problem of surface and finite-size effects, and therefore important in the study of the long-range effects in bulk systems.

To study proton dissociation and transfer in  $\text{H}^+(\text{H}_3\text{PO}_4)(\text{Im})_n$  ( $n = 1-4$ ), NVT BOMD simulations were performed at the B3LYP/TZVP level. Two thousand steps of 1 fs each were used in the equilibration and 10,000 steps were used in the property calculations, corresponding to 2 and 10 ps, respectively. The NVT ensemble was concluded to be appropriate for the dynamic processes that take place on relatively short time scales and in the continuum solvent (Basconi and Shirts, 2013) and the time step proved to be small enough to determine reliable vibrational spectra, activation energies and dynamic properties of the transferring protons. (Chaiwongwattana, Lao-ngam, Phonyiem, Vchirawongkwin, and Sagarik; Lao-ngam *et al.*, 2011; Lao-ngam *et al.*,

2013; Phonyiem *et al.*, 2011; Chaiwongwattana *et al.*, 2012; Sagarik *et al.*, 2010; Sagarik *et al.*, 2008)

Because realistic dynamics at constant temperatures are desirable in this work, the BOMD simulation conditions were carefully chosen, especially the temperature control algorithm. The Nosé-Hoover thermostat was selected based on the conclusion that the transport properties and thermodynamic distributions that are statistically indistinguishable from the NVE ensemble can be achieved when globally applied to the system using any coupling strength (Basconi *et al.*, 2013); the Nosé-Hoover thermostat adjusts velocities by coupling the equations of motion to extended dynamic variables and gives an oscillatory relaxation to the target temperature. To ensure the minimum perturbation on the dynamics of the transferring protons, the energy conservation and stability of the numerical integration in the NVT BOMD simulations were assessed at 323 K, using the smallest, most active intermediate complex as a representative. To test the stability of the numerical integration, a drift in property A ( $\delta_A$ ) over a time interval  $[0, t_{\max}]$  was computed from  $\delta_A = b_A t_{\max} / \sigma_A$  (Davidchack, 2010);  $b_A$  is obtained from a linear least-square fit to the data,  $A(t) = a_A + b_A t + \varepsilon(t)$ , and  $\sigma_A$  is the standard deviation of  $\varepsilon(t)$ . Therefore, for an ideal, isolated-energy conserved system,  $b_A$  is 0, and hence,  $|\delta_A| = 0$ . The drift in property A is significant if  $|\delta_A| \sim 1$  and the result obtained by averaging  $A(t)$  over the simulation time  $t_{\max}$  is considered to be unreliable. Based on this definition, the drifts in energies ( $E^{\text{tot}}$ ,  $E^{\text{pot}}$  and  $E^{\text{kin}}$ ), the H-bond structures ( $R_{\text{N-O}}$ ,  $R_{\text{N-H}}$  and  $R_{\text{O-H}}$ ) and the velocity of the transferring proton ( $v^{\text{H}^+}$ ) were calculated over the integration period of  $t_{\max} = 2$  ps and included in Table 2.2. The energy conservation and velocity plots over the entire simulation length (10 ps) are illustrated in Figure 2.3. Additionally, to confirm that the dynamics are not perturbed by the Nosé-Hoover

thermostat, the mean-square displacement (MSD) of the transferring proton was computed and included in Figure 2.3. Because the trends of the energy conservation and velocity plots showed no systematic drifts and a general linear relationship was observed for the MSD plot, the dynamic properties computed under the present NVT BOMD simulation conditions, including the Nosé-Hoover thermostat, were determined to be well represented. Additionally, as the energy and velocity drifts are only 0.22, the numerical integration in the NVT BOMD simulations is confirmed to be stable.



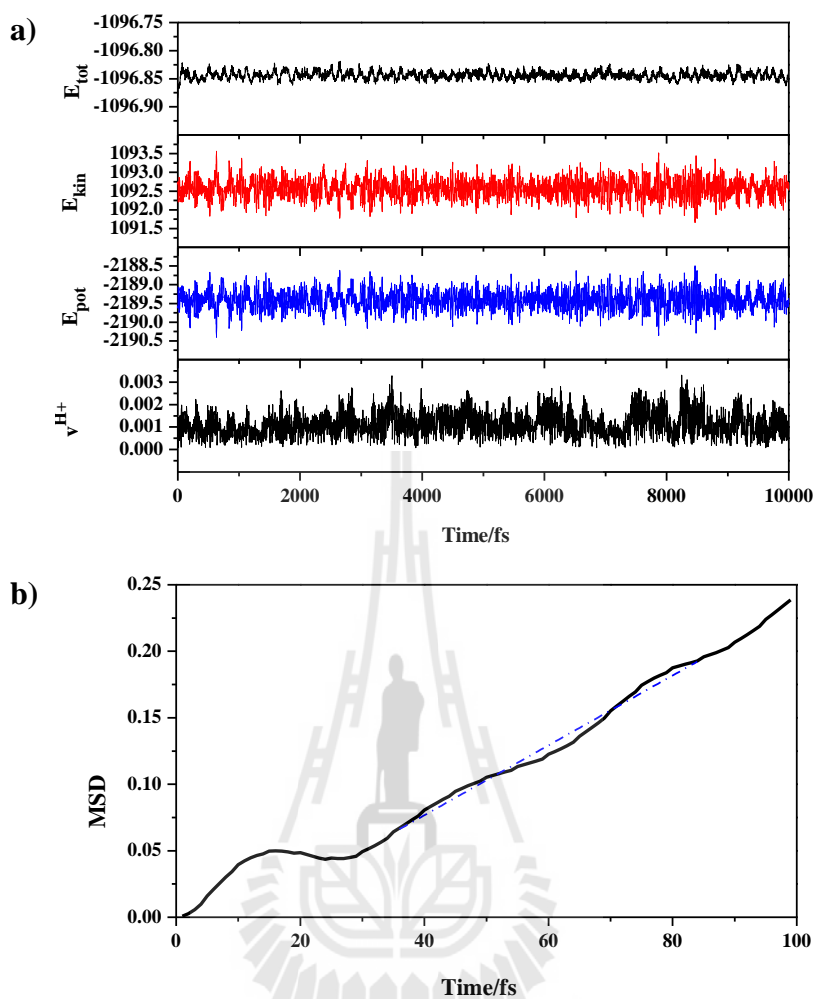


**Figure 2.3** a) Energy conservation and velocity plots obtained from NVT BOMD simulations on structure  $G2-[1]^{(I,II)}$  at 323 K. b) Plot of MSD and BOMD simulation time ( $t$ ) for proton in H-bond (1) of structure  $G2-[1]^{(I,II)}$  at 323 K.

**Table 2.2** Drifts in the energies, H-bond properties and velocity of proton obtained from NVT BOMD simulations at 323 K. Energies and velocity are in atomic unit (au). Distances and temperature are in Å and K, respectively.

Property A	$\delta_A$	$\langle A \rangle$	$\sigma_A$
$E^{\text{tot}}$	0.2223	-1096.8061	0.0083
$E^{\text{pot}}$	0.2292	-1096.8438	0.0060
$E^{\text{kin}}$	0.0761	0.0376	0.0060
$v^{\text{H}^+}$	-0.2192	0.0013	0.0005
$R_{\text{N-O}}$	0.0546	2.55	0.0726
$R_{\text{N-H}}$	-0.3945	1.12	0.0674
$R_{\text{O..H}}$	0.2718	1.46	0.1203
T	0.0460	317.4	34.8

$\delta_A$  = drift of property A;  $\langle A \rangle$  = average of property A;  $\sigma_A$  = SD of property A;  $E^{\text{tot}}$  = total energy;  $E^{\text{pot}}$  = potential energy;  $E^{\text{kin}}$  = kinetic energy;  $v^{\text{H}^+}$  = velocity of proton in H-bond;  $R_{\text{N-O}}$ ,  $R_{\text{N-H}}$  and  $R_{\text{O..H}}$  = H-bond distances; T = temperature.

The dynamic behaviors of proton dissociation and transfer in the  $\text{H}_3\text{PO}_4$  doped Im system were primarily discussed using proton transfer profiles, with variations of  $R_{\text{A-B}}$ ,  $R_{\text{A-H}}$  and  $R_{\text{B-H}}$  with the simulation time (Sagarik *et al.*, 2008). Proton transfer reactions are generally not concerted and can take place in both the forward and reverse directions, with the oscillatory shuttling motion being the rate-determining process (Sagarik *et al.*, 2008). This is because the transfer reactions involve quasi-dynamic equilibrium between the close-contact  $\text{A-H}\cdots\text{B}$  and the shared-proton  $\text{A}\cdots\text{H}\cdots\text{B}$  H-bonds (Sagarik *et al.*, 2008). It is therefore not straightforward to determine the

direction of the proton displacement in the Im H-bond chain. Because a stable covalent bond must be formed in the direction of the proton displacement to complete proton hopping in a single H-bond, it is reasonable to correlate the probability of finding a proton moving in a specific direction with the probability of covalent bond formation. Hence, to estimate the probability of finding a proton transfer from atom B to A ( $P_{BA}$ ), the distribution of the A–H covalent bond distance ( $R_{A-H}$ ) is first computed from the BOMD simulations. Then, based on the criterion for the N–H covalent bond formation ( $R_{N-H} \leq 1.3 \text{ \AA}$ ),  $P_{BA}$  is approximated by the number of counts of the N–H covalent bond divided by the total number of samples. In this work, a proton is considered to have favorably transferred from B to A when  $P_{BA} \geq 0.5$ . Likewise, the probability of finding the intermediate complex with the shared-proton  $A \cdots H \cdots B$  H-bond ( $P_{A \cdots H \cdots B}$ ) can be approximated by the number of counts of  $R_{A-H}$  in the range between 1.3 and 1.5  $\text{\AA}$ , divided by the total number of samples.

The dynamics and mechanisms of proton dissociation and transfer were finally confirmed using the vibrational spectra obtained from Fourier transformations of the velocity autocorrelation functions (VACF) of the atoms in H-bonds (Phonyiem *et al.*, 2011; Chaiwongwattana *et al.*, 2012). Only the characteristic N–O and N–N vibrational frequencies ( $v^{NO,MD}$  and  $v^{NN,MD}$ , respectively), as well as the asymmetric N–H stretching frequencies ( $v^{NH,MD}$ ), were reported and discussed in detail. As an example, the definitions of the velocity vectors used in the calculations of the symmetric and asymmetric O–H stretching modes, as well as the O–O vibrations, are shown in Figure 2.4.

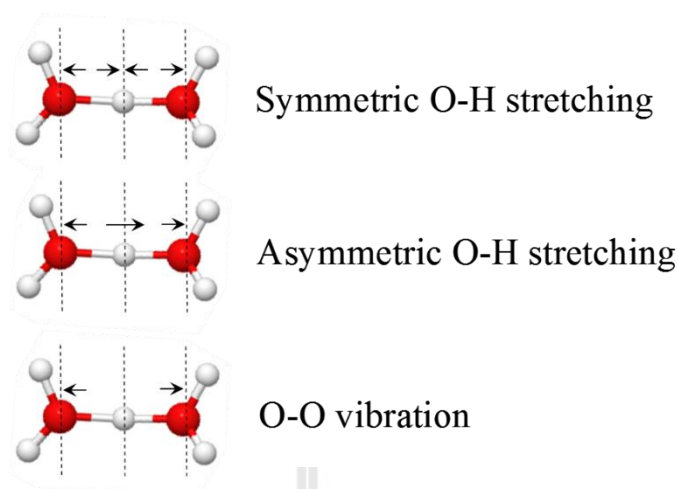


**Figure 2.4** Definitions of the velocity vectors used in the calculations of the symmetric and asymmetric O–H stretching modes, as well as the O–O vibration (Sagarik *et al.*, 2010)-Reproduced by permission of the PCCP Owner Societies.

The activation energies of the rate-determining processes in the proton dissociation and transfer pathways were determined by performing BOMD simulations over the temperature range of 298 to 423 K. The first-order rate constants ( $k$ ) for proton exchanges were approximated from the exponential relaxation behavior of the envelope of VACF of the N–O and N–N vibrations, which are based on the assumption that the decay process follows the first-order kinetics:  $k = \ln(2)/\tau_{1/2}$ , where  $\tau_{1/2}$  is the half-life of the exponential decay function. The Arrhenius plots were constructed and the activation energies ( $\Delta E^{\ddagger, \text{Arr}}$ ) of proton dissociation and transfer were approximated from the slopes of the linear relationship between  $\ln(k)$  and  $1000/T$  (Lao-ngam *et al.*, 2013). Examples of the VACF, the corresponding exponential relaxation behavior of the envelope, and the Arrhenius plot of the Zundel complex obtained from BOMD simulations at 350 K (Lao-ngam *et al.*, 2013) are shown in Figure 2.5.

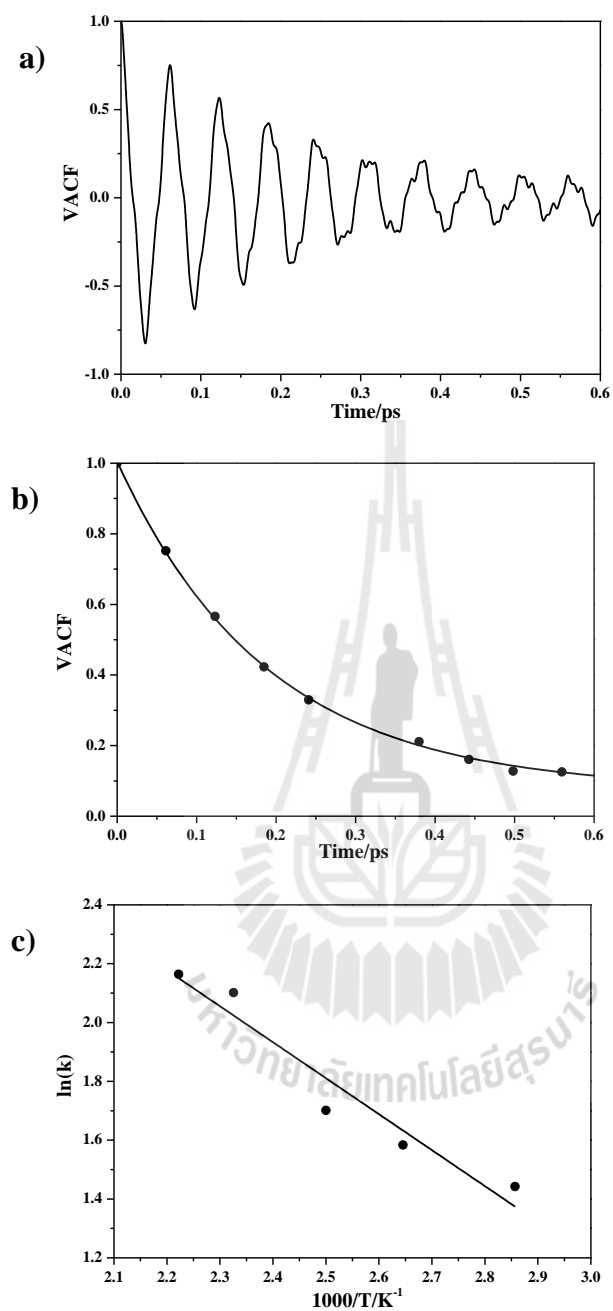


**Figure 2.5** a) VACF of the proton in the Zundel complex obtained from BOMD simulations at 350 K. b) The exponential relaxation behavior of the envelope of the VACF. c) Plot of the natural log of the first-order rate constant ( $\ln(k)$ ) and  $1000/T$ . (Lao-ngam *et al.*, 2013)-Reproduced by permission of the Elsevier B.V.

## 2.5 References

- Ahlrichs, R., Baer, M., Haeser, M., Horn, H., and Koelmel, C. (1989). Electronic structure calculations on workstation computers: The program system turbomole. **Chemical Physics Letters**. 162: 165-169.
- Basconi, J. E. and Shirts, M. R. (2013). Effects of temperature control algorithms on transport properties and kinetics in molecular dynamics simulations. **Journal of Chemical Theory and Computation**. 9: 2887-2899.
- Buagern, V. and Sagarik, K. Proton dissociation and transfer in an imidazole clusters. (*in preparation*).
- Chaiwongwattana, S., Lao-ngam, C., Phonyiem, M., Vchirawongkwin, V., and Sagarik, K. Temperature dependence of proton transfer in linear hydrogen-bond chains. (*in preparation*).
- Chaiwongwattana, S., Phonyiem, M., Vchirawongkwin, V., Prueksaaron, S., and Sagarik, K. (2012). Dynamics and mechanism of structural diffusion in linear hydrogen bond. **Journal of Computational Chemistry**. 33: 175-188.
- Chen, H., Yan, T., and Voth, G. A. (2009). A computer simulation model for proton transport in liquid imidazole. **The Journal of Physical Chemistry A**. 113: 4507-4517.
- Davidchack, R. L. (2010). Discretization errors in molecular dynamics simulations with deterministic and stochastic thermostats. **Journal of Computational Physics**. 229: 9323-9346.
- Greenwood, N. N. and Thompson, A. (1959). The mechanism of electrical conduction in fused phosphoric and trideuterophosphoric acids. **Journal of the Chemical Society**. 3485-3492.

- Hobza, P., Selzle, H. L., and Schlag, E. W. (1994). Structure and properties of benzene-containing molecular clusters: Nonempirical *ab Initio* calculations and experiments. **Chemical Reviews**. 94: 1767-1785.
- Iannuzzi, M. (2006). Proton transfer in imidazole-based molecular crystals. **The Journal of Chemical Physics**. 124: 204710.
- Kawada, A., McGhie, A. R., and Labes, M. M. (1970). Protonic conductivity in imidazole single crystal. **The Journal of Chemical Physics**. 52: 3121-3125.
- Knee, J. L., Knundkar, L. R., and Zewail, A. H. (1985). Picosecond mass spectrometry of a collisionless photodissociation reaction. **The Journal of Chemical Physics**. 82: 4715.
- Kwac, K., Lee, C., Jung, Y., Han, J., Kwak, K., Zheng, J., Fayer, M. D., and Cho, M. (2006). Phenol-benzene complexation dynamics: Quantum chemistry calculation, molecular dynamics simulations, and two dimensional IR spectroscopy. **The Journal of Chemical Physics**. 125: 244508.
- Lao-ngam, C., Asawakun, P., Wannarat, S., and Sagarik, K. (2011). Proton transfer reactions and dynamics in protonated water clusters. **Physical Chemistry Chemical Physics**. 13: 4562-4575.
- Lao-ngam, C., Phonyiem, M., Chaiwongwattana, S., Kawazoe, Y., and Sagarik, K. (2013). Characteristic NMR spectra of proton transfer in water clusters. **Chemical Physics**. 420: 50-61.
- Li, A., Cao, Z., Li, Y., Yan, T., and Shen, P. (2012). Structure and dynamics of proton transfer in liquid imidazole. A molecular dynamics simulation. **The Journal of Physical Chemistry B**. 116: 12793-12800.

- Marx, D., Chandra, A., and Tuckerman, M. E. (2010). Aqueous basic solutions: Hydroxide solvation, structural diffusion, and comparison to the hydrated proton. **Chemical Reviews**. 110: 2174-2216.
- Münch, W., Kreuer, K. D., Silvestri, W., Maier, J., and Seifert, G. (2001). The diffusion mechanism of an excess proton in imidazole molecule chains: First results of an ab initio molecular dynamics study. **Solid State Ionics**. 145: 437-443.
- Munson, R. A. and Lazarus, M. E. (1967). The influence of ionic solutes upon the conductivity of molten phosphoric acid. **The Journal of Physical Chemistry**. 71: 3245-3248.
- Paddison, S. J. (2001). The modeling of molecular structure and ion transport in sulfonic acid based ionomer membranes. **Journal of New Materials for Electrochemical Systems**. 4: 197-207.
- Phonyiem, M., Chaiwongwattana, S., Lao-ngam, C., and Sagarik, K. (2011). Proton transfer reactions and dynamics of sulfonic acid groups of Nafion<sup>®</sup>. **Physical Chemistry Chemical Physics**. 13: 10923.
- Sagarik, K. P. and Ahlrichs, R. (1987). A test particle model potential for formamide and molecular dynamics simulations of the liquid. **The Journal of Chemical Physics**. 86: 5117.
- Sagarik, K. P. and Asawakun, P. (1997). Intermolecular potential for phenol based on the test particle model. **Chemical Physics**. 219: 173-191.
- Sagarik, K. P., Chaiwongwattana, S., and Sisot, P. (2004). A theoretical study on clusters of benzoic acid-water in benzene solutions. **Chemical Physics**. 306: 1-12.

- Sagarik, K., Chaiwongwattana, S., Vchirawongkwin, V., and Prueksaaroon, S. (2010). Proton transfer reactions and dynamics in  $\text{CH}_3\text{OH-H}_3\text{O}^+\text{-H}_2\text{O}$  complexes. **Physical Chemistry Chemical Physics**. 12: 918-929.
- Sagarik, K. P. and Dokmaisrijan, S. (2005). A theoretical study on hydration of alanine zwitterions. **Journal of Molecular Structure: THEOCHEM**. 718: 31-47.
- Sagarik, K., Phonyiem, M., Lao-Ngam, C., and Chaiwongwattana, S. (2008). Mechanisms of proton transfer in Nafion<sup>®</sup>: Elementary reactions at the sulfonic acid groups. **Physical Chemistry Chemical Physics**. 10: 2098-2112.
- Sagarik, K. P., Pongpituk, V., Chiyapongs, S., and Sisot, P. (1991). Test-particle model potentials for hydrogen-bonded complexes: Complexes formed from HCN, HF,  $\text{H}_2\text{O}$ ,  $\text{HCONH}_2$ ,  $\text{HCONHCH}_3$ , guanine and cytosine. **Chemical Physics**. 156: 439-456.
- Scott, A. P. and Radom, L. (1996). Harmonic vibrational frequencies: An evaluation of Hartree-Fock, Møller-Plesset, quadratic configuration interaction, density functional theory, and semiempirical scale factors. **The Journal of Physical Chemistry**. 100: 16502-16513.
- SURFER for Window (Version 6.04). (1997): Golden Software Inc., USA.
- Suwannakham, P., Chaiwongwattana, S., and Sagarik, K. (2015). Proton dissociation and transfer in hydrated phosphoric acid clusters. **International Journal of Quantum Chemistry**. 115: 486-501.
- Treutler, O. and Ahlrichs, R. (1995). Efficient molecular numerical integration schemes. **The Journal of Chemical Physics**. 102: 346.

# CHAPTER III

## RESULTS AND DISCUSSION

### 3.1 Static results

The equilibrium structures and the interaction ( $\Delta E$ ) and solvation ( $\Delta E^{\text{sol}}$ ) energies obtained from the B3LYP/TZVP calculations in the gas phase and the continuum solvent are listed in Table 2.1, together with the H-bond distances ( $R_{\text{N-N}}$ ,  $R_{\text{N-O}}$  and  $\Delta d_{\text{DA}}$ ) and the asymmetric N-H stretching frequencies ( $\nu^{\text{NH}}$ ). The  $\text{H}_3\text{PO}_4$  doped Im H-bond structures in Table 2.1 are labelled with a four character code, *e.g.*, **Gn-[m]<sup>(I-VII)</sup>** and **Cn-[m]<sup>(I-VII)</sup>**, where **G** = equilibrium structure in the gas phase; **C** = equilibrium structure in continuum solvent; and **n** = number of Im molecules. Different H-bond structures with the same number of Im molecules are distinguished by **[m]**. Positively charged Im molecules are designated by a Roman numeral in parenthesis, from **(I)** to **(VII)**. As an example, **G3-[2]<sup>(I)</sup>** and **G3-[2]<sup>(II)</sup>** are the same H-bond structures (**m** = 2 and **n** = 3) with different positively charged Im molecules, at Im **(I)** and Im **(II)**, respectively.

### 3.1.1 Excess proton conditions and tendencies of proton dissociation and transfer

Investigation of the embedded structures and their H-bond properties in Table 2.1 reveals outstanding acid-base interaction in the H<sub>3</sub>PO<sub>4</sub> doped Im system, specifically two protons are readily dissociated from H<sub>4</sub>PO<sub>4</sub><sup>+</sup> and protonate the two neighboring Im molecules (Im **(I)** and Im **(II)**), forming the ImH<sup>+</sup>-H<sub>2</sub>PO<sub>4</sub><sup>-</sup>-ImH<sup>+</sup> complex, *e.g.*, in the gas phase, structures **G2-[1]<sup>(I,II)</sup>** and **G3-[1]<sup>(I,II)</sup>**, and in the continuum solvent, structures **C2-[1]<sup>(I,II)</sup>** and **C3-[1]<sup>(I,II)</sup>**. Because the B3LYP/TZVP calculations (not shown here) suggest no proton dissociation from the corresponding unprotonated (neutral) embedded structures, one can conclude that proton dissociation and transfer in the Im system takes place preferentially under excess proton conditions (Chin *et al.*, 1989; He *et al.*, 2003), with the Im-H<sub>4</sub>PO<sub>4</sub><sup>+</sup>-Im complexes as the precursors. This is in agreement with experiments in which dipping the PBI film into a H<sub>3</sub>PO<sub>4</sub> solution is a necessary step for the conductivity measurement (He *et al.*, 2003). Therefore, to obtain realistic proton dissociation and transfer mechanisms, excess proton conditions must be included in the presolvation models (Lao-ngam *et al.*, 2011; Phonyiem *et al.*, 2011; Chaiwongwattana *et al.*, 2012; Suwannakham *et al.*, 2015).

The tendencies of proton dissociation and transfer are primarily discussed using the relationships between  $\nu^{\text{NH}}$  and  $\Delta d_{\text{DA}}$  in Figure 3.1. The plot of  $\nu^{\text{NH}}$  and  $\Delta d_{\text{DA}}$  in Figure 3.1a suggests that the threshold asymmetric N–H stretching frequency ( $\nu^{\text{NH}^*}$ ) for the proton dissociation in the gas phase is at  $\nu^{\text{NH}^*} = 2158 \text{ cm}^{-1}$  and  $\Delta d_{\text{DA}}^* = 0.37 \text{ \AA}$ , approximately  $150 \text{ cm}^{-1}$  lower than in aqueous solution ( $\nu^{\text{OH}^*} = 2306 \text{ cm}^{-1}$ ) (Suwannakham *et al.*, 2015), reflecting a stronger acid-base interaction in the H<sub>3</sub>PO<sub>4</sub> doped Im system. In the continuum solvent, the  $\nu^{\text{NH}}$  values are all above  $2500 \text{ cm}^{-1}$

without an inflection point ( $\nu^{\text{NH}^*}$ ), suggesting that the close-contact N–H···O H-bond with localized positive charge is more favorable than the shared-proton structure (N···H···O) with delocalized positive charge in COSMO, which is in accordance with the localized charge solvent (LCS) concept: “a polar solvent solvates species with localized charges more efficiently than species with more delocalized charges” (Koepp, Guo, Tolstoy, Denisov, and Limbach, 2013). Similar results were obtained for proton transfer in the Im H-bond chains, for which the plot of  $\nu^{\text{NH}}$  and  $\Delta d_{\text{DA}}$  in Figure 3.1b yielded the threshold frequency only in a low local-dielectric environment, in the gas phase at  $\nu^{\text{NH}^*} = 1925 \text{ cm}^{-1}$  and  $\Delta d_{\text{DA}}^* = 0.44 \text{ \AA}$ . The threshold frequency is approximately  $70 \text{ cm}^{-1}$  lower than that of the undoped Im H-bond chains ( $1992 \text{ cm}^{-1}$ ) (Buagern *et al.*), reflecting the strong polarization effect of the dopant and a higher probability of finding the shared-proton structure and delocalized protons in the  $\text{H}_3\text{PO}_4$  doped Im system; the shared-proton structure is an important intermediate in the proton transfer pathway.

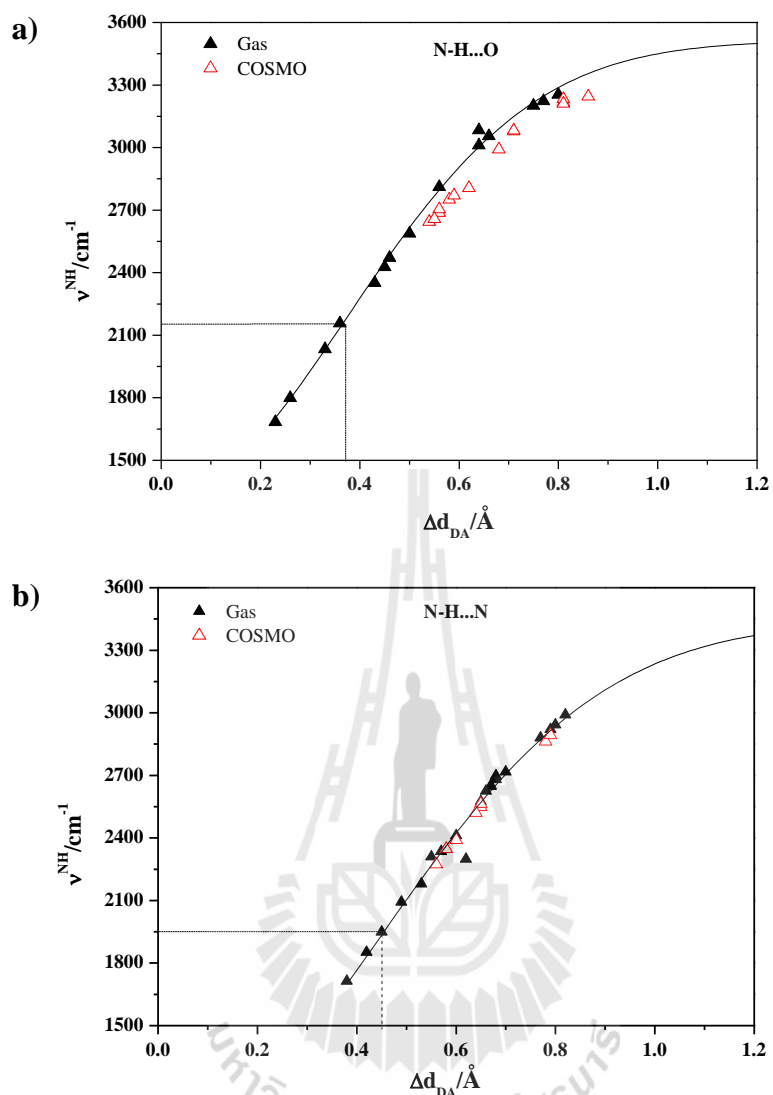


**Figure 3.1** Plots of asymmetric N–H stretching frequencies ( $\nu^{\text{NH}}$ ) as a function of asymmetric stretching coordinates ( $\Delta d_{\text{DA}}$ ), obtained from B3LYP/TZVP calculations. The dashed lines separate the protons that are susceptible and not susceptible to exchange. a) N–H...O H-bonds in the first solvation shell. b) N–H...N H-bonds in Im H-bond chains.

### 3.1.2 Two-dimensional potential energy surfaces and solvent effects

The two-dimensional potential energy surfaces (2D-PES) for proton dissociation in the smallest embedded structure in the gas phase and the continuum solvent are shown in Figure 3.2. The absolute minimum on the 2D-PES of structure **G2-[1]<sup>(L,II)</sup>** is represented by an asymmetric single-well potential at  $R_{N-O} = 2.54 \text{ \AA}$  and  $\Delta d_{DA} = 0.33 \text{ \AA}$ . At longer  $R_{N-O}$  distance ( $R_{N-O} \approx 2.67 \text{ \AA}$ ), a double-well potential emerges. On the 2D-PES, a low-interaction energy, barrier-less path connecting the single- and double-well potentials spans from **A** to **C**, regarded hereafter as the “dissociation path” (or path **AC**), whereas the “association path” spanning from **A** to **B** (or path **AB**) is uphill and therefore unfavorable in this H-bond complex. The shapes of the cross-sectional plots in Figure 3.2a suggest at least three N–H stretching modes associated with proton dissociation, namely a vibrational mode associated with a proton moving in the single-well potential and two vibrational modes with a proton moving on the dissociation and association paths. Because conventional quantum chemical calculations on vibrational spectra are based on the harmonic approximation, which requires well-optimized geometry, only the  $\nu^{NH}$  value of a proton moving in the single-well potential is obtainable from the static calculations; for proton dissociation in structure **G2-[1]<sup>(L,II)</sup>**,  $\nu^{NH} = 2033 \text{ cm}^{-1}$ . Therefore, BOMD simulations must be performed to study the other two characteristic modes that involve H-bond structures distorted from the absolute minimum energy geometry.

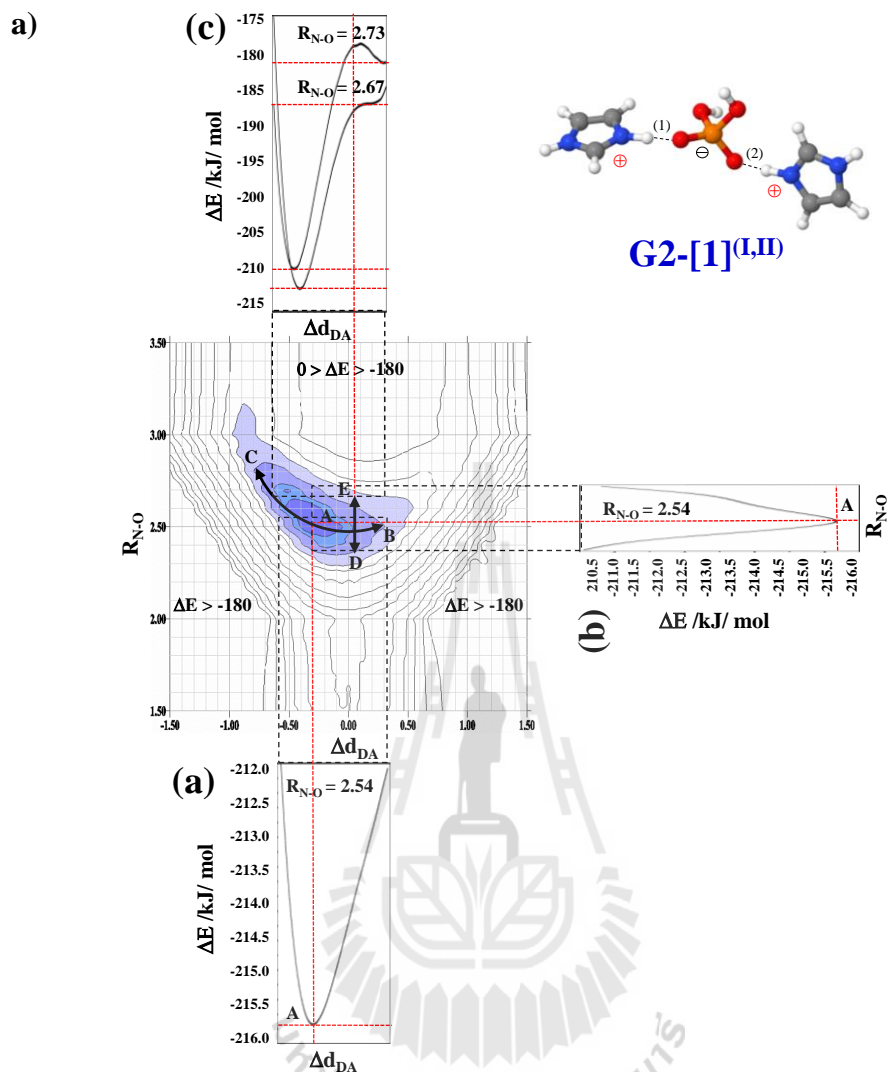


**Figure 3.2** Two-dimensional potential energy surfaces (2D-PES) of proton dissociation in the gas phase and continuum solvent. a) Proton dissociation in H-bond (1) of the embedded structure **G2-[1]<sup>(I,II)</sup>**. b) Proton dissociation in H-bond (1) of the embedded structure **C2-[1]<sup>(I,II)</sup>**. (a), (b) and (c) are the cross-sectional plots of the single- and double-well potentials, respectively.

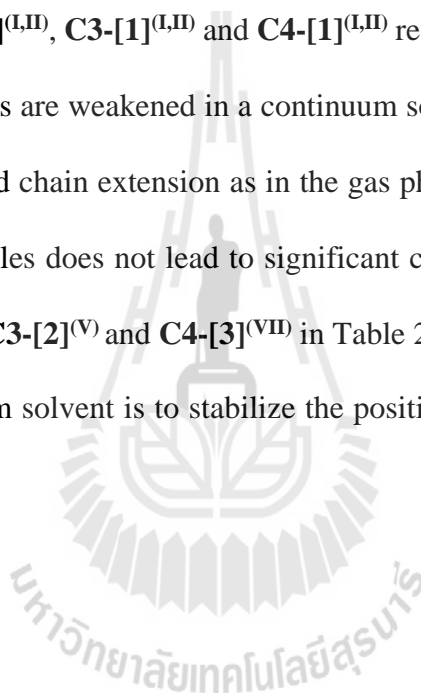


A comparison of the cross-sectional plots in Figure 3.2a and 3.2b reveals the effects of the continuum solvent on the shapes of the 2D-PES, namely the single- and double-well potentials are shifted closer to the Im molecules, suggesting stronger N–H covalent bonds and weaker N–H···O H-bonds in structure **C2-[1]<sup>(I,II)</sup>**. In other words, due to the partial neutralization of positive charges by the continuum solvent, protons are localized nearer to the nitrogen atoms, resulting in a lower probability of finding the shared-proton structure and the oscillatory shuttling motion. These findings confirm that the intermediate complexes of proton dissociation and transfer in the H<sub>3</sub>PO<sub>4</sub> doped Im system are favorably formed in a low local-dielectric environment and that a high local-dielectric environment is required to stabilize the transferred proton before the successive transfer.

### 3.1.3 Mechanisms of proton transfer in the Im H-bond chains

Apart from the excess proton condition and the effects of the local-dielectric environment, to propose the elementary steps of proton transfer in the H<sub>3</sub>PO<sub>4</sub> doped Im system, the effects of fluctuations of the H-bond chain lengths are discussed in detail. In this case,  $\Delta d_{\text{DA}}$  of the embedded structures **G2-[1]<sup>(I,II)</sup>**, **G3-[1]<sup>(I,II)</sup>** and **G4-[2]<sup>(I,II)</sup>** are analyzed and the effects of the H-bond chain extension are shown schematically in Figure 3.3a. Starting from the smallest, most active embedded structure **G2-[1]<sup>(I,II)</sup>**, an extension of the Im H-bond chain at Im (**II**) leads to structure **G3-[1]<sup>(I,II)</sup>**, with a decrease in  $\Delta d_{\text{DA}}$  of H-bond (**1**) from 0.33 to 0.26 Å and an increase in  $\Delta d_{\text{DA}}$  of the H-bond (**2**) from 0.36 to 0.46 Å. These findings suggest that an increase in the Im H-bond chain length at one side of the embedded structure results in a stronger N–H···O H-bond on the other side. Further extension of the Im H-bond chain at Im (**IV**) of structure **G3-[1]<sup>(I,II)</sup>** yields structure **G4-[2]<sup>(I,II)</sup>**, with a decrease in the

$\Delta d_{DA}$  of H-bond (1) from 0.26 to 0.23 Å and an increase in the  $\Delta d_{DA}$  of H-bond (2) from 0.46 to 0.50 Å. Because the two N–H···O H-bonds in the embedded structures are simultaneously stabilized and destabilized by the H-bond chain extension, it is reasonable to anticipate that terminal structures, which are precursors for proton transfer in the Im H-bond chain, can be formed in a low local-dielectric environment. In a high local-dielectric environment, a comparison of the  $\Delta d_{DA}$  of H-bonds (1) and (2) in structures C2-[1]<sup>(I,II)</sup>, C3-[1]<sup>(I,II)</sup> and C4-[1]<sup>(I,II)</sup> reveals different results. Because the protonated H-bonds are weakened in a continuum solvent, the  $\Delta d_{DA}$  values are not sensitive to the H-bond chain extension as in the gas phase. Therefore, the successive addition of Im molecules does not lead to significant changes in the  $\Delta d_{DA}$ . However, structures C2-[2]<sup>(III)</sup>, C3-[2]<sup>(V)</sup> and C4-[3]<sup>(VII)</sup> in Table 2.1 suggest that the outstanding effect of the continuum solvent is to stabilize the positive charge at the end of the Im H-bond chains.



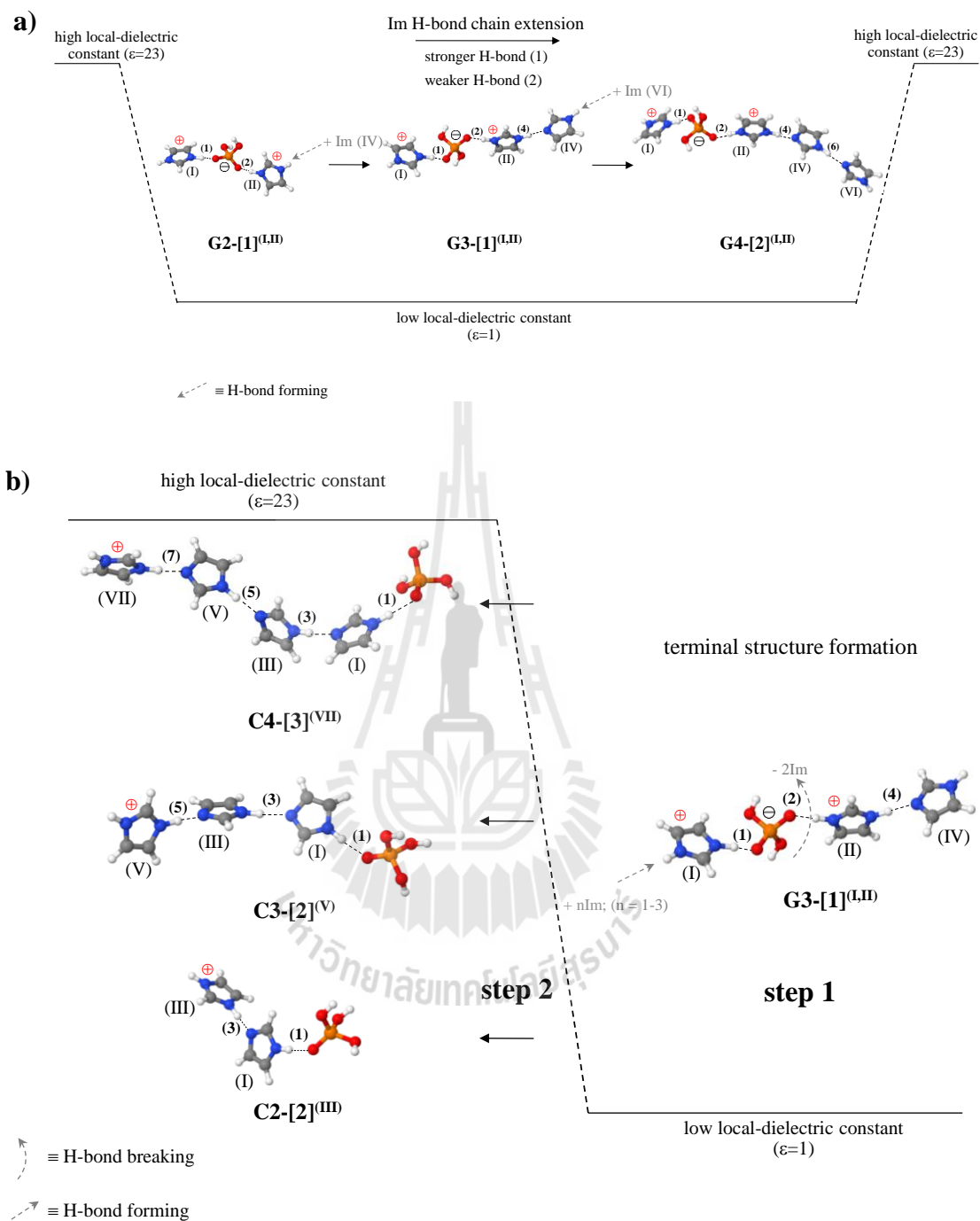


**Figure 3.3** a) The effects of Im H-bond chain extension in low local-dielectric environment. b) Examples of elementary steps of proton transfer in Im H-bond chains. **step 1** = Terminal structure formation. **step 2** = Proton transfer in Im H-bond chains.

Because the intermediate complexes (strong H-bonds with shared-proton structures) are favorably formed in a low local-dielectric environment and a high local-dielectric environment is required to stabilize the positive charge and drive protons in the Im H-bond chain, the fluctuations of the local-dielectric environment must be included as a part of the mechanisms of proton dissociation and transfer. Therefore, based on the analyses of the static results, examples of the elementary steps, which involve the fluctuations of the H-bond chain lengths ( $n = 2$  to 4) and the local-dielectric environment ( $\epsilon = 1$  and 23) are proposed in Figure 3.3b. The elementary steps show the terminal structure formation in step 1 and proton displacement to the end of the Im H-bond chains in step 2.

Similar effects of fluctuations of the H-bond chain lengths and dopant were reported by Sadeghi *et al.* (Sadeghi and Cheng, 1999) in which BOMD simulations revealed that proton transfer in the protonated linear H-bond chains of water molecules ( $n = 6$ ) occurs through a series of semi-collective motions, resulting from the fluctuations of the H-bond chain lengths and reorganization of the water molecules. Additionally, based on the BOMD results on the protonated linear H-bond chains of water molecules ( $n = 5$ ) with an ammonia molecule ( $\text{NH}_3$ ) attached to one end of the chain, it was demonstrated that the doping effect is described by proton transfer throughout the H-bond chain until it reaches the  $\text{NH}_3$  dopant (Sadeghi *et al.*, 1999). Because the dopant in the present system is an acid, proton transfer takes place in the opposite direction, from the proton donor ( $\text{H}_4\text{PO}_4^+$ ) to the end of the Im H-bond chains, as shown in Figure 3.3b.

It should be noted that due to the thermal energy fluctuations and dynamics, as well as the local geometrical requirements, H-bonds in liquids can be

considered as “forming” and “breaking” (Watts and McGee, 1976). For liquid Im in excess proton conditions, MD simulations based on an MS-EVB model suggested continuous forming and breaking of protonated H-bond chains in which the average H-bond cluster size is approximately four ( $\text{H}^+(\text{Im})_4$ ). The proton transfer in the Im H-bond chain is therefore considered to be a local event, characterized by the fluctuations of the H-bond chain lengths between the Eigen-like ( $n = 3$ ) and Zundel-like ( $n = 2$ ) complexes (Li *et al.*, 2012). Because the fluctuations of the Im H-bond chain lengths and the structure reorganization lead to fluctuations of the local polarization that determine the local-dielectric environment, and because the dielectric spectra of imidazolium compounds suggested that the dipolar relaxation times can be quite short (Schmollngruber, Schröde, and Steinhauser, 2014) and could synchronize with the lifetimes of the intermediate complexes in the proton transfer pathways, it is justifiable to include the effects of the local-dielectric environment in the proton dissociation and transfer mechanisms.

#### 3.1.4 Effects of Im H-bond chain structure reorganization

To discuss the effects of Im H-bond chain structure reorganization, the relative energy diagrams and potential energy curves for proton displacement in  $\text{H}^+(\text{H}_3\text{PO}_4)(\text{Im})_4$  are constructed and shown in Figure 3.4a. The relative energy diagram shows that structures **G4-[3]<sup>(I)</sup>**, **G4-[3]<sup>(III)</sup>** and **G4-[3]<sup>(V)</sup>** are close in energy and are accessible through the Im H-bond chain structure reorganization, *e.g.*, through the rotations of the dihedral angles  $\omega_3$  and  $\omega_5$ . It appears that in a low local-dielectric environment ( $\epsilon = 1$ ), the orientations of the Im molecules, especially Im **(III)** and Im **(V)**, determine the relative stabilities and the shapes of the potential energy curves that define the energy barriers for proton displacement; *e.g.*, to convert structure

**G4-[3]<sup>(I)</sup>** to **G4-[3]<sup>(III)</sup>**,  $\omega_5$  decreases from 107 to 93 degrees. The rotation of  $\omega_5$  results in the modification of the shape of the potential energy curve of H-bond (**3**) in such a way that the lowest minimum of the double-well potential shifts from Im (**I**) to Im (**III**). As a consequence, the positive charge (the proton in H-bond (**3**)) displaces from Im (**I**) to Im (**III**). Similarly, to further drive the proton away from the H<sub>3</sub>PO<sub>4</sub> dopant (from Im (**III**) to Im (**V**)), structure **G4-[3]<sup>(III)</sup>** must be changed to structure **G4-[3]<sup>(V)</sup>** by the rotation of  $\omega_3$  from 87 to 101 degrees. It should be recognized that in a low local-dielectric environment, although the rotations of  $\omega_5$  and  $\omega_3$  modify the shapes of the potential energy curves, the energy barriers ( $\Delta E^\ddagger$ ) in the double-well potentials are not high enough to prohibit protons from returning to the original Im molecules, *e.g.*, in H-bond (**5**),  $\Delta E^\ddagger$  is only approximately 3.3 kJ/mol, compared with the thermal energy fluctuation at room temperature of approximately 2.5 kJ/mol. To visualize the roles played by the continuum solvent, the relative energy diagram and potential energy curves for proton displacement in structures **C4-[3]<sup>(I)</sup>**, **C4-[3]<sup>(III)</sup>**, **C4-[3]<sup>(V)</sup>** and **C4-[3]<sup>(VII)</sup>**, which are shown in Figure 3.4b, are discussed. It appears that in general, in a high local-dielectric environment (when COSMO is switched on), the energy barriers are substantially higher than in the gas phase. It is therefore reasonable to conclude that a high local-dielectric environment stabilizes the positive charge and prohibits protons from shuttling back to the original Im molecule.

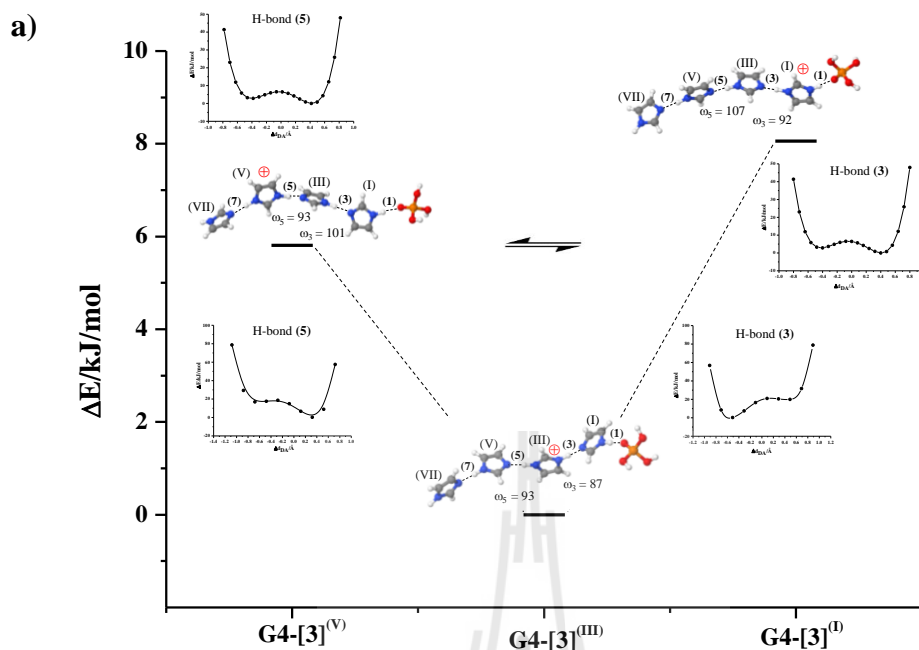


**Figure 3.4** Effects of Im H-bond chain structure reorganization on the energetics of proton transfer. Potential energy curves of proton displacement in H-bonds (3) and (5) are included. a) Proton displacement in  $\text{H}^+(\text{H}_3\text{PO}_4)(\text{Im})_4$  in low local-dielectric environment ( $\epsilon = 1$ ). b) Proton displacement in  $\text{H}^+(\text{H}_3\text{PO}_4)(\text{Im})_4$  in high local-dielectric environment (COSMO,  $\epsilon = 23$ ).

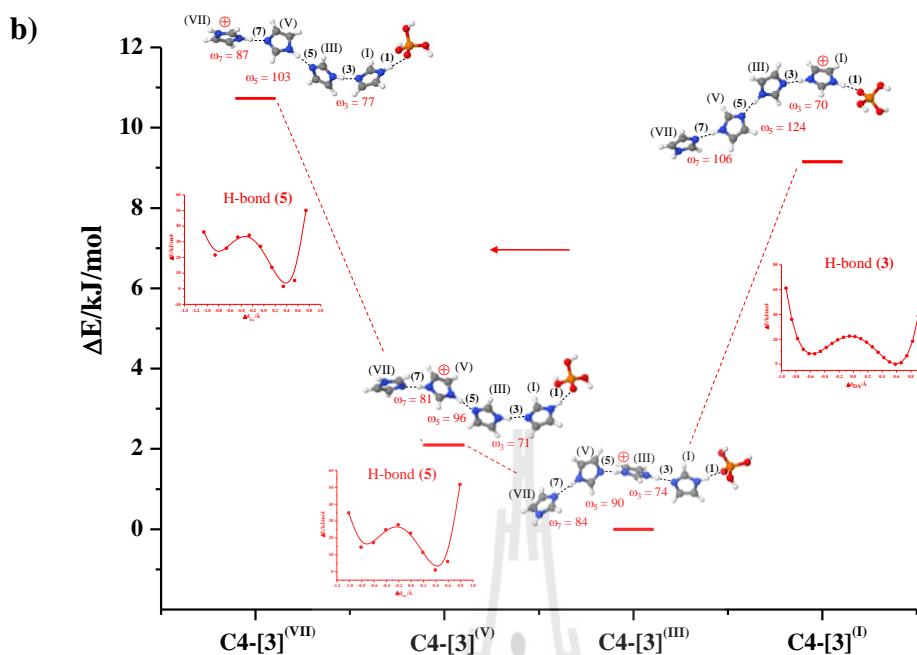


**Figure 3.4** (Continued) Effects of Im H-bond chain structure reorganization on the energetics of proton transfer. Potential energy curves of proton displacement in H-bonds (3) and (5) are included. a) Proton displacement in  $\text{H}^+(\text{H}_3\text{PO}_4)(\text{Im})_4$  in low local-dielectric environment ( $\epsilon = 1$ ). b) Proton displacement in  $\text{H}^+(\text{H}_3\text{PO}_4)(\text{Im})_4$  in high local-dielectric environment (COSMO,  $\epsilon = 23$ ).

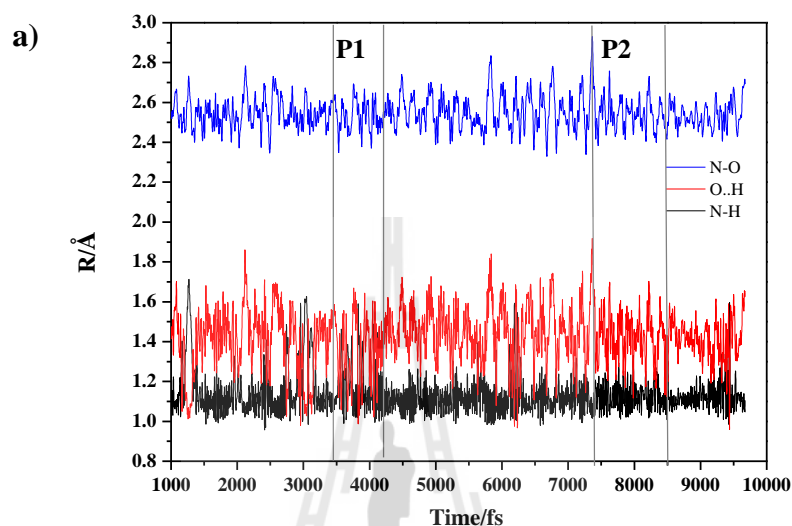
## 3.2 Dynamic results

BOMD simulations on the presolvation models reveal that in the continuum solvent (COSMO,  $\epsilon = 23$ ), a proton spends the majority of the time at the bottom of the double-well potential (a close-contact A–H $\cdots$ B H-bond structure) and there is no intermediate complex with the oscillatory shuttling motion (the shared-proton A $\cdots$ H $\cdots$ B H-bond structure) observed at any temperature. This is in accordance with the static results and confirms that the intermediate complexes are effectively formed in a low local-dielectric environment. Because the quasi-dynamic equilibrium between the oscillatory shuttling and structural diffusion motions has been shown in the previous studies to be a rate-determining process (Chaiwongwattana *et al.*, 2011; Lao-ngam *et al.*, 2011; Phonyiem *et al.*, 2011; Sagarik *et al.*, 2010; Sagarik *et al.*, 2008), the dynamics of proton dissociation and transfer are discussed based only on the BOMD results on the intermediate complexes in a low local-dielectric environment ( $\epsilon = 1$ ).

### 3.2.1 Dynamics of proton dissociation

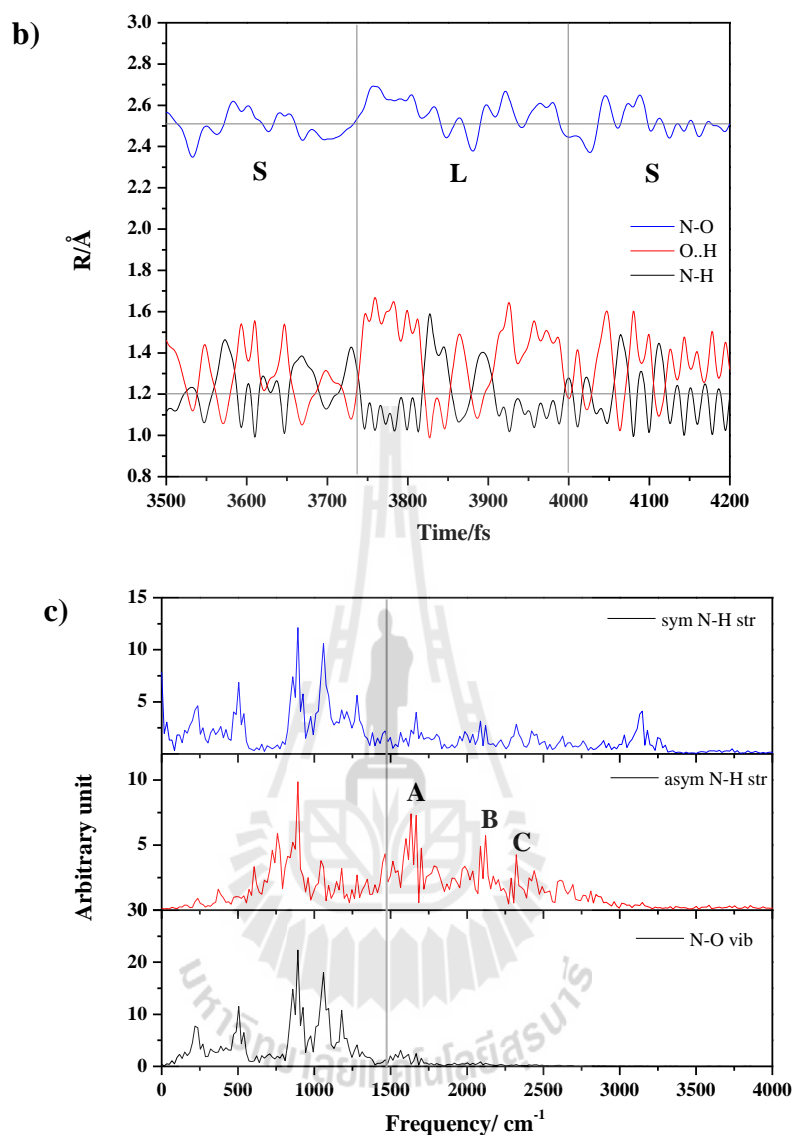
To verify the elementary steps of proton dissociation and transfer suggested by the static calculations, the BOMD results on structures **G2-[1]<sup>(I,II)</sup>**, **G3-[1]<sup>(I,II)</sup>** and **G3-[2]<sup>(III)</sup>** at 353 K are analyzed in detail. Structures **G2-[1]<sup>(I,II)</sup>** and **G3-[2]<sup>(III)</sup>** are, according to  $v^{\text{NH}}$  ( $v^{\text{NH}} < v^{\text{NH}^*}$ ), intermediate complexes for the proton transfer in the embedded and terminal presolvation models, respectively. Because H-bonds **(1)** and **(2)** in structure **G2-[1]<sup>(I,II)</sup>** are equivalent, only the dynamics in H-bond **(1)** are discussed. The proton transfer profile (variations of the  $R_{\text{N-O}}$ ,  $R_{\text{N-H}}$  and  $R_{\text{O-H}}$  distances) in Figure 3.5a is dominated by a close-contact N–H $\cdots$ O H-bond, with an occasional shared-proton N $\cdots$ H $\cdots$ O H-bond, examples of which are shown in panels **P1** and **P2**. Due to

the strong acid-base interaction, a stable  $\text{Im}^+\text{-H}_2\text{PO}_4^-\text{-Im}^+$  structure is formed, evident from the probability of proton transfer from O to N,  $P_{\text{ON}} = 0.87$ , computed from the distribution of the N–H covalent bond distance ( $R_{\text{N-H}}$ ) in Figure 3.6a

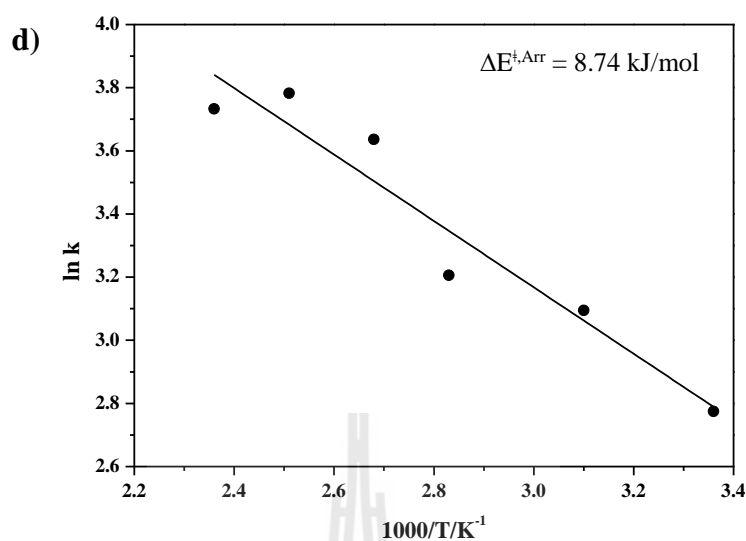


**Figure 3.5** a) - b) Variations of the  $R_{\text{N-O}}$  and  $R_{\text{N-H}}$  distances in H-bond (1) of structure  $\text{G2-}[1]^{(\text{I,II})}$ , obtained from BOMD simulations at 353 K. c) Characteristic vibrational spectra of proton dissociation in H-bond (1) of structure  $\text{G2-}[1]^{(\text{I,II})}$ , obtained from BOMD simulations at 353 K. d) Arrhenius plot of proton dissociation in H-bond (1) of structure  $\text{G2-}[1]^{(\text{I,II})}$ , obtained from BOMD simulations over the temperature range of 298 to 423 K. **S** and **L** = small- and large-amplitude N–O vibrations, respectively.

$\Delta E^{\ddagger, \text{Arr}}$  = Arrhenius activation energy of proton dissociation.



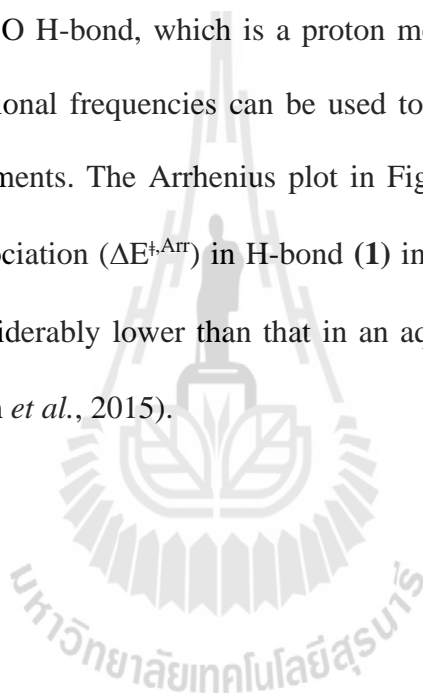
**Figure 3.5** (Continued) a) - b) Variations of the  $R_{\text{N-O}}$  and  $R_{\text{N-H}}$  distances in H-bond (1) of structure  $\text{G2-[1]}^{(\text{L,II})}$ , obtained from BOMD simulations at 353 K. c) Characteristic vibrational spectra of proton dissociation in H-bond (1) of structure  $\text{G2-[1]}^{(\text{L,II})}$ , obtained from BOMD simulations at 353 K. d) Arrhenius plot of proton dissociation in H-bond (1) of structure  $\text{G2-[1]}^{(\text{L,II})}$ , obtained from BOMD simulations over the temperature range of 298 to 423 K. **S** and **L** = small- and large-amplitude N–O vibrations, respectively.  $\Delta E^{\ddagger, \text{Arr}}$  = Arrhenius activation energy of proton dissociation.



**Figure 3.5** (Continued) a) - b) Variations of the  $R_{N-O}$  and  $R_{N-H}$  distances in H-bond (**1**) of structure  $G2-[1]^{(L,II)}$ , obtained from BOMD simulations at 353 K. c) Characteristic vibrational spectra of proton dissociation in H-bond (**1**) of structure  $G2-[1]^{(L,II)}$ , obtained from BOMD simulations at 353 K. d) Arrhenius plot of proton dissociation in H-bond (**1**) of structure  $G2-[1]^{(L,II)}$ , obtained from BOMD simulations over the temperature range of 298 to 423 K. **S** and **L** = small- and large-amplitude N–O vibrations, respectively.  $\Delta E^{\ddagger,Arr}$  = Arrhenius activation energy of proton dissociation.

Investigation of the proton transfer profile in panel **P1** of Figure 3.5b reveals two characteristic N–O vibrations associated with proton dissociation, namely small (**S**) and large (**L**) amplitude vibrations. In our previous study, these two characteristic modes were shown to underlie the oscillatory shuttling and structural diffusion motions of protons in H-bonds, respectively (Sagarik *et al.*, 2008). For structure  $G2-[1]^{(L,II)}$ , the Fourier transformation of VACF of the atoms in panel **P1** (between 3500 and 4200 fs) yields the vibrational spectra in Figure 3.5c in which the N–O vibrational frequency

( $\nu^{\text{NO,MD}}$ ) is outstanding at  $894\text{ cm}^{-1}$ , with strong interferences of torsional oscillations at frequencies below  $500\text{ cm}^{-1}$  and bending motions in the range between  $1000$  and  $1550\text{ cm}^{-1}$  (Buagern *et al.*). According to the static results in Table 2.1, peak **B** at  $2177\text{ cm}^{-1}$  and peak **C** at  $2322\text{ cm}^{-1}$  are characteristic asymmetric N–H stretching frequencies ( $\nu^{\text{NH,MD}}$ ) of protons moving on the dissociation and association paths (see Figure 3.2), respectively, whereas peak **A** at  $1633\text{ cm}^{-1}$  is the vibrational signature of the shared-proton in the  $\text{N}\cdots\text{H}\cdots\text{O}$  H-bond, which is a proton moving in single-well potential. These transient vibrational frequencies can be used to monitor the acid-base proton dissociation in experiments. The Arrhenius plot in Figure 3.5d yields the activation energy of proton dissociation ( $\Delta E^{\ddagger,\text{Arr}}$ ) in H-bond (**1**) in structure **G2-[1]<sup>(I,II)</sup>** to be  $8.7\text{ kJ/mol}$ , which is considerably lower than that in an aqueous solution,  $\Delta E^{\ddagger,\text{Arr}} = 13.1\text{ kJ/mol}$  (Suwannakham *et al.*, 2015).



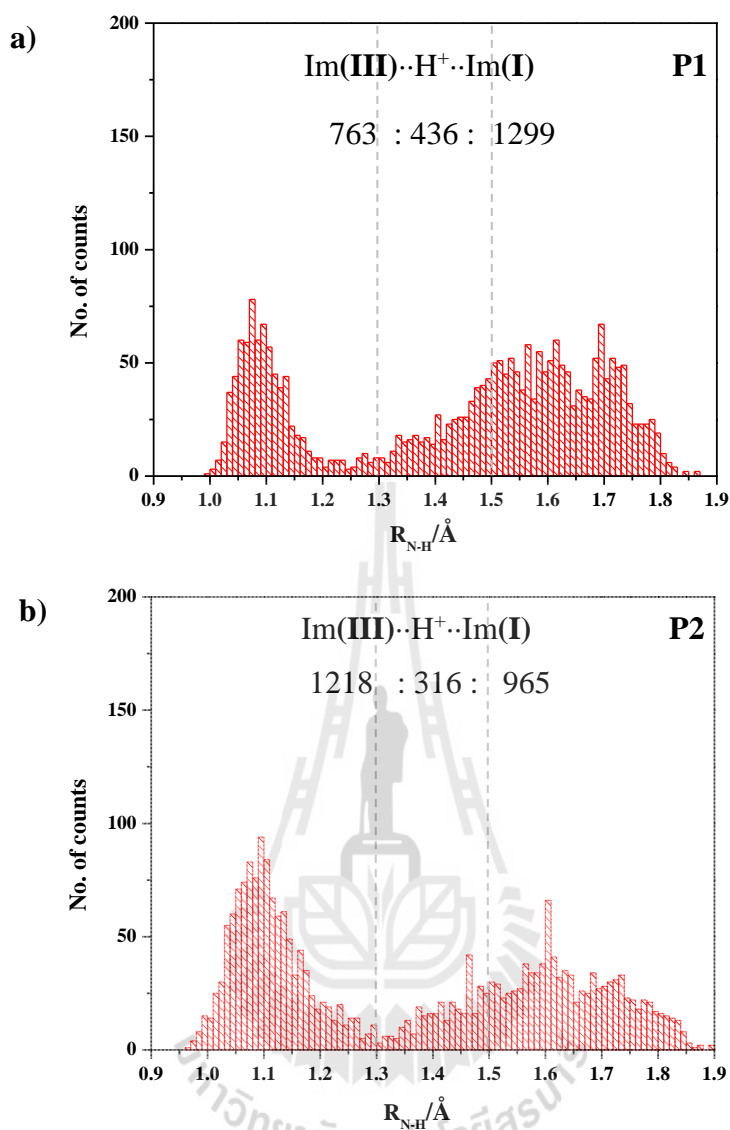


**Figure 3.6** Distributions of the N–H covalent bond distances ( $R_{\text{N-H}}$ ) in H-bonds of the intermediate complexes, obtained from BOMD simulations. a) Distribution of  $R_{\text{N-H}}$  in H-bond (1) of structure **G2-[1]<sup>(I,II)</sup>** at 353 K. b) - c) Distributions of  $R_{\text{N-H}}$  in H-bonds (1) and (2) of structure **G3-[1]<sup>(I,II)</sup>** at 353 K, respectively. d) Distribution of  $R_{\text{N-H}}$  in H-bond (3) of structure **G3-[2]<sup>(III)</sup>** at 298 K.

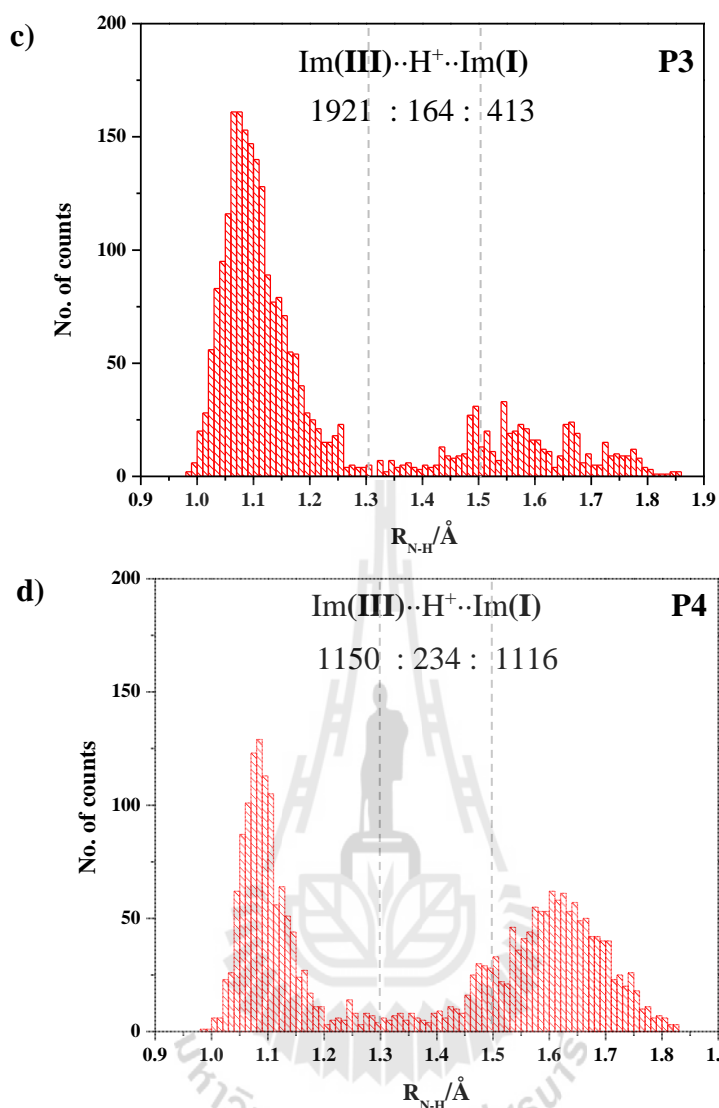


**Figure 3.6** (Continued) Distributions of the N-H covalent bond distances ( $R_{N-H}$ ) in H-bonds of the intermediate complexes, obtained from BOMD simulations. a) Distribution of  $R_{N-H}$  in H-bond (1) of structure **G2-[1]<sup>(I,II)</sup>** at 353 K. b) - c) Distributions of  $R_{N-H}$  in H-bonds (1) and (2) of structure **G3-[1]<sup>(I,II)</sup>** at 353 K, respectively. d) Distribution of  $R_{N-H}$  in H-bond (3) of structure **G3-[2]<sup>(III)</sup>** at 298 K.

To confirm the effects of the Im H-bond chain extension suggested by the static results, the proton transfer profiles, distributions of the N–H covalent bond distances ( $R_{N-H}$ ) and vibrational spectra of protons in H-bonds (1) and (2) of structures **G2-[1]<sup>(I,II)</sup>** and **G3-[1]<sup>(I,II)</sup>** are discussed. Extension of the Im H-bond chain at Im (II) of structure **G2-[1]<sup>(I,II)</sup>** leads to structure **G3-[1]<sup>(I,II)</sup>**. The analyses of the proton transfer profiles in Figures 3.5a, 3.7a and 3.7e and the distributions of  $R_{N-H}$  in Figure 3.6 confirm that H-bond (1) is stabilized and H-bond (2) is destabilized upon the Im H-bond chain extension. The former is evident from a significant increase in the probability of finding the shared-proton structure ( $R_{N-H}$  between 1.3 and 1.5 Å) in H-bond (1), from  $P_{N...H...O} = 0.10$  in structure **G2-[1]<sup>(I,II)</sup>** to 0.22 in structure **G3-[1]<sup>(I,II)</sup>** (see Figures 3.6a and 3.6b), whereas in H-bond (2),  $P_{N...H...O}$  decreases from 0.10 to 0.01 (see Figures 3.6a and 3.6c, where H-bond (1) and H-bond (2) in structure **G2-[1]<sup>(I,II)</sup>** are equivalent). Because the shared-proton structure of H-bond (1) is more stable, the activation energy ( $\Delta E^{+A_{PT}}$ ) for proton dissociation in structure **G3-[1]<sup>(I,II)</sup>** is higher; the Arrhenius plot in Figure 3.7d yields  $\Delta E^{+A_{PT}} = 10.8$  kJ/mol, compared with 8.7 kJ/mol in structure **G2-[1]<sup>(I,II)</sup>**. The stabilization effect of H-bond (1) in structure **G3-[1]<sup>(I,II)</sup>** is also indicated by the red-shifts of  $\nu^{NH,MD}$  of peaks **A**, **B** and **C** in Figure 3.7c compared with those of structure **G2-[1]<sup>(I,II)</sup>** in Figure 3.5c. The destabilization effect of H-bond (2) is manifested by the very rare proton exchange event observed in Figure 3.7e and the disappearance of the three characteristic peaks in Figure 3.7g. Additionally, in Figure 3.7c, as the relative intensity of peak **A** is higher than peaks **B** and **C**, the extension of the Im H-bond chain is confirmed to increase the probability of finding the oscillatory shuttling motion, leading to a longer lifetime of the rate-

determining process in H-bond (1) and a higher  $\Delta E^{\ddagger, \text{Arr}}$  in structure **G3-[1]<sup>(I,II)</sup>** compared with structure **G2-[1]<sup>(I,II)</sup>**.

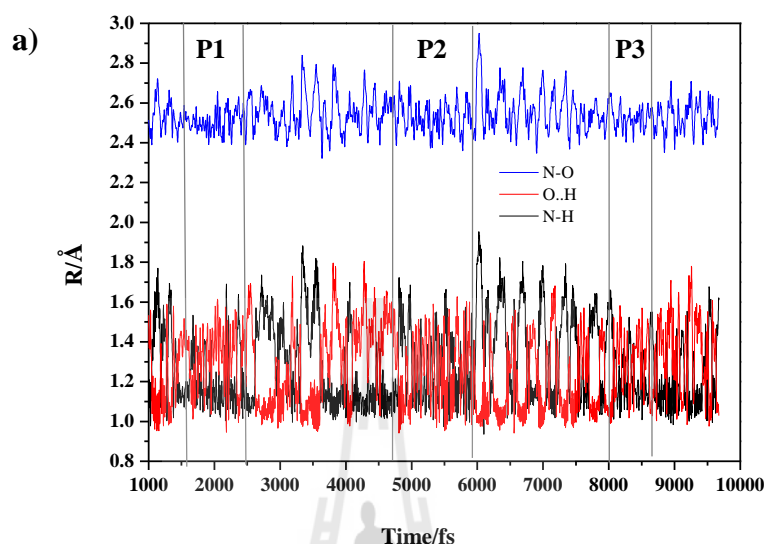


**Figure 3.7** a) - b) Variations of the  $R_{\text{N-O}}$  and  $R_{\text{N-H}}$  distances in H-bond (1) of structure **G3-[1]<sup>(I,II)</sup>**, obtained from BOMD simulations at 353 K. c) Characteristic vibrational spectra of proton dissociation in H-bond (1) of structure **G3-[1]<sup>(I,II)</sup>**, obtained from BOMD simulations at 353 K. d) Arrhenius plot of proton dissociation in H-bond (1) of structure **G3-[1]<sup>(I,II)</sup>**, obtained from BOMD simulations over the temperature range of 298 to 423 K. e) - f) Variations of the  $R_{\text{N-O}}$  and  $R_{\text{N-H}}$  distances in H-bond (2) of structure **G3-[1]<sup>(I,II)</sup>**, obtained from BOMD simulations at 353 K. g) Characteristic vibrational spectra of H-bond (2) of structure **G3-[1]<sup>(I,II)</sup>**, obtained from BOMD simulations at 353 K. **S** and **L** = small- and large-amplitude N–O vibrations, respectively.  $\Delta E^{\ddagger, \text{Arr}}$  = Arrhenius activation energy of proton dissociation.

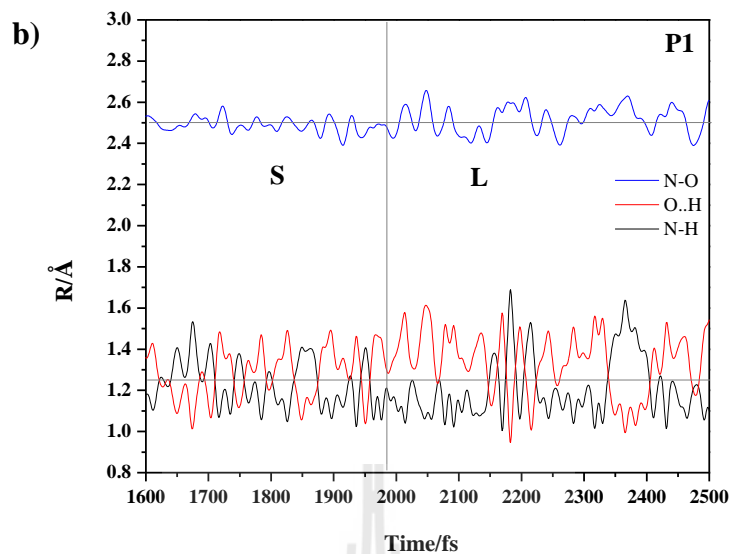


**Figure 3.7** (Continued) a) - b) Variations of the  $R_{N-O}$  and  $R_{N-H}$  distances in H-bond (1) of structure  $G3-[1]^{(L,II)}$ , obtained from BOMD simulations at 353 K. c) Characteristic vibrational spectra of proton dissociation in H-bond (1) of structure  $G3-[1]^{(L,II)}$ , obtained from BOMD simulations at 353 K. d) Arrhenius plot of proton dissociation in H-bond (1) of structure  $G3-[1]^{(L,II)}$ , obtained from BOMD simulations over the temperature range of 298 to 423 K. e) - f) Variations of the  $R_{N-O}$  and  $R_{N-H}$  distances in H-bond (2) of structure  $G3-[1]^{(L,II)}$ , obtained from BOMD simulations at 353 K. g) Characteristic vibrational spectra of H-bond (2) of structure  $G3-[1]^{(L,II)}$ , obtained from BOMD simulations at 353 K. **S** and **L** = small- and large-amplitude N–O vibrations, respectively.  $\Delta E^{\ddagger, Arr}$  = Arrhenius activation energy of proton dissociation.

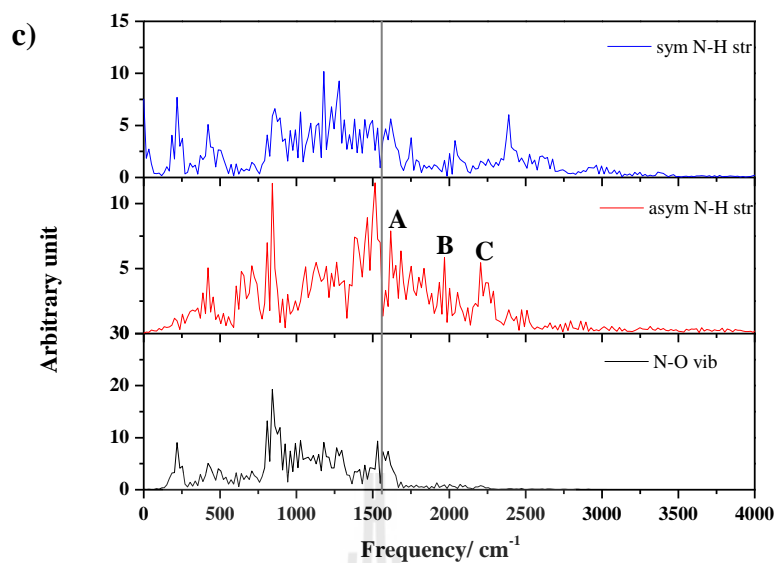


**Figure 3.7** (Continued) a) - b) Variations of the  $R_{N-O}$  and  $R_{N-H}$  distances in H-bond (1) of structure  $G3-[1]^{(L,II)}$ , obtained from BOMD simulations at 353 K. c) Characteristic vibrational spectra of proton dissociation in H-bond (1) of structure  $G3-[1]^{(L,II)}$ , obtained from BOMD simulations at 353 K. d) Arrhenius plot of proton dissociation in H-bond (1) of structure  $G3-[1]^{(L,II)}$ , obtained from BOMD simulations over the temperature range of 298 to 423 K. e) - f) Variations of the  $R_{N-O}$  and  $R_{N-H}$  distances in H-bond (2) of structure  $G3-[1]^{(L,II)}$ , obtained from BOMD simulations at 353 K. g) Characteristic vibrational spectra of H-bond (2) of structure  $G3-[1]^{(L,II)}$ , obtained from BOMD simulations at 353 K. **S** and **L** = small- and large-amplitude N–O vibrations, respectively.  $\Delta E^{\ddagger, Arr}$  = Arrhenius activation energy of proton dissociation.

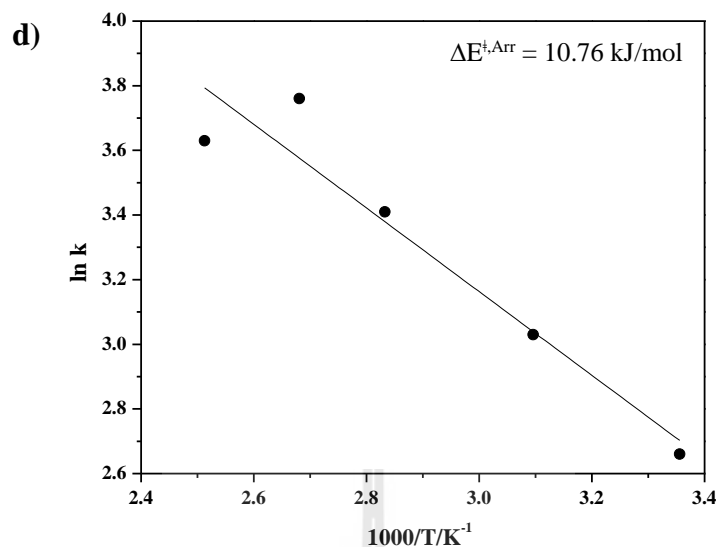


**Figure 3.7** (Continued) a) - b) Variations of the  $R_{N-O}$  and  $R_{N-H}$  distances in H-bond (1) of structure  $G3-[1]^{(L,II)}$ , obtained from BOMD simulations at 353 K. c) Characteristic vibrational spectra of proton dissociation in H-bond (1) of structure  $G3-[1]^{(L,II)}$ , obtained from BOMD simulations at 353 K. d) Arrhenius plot of proton dissociation in H-bond (1) of structure  $G3-[1]^{(L,II)}$ , obtained from BOMD simulations over the temperature range of 298 to 423 K. e) - f) Variations of the  $R_{N-O}$  and  $R_{N-H}$  distances in H-bond (2) of structure  $G3-[1]^{(L,II)}$ , obtained from BOMD simulations at 353 K. g) Characteristic vibrational spectra of H-bond (2) of structure  $G3-[1]^{(L,II)}$ , obtained from BOMD simulations at 353 K. **S** and **L** = small- and large-amplitude N–O vibrations, respectively.  $\Delta E^{\ddagger, \text{Arr}}$  = Arrhenius activation energy of proton dissociation.

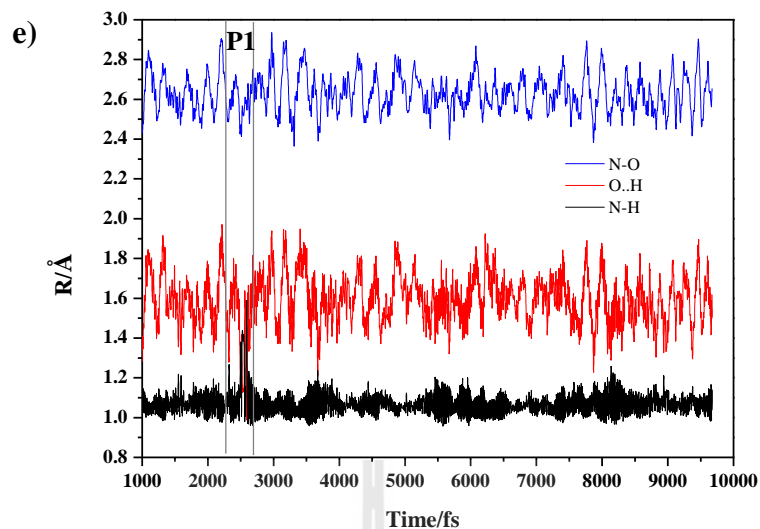


**Figure 3.7** (Continued) a) - b) Variations of the  $R_{N-O}$  and  $R_{N-H}$  distances in H-bond (1) of structure  $G3-[1]^{(L,II)}$ , obtained from BOMD simulations at 353 K. c) Characteristic vibrational spectra of proton dissociation in H-bond (1) of structure  $G3-[1]^{(L,II)}$ , obtained from BOMD simulations at 353 K. d) Arrhenius plot of proton dissociation in H-bond (1) of structure  $G3-[1]^{(L,II)}$ , obtained from BOMD simulations over the temperature range of 298 to 423 K. e) - f) Variations of the  $R_{N-O}$  and  $R_{N-H}$  distances in H-bond (2) of structure  $G3-[1]^{(L,II)}$ , obtained from BOMD simulations at 353 K. g) Characteristic vibrational spectra of H-bond (2) of structure  $G3-[1]^{(L,II)}$ , obtained from BOMD simulations at 353 K. **S** and **L** = small- and large-amplitude N–O vibrations, respectively.  $\Delta E^{\ddagger, Arr}$  = Arrhenius activation energy of proton dissociation.

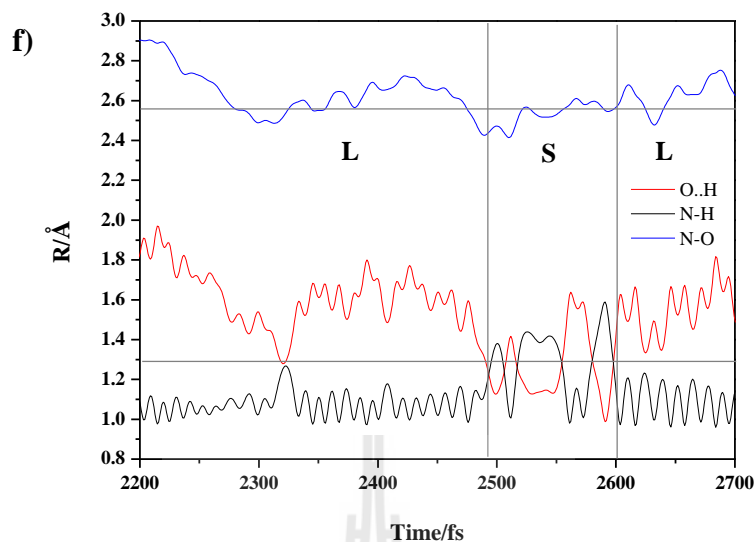


**Figure 3.7** (Continued) a) - b) Variations of the  $R_{N-O}$  and  $R_{N-H}$  distances in H-bond (1) of structure  $G3-[1]^{(L,II)}$ , obtained from BOMD simulations at 353 K. c) Characteristic vibrational spectra of proton dissociation in H-bond (1) of structure  $G3-[1]^{(L,II)}$ , obtained from BOMD simulations at 353 K. d) Arrhenius plot of proton dissociation in H-bond (1) of structure  $G3-[1]^{(L,II)}$ , obtained from BOMD simulations over the temperature range of 298 to 423 K. e) - f) Variations of the  $R_{N-O}$  and  $R_{N-H}$  distances in H-bond (2) of structure  $G3-[1]^{(L,II)}$ , obtained from BOMD simulations at 353 K. g) Characteristic vibrational spectra of H-bond (2) of structure  $G3-[1]^{(L,II)}$ , obtained from BOMD simulations at 353 K. **S** and **L** = small- and large-amplitude N–O vibrations, respectively.  $\Delta E^{\ddagger, Arr}$  = Arrhenius activation energy of proton dissociation.

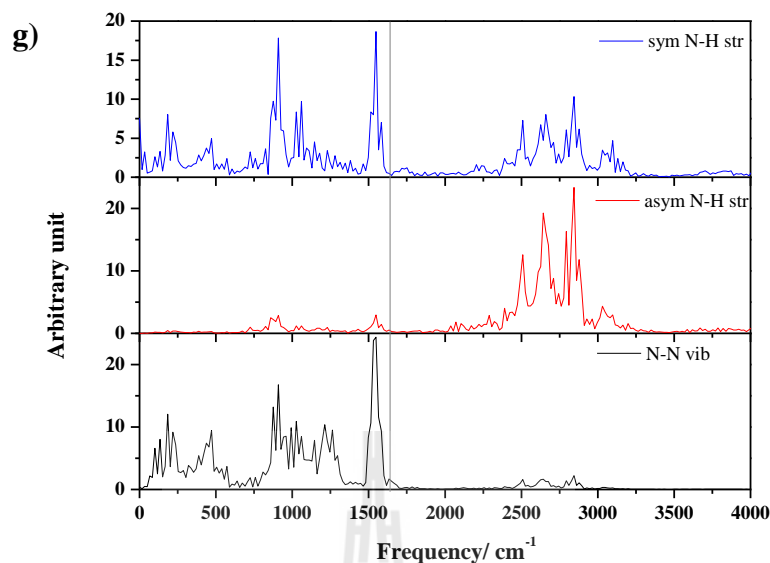


**Figure 3.7** (Continued) a) - b) Variations of the  $R_{N-O}$  and  $R_{N-H}$  distances in H-bond (1) of structure  $\mathbf{G3-[1]^{(I,II)}}$ , obtained from BOMD simulations at 353 K. c) Characteristic vibrational spectra of proton dissociation in H-bond (1) of structure  $\mathbf{G3-[1]^{(I,II)}}$ , obtained from BOMD simulations at 353 K. d) Arrhenius plot of proton dissociation in H-bond (1) of structure  $\mathbf{G3-[1]^{(I,II)}}$ , obtained from BOMD simulations over the temperature range of 298 to 423 K. e) - f) Variations of the  $R_{N-O}$  and  $R_{N-H}$  distances in H-bond (2) of structure  $\mathbf{G3-[1]^{(I,II)}}$ , obtained from BOMD simulations at 353 K. g) Characteristic vibrational spectra of H-bond (2) of structure  $\mathbf{G3-[1]^{(I,II)}}$ , obtained from BOMD simulations at 353 K. **S** and **L** = small- and large-amplitude N–O vibrations, respectively.  $\Delta E^{\text{Arr}}$  = Arrhenius activation energy of proton dissociation.

### 3.2.2 The effects of doping on the dynamics of proton transfer

The effects of doping are verified by comparing the proton transfer profiles and vibrational spectra of a proton in H-bond (3) of structure  $\mathbf{G3-[2]^{(III)}}$  with those in  $\text{H}^+(\text{Im})_4$  (Buagern *et al.*). The proton transfer profile in panel **P1** of Figures

3.8a and 3.8b is dominated by a large-amplitude N–N vibration in which  $R_{N-N}$  varies over a very wide range, between 2.4 and 2.9 Å. It is shown in panel **P1** that the proton exchange in H-bond (**3**) takes place almost exclusively through the structural diffusion mechanism, without the oscillatory shuttling motion as the rate-determining process (Sagarik *et al.*, 2008). In contrast, in the undoped Im H-bond system ( $H^+(Im)_4$ ), the proton transfer profile in Figure 3.9a is characterized by both large- and small-amplitude N–N vibrations, labeled **L** and **S**, respectively, in panel **P1** of Figure 3.9b. Due to the interference between various modes of vibrations, especially below 2500  $cm^{-1}$ , the oscillatory shuttling and structural diffusion frequencies of a proton in H-bond (**3**) cannot be precisely determined from the vibrational spectra in Figure 3.8c. However, based on the static results in Table 2.1, the two vibrational frequencies associated with the proton exchange in H-bond (**3**) can be estimated: peaks **B** and **C** at 1901 and 2345  $cm^{-1}$ , respectively. For  $H^+(Im)_4$  (Buagern *et al.*), the oscillatory shuttling and structural diffusion frequencies can be easily assigned from the vibrational spectra in Figure 3.9c, for peaks **A**, **B** and **C** at 1195  $cm^{-1}$ , 2205 and 2508  $cm^{-1}$ , respectively. The red shifts of peaks **B** and **C** in structure **G3-[2]<sup>(III)</sup>**, compared with those in  $H^+(Im)_4$ , confirm that  $H_3PO_4$  helps promote the structural diffusion process by strengthening the Im H-bond chain and enhancing the large-amplitude N–N vibration in the  $H_3PO_4$  doped Im H-bond system. This results in a lower activation energy ( $\Delta E^{\ddagger, Arr}$ ) and a higher rate of proton transfer in H-bond (**3**) of the doped system; the Arrhenius plot in Figure 3.8d yields  $\Delta E^{\ddagger, Arr}$  of 1.22 kJ/mol, compared with  $\Delta E^{\ddagger, Arr} = 3.28$  kJ/mol in  $H^+(Im)_4$  (see Figure 3.9d) (Buagern *et al.*).

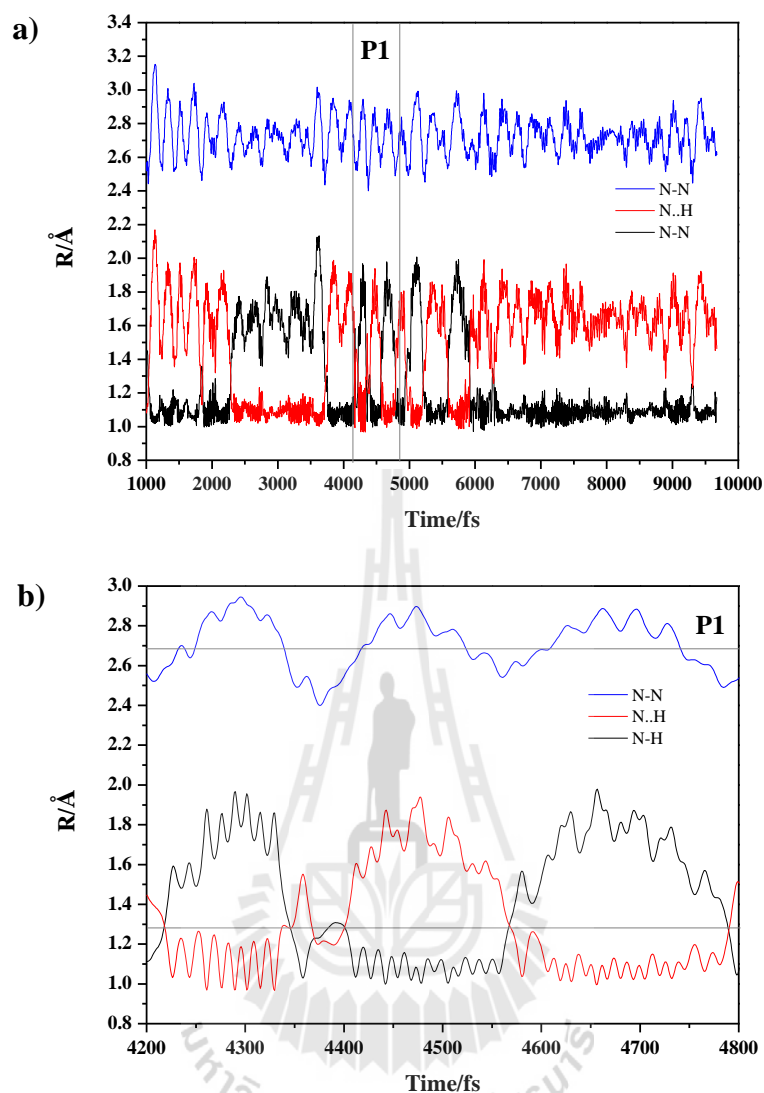


**Figure 3.8** a) - b) Variations of the  $R_{N-N}$  and  $R_{N-H}$  distances in H-bond (3) of structure  $G3-[2]^{(III)}$ , obtained from BOMD simulations at 353 K. c) Characteristic vibrational spectra of proton transfer in H-bond (3) of structure  $G3-[2]^{(III)}$ , obtained from BOMD simulations at 353 K. d) Arrhenius plot of proton transfer in H-bond (3) of structure  $G3-[2]^{(III)}$ , obtained from BOMD simulations over the temperature range of 298 to 423 K.  $\Delta E^{\ddagger, \text{Arr}}$  = Arrhenius activation energy of proton transfer.

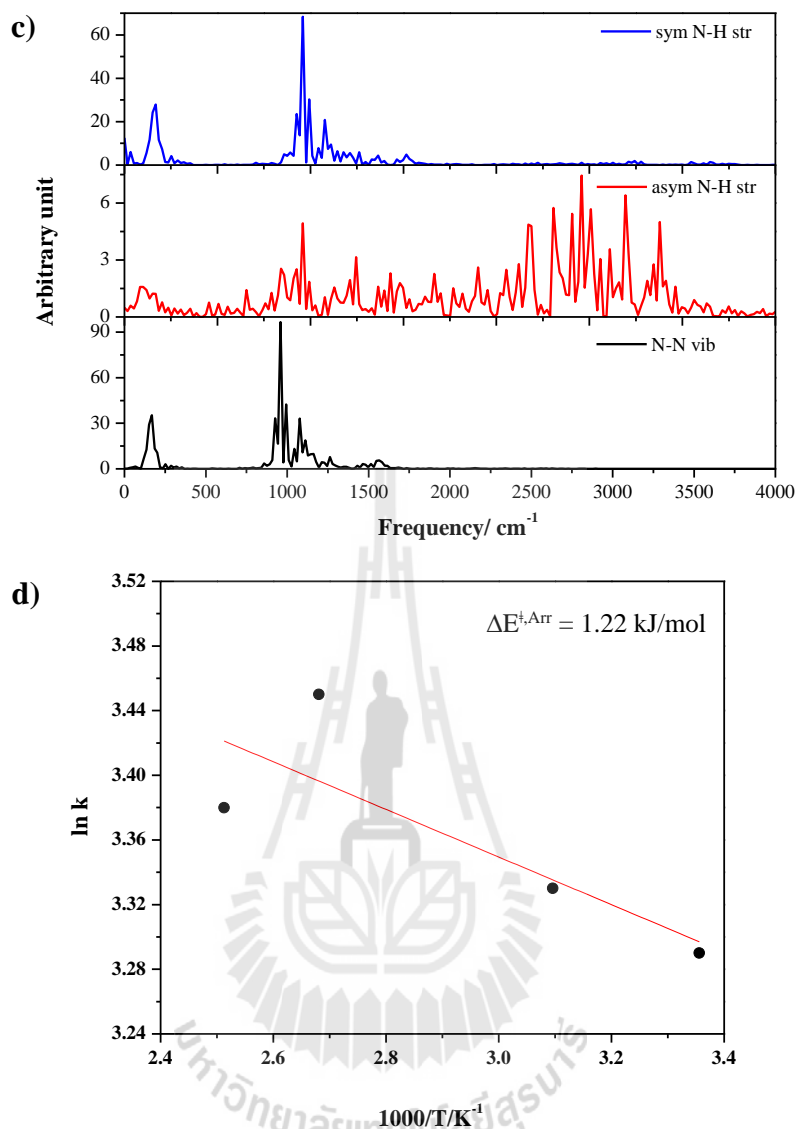


**Figure 3.8** (Continued) a) - b) Variations of the  $R_{N-N}$  and  $R_{N-H}$  distances in H-bond (3) of structure **G3-[2]<sup>(III)</sup>**, obtained from BOMD simulations at 353 K. c) Characteristic vibrational spectra of proton transfer in H-bond (3) of structure **G3-[2]<sup>(III)</sup>**, obtained from BOMD simulations at 353 K. d) Arrhenius plot of proton transfer in H-bond (3) of structure **G3-[2]<sup>(III)</sup>**, obtained from BOMD simulations over the temperature range of 298 to 423 K.  $\Delta E^{\ddagger, Arr}$  = Arrhenius activation energy of proton transfer.

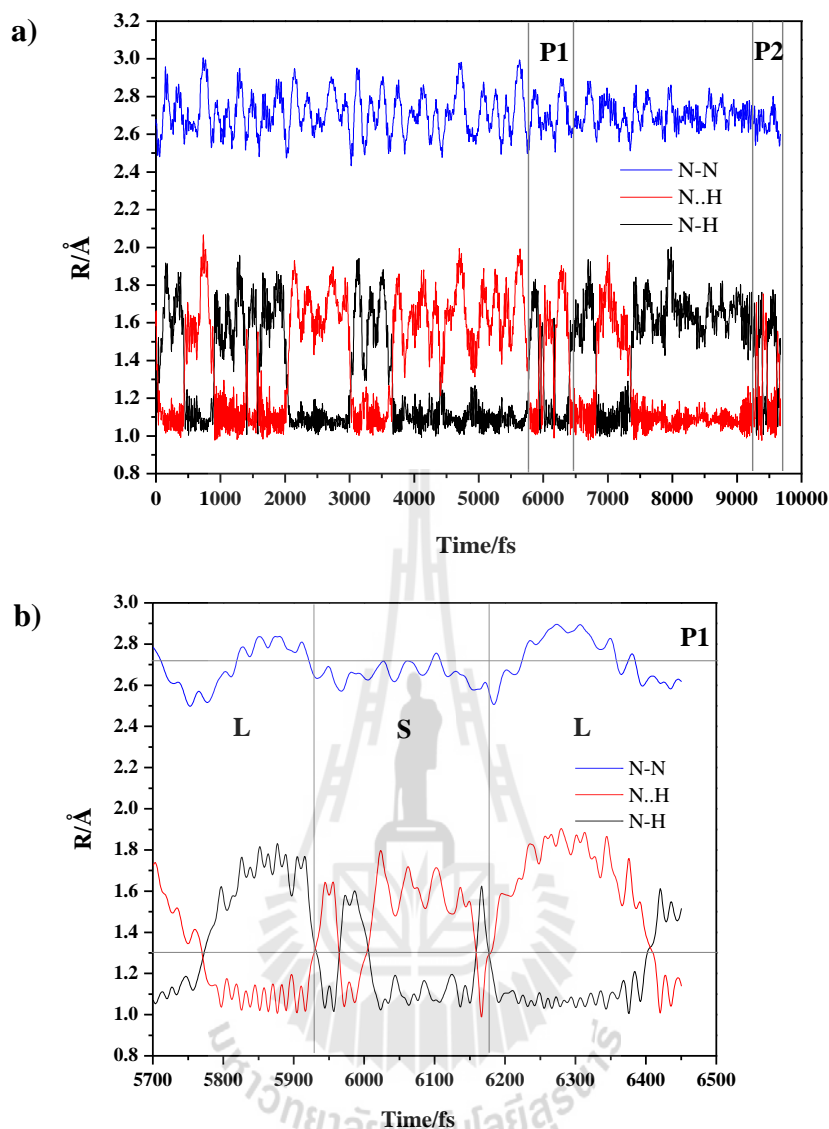


**Figure 3.9** a) - b) Variations of the  $R_{N-N}$  and  $R_{N-H}$  distances in H-bond of  $H^+(Im)_4$ , obtained from BOMD simulations at 350 K. c) Characteristic vibrational spectra of proton transfer in H-bond of  $H^+(Im)_4$ , obtained from BOMD simulations at 350 K. d) Arrhenius plot of proton transfer in H-bond of  $H^+(Im)_4$ , obtained from BOMD simulations over the temperature range of 298 to 423 K. e) Distribution of  $R_{N-H}$  in H-bond of  $H^+(Im)_4$ , obtained from BOMD simulations at 350 K.  $\Delta E^{\ddagger, Arr}$  = Arrhenius activation energy of proton transfer (Buagern *et al.*).

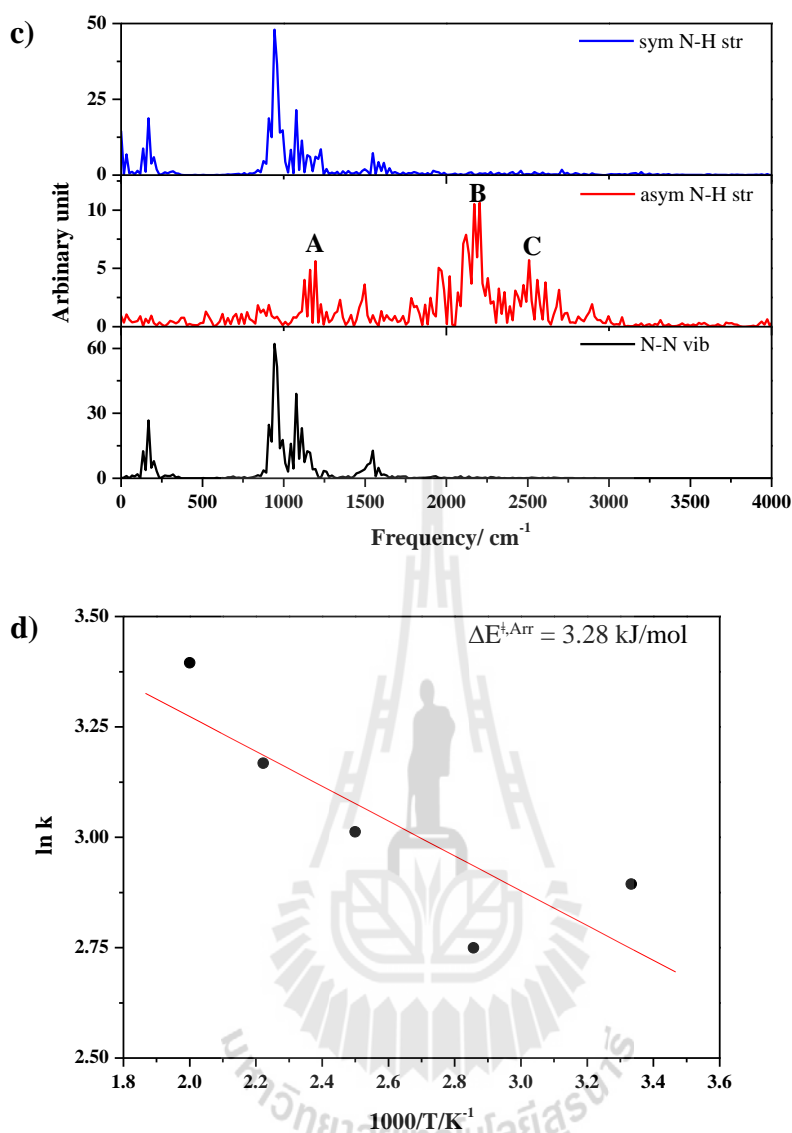


**Figure 3.9** (Continued) a) - b) Variations of the  $R_{\text{N-N}}$  and  $R_{\text{N-H}}$  distances in H-bond of  $\text{H}^+(\text{Im})_4$ , obtained from BOMD simulations at 350 K. c) Characteristic vibrational spectra of proton transfer in H-bond of  $\text{H}^+(\text{Im})_4$ , obtained from BOMD simulations at 350 K. d) Arrhenius plot of proton transfer in H-bond of  $\text{H}^+(\text{Im})_4$ , obtained from BOMD simulations over the temperature range of 298 to 423 K. e) Distribution of  $R_{\text{N-H}}$  in H-bond of  $\text{H}^+(\text{Im})_4$ , obtained from BOMD simulations at 350 K.  $\Delta E^{\ddagger, \text{Arr}}$  = Arrhenius activation energy of proton transfer (Buagern *et al.*).

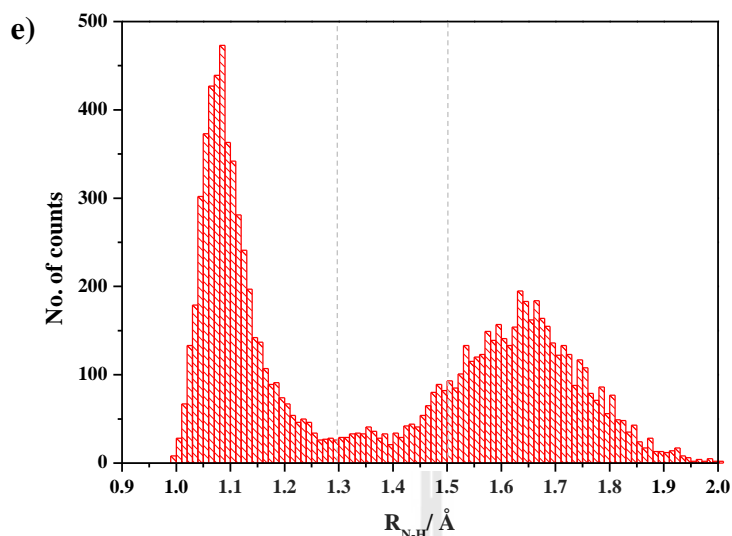


**Figure 3.9** (Continued) a) - b) Variations of the  $R_{N-N}$  and  $R_{N-H}$  distances in H-bond of  $H^+(Im)_4$ , obtained from BOMD simulations at 350 K. c) Characteristic vibrational spectra of proton transfer in H-bond of  $H^+(Im)_4$ , obtained from BOMD simulations at 350 K. d) Arrhenius plot of proton transfer in H-bond of  $H^+(Im)_4$ , obtained from BOMD simulations over the temperature range of 298 to 423 K. e) Distribution of  $R_{N-H}$  in H-bond of  $H^+(Im)_4$ , obtained from BOMD simulations at 350 K.  $\Delta E^{\ddagger, Arr}$  = Arrhenius activation energy of proton transfer (Buagern *et al.*).

It should be noted that  $\Delta E^{\ddagger, Arr}$  is computed during the proton exchange process, *e.g.*, in panel **P1** of Figures 3.8a and 3.8b, which involves the quasi-dynamic equilibrium between the oscillatory shuttling and structural diffusion motions. Therefore,  $\Delta E^{\ddagger, Arr}$  might not be directly measurable in an experiment in which different experimental techniques generally yield different activation energies and where other effects could play important roles. As the proton transfer profile in Figure 3.8a shows both the shared-proton and close-contact structures, the actual proton transfer is expected to take place not very often and a frequency factor must be included in the

model calculations to obtain a more accurate first-order rate constant for the proton displacement in the Im H-bond chain. It should be added that although our presolvation models do not take into account a continuous H-bond network, because proton transfer in the Im H-bond system can be considered a local process with a short spatial, temporal correlation (Li *et al.*, 2012), it is reasonable to investigate only the rate-determining process (the dynamic behavior of the intermediate complex), which, in this case, is the quasi-dynamic equilibrium between the oscillatory shuttling and structural diffusion motions (the close-contact N–H···O and shared-proton N···H···O H-bonds).

### 3.2.3 Dynamics of the Im H-bond chain structure reorganization

Because the static results suggest that the shapes of the potential energy curves for proton displacement are sensitive to the Im H-bond chain structure reorganization (see Figure 3.4), the effects of a conformation change on the dynamics of proton transfer are discussed using the proton transfer profiles of structure **G3-[2]<sup>(III)</sup>**, which were obtained from the BOMD simulations at 298 K. Variations of  $R_{N-N}$  and  $R_{N-H}$  in H-bonds **(3)** and **(5)**, as well as the time evolutions of  $\omega_3$  and  $\omega_5$ , as shown in Figure 3.10, confirm that the Im H-bond chain structure reorganization does affect the dynamics of proton transfer. Investigation of the time evolutions of the torsional angles suggests division of the proton transfer profiles into four panels of 2500 fs each (**P1** to **P4**).

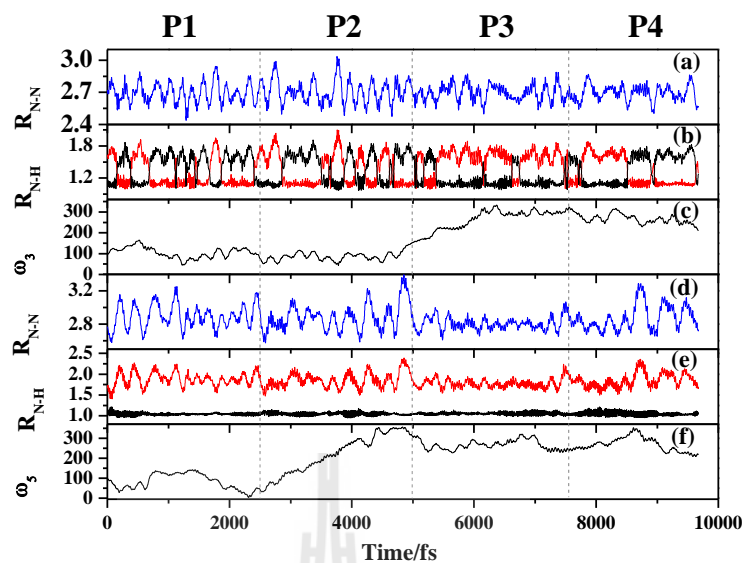


**Figure 3.10** Proton transfer profiles of H-bonds (3) and (5), and time evolutions of  $\omega_3$  and  $\omega_5$  in the terminal structure  $\text{G3-[2]}^{(\text{III})}$ , obtained from BOMD simulations at 298 K. (a) - (c) = H-bond (3); (d) - (f) = H-bond (5).

To visualize the effects of the conformation change on the proton displacement in H-bond (3), a reference vector ( $v^{\text{ref}}$ ) coinciding with the  $C_2$  axis of  $\text{ImH}^+$  is defined, and projections of  $v^{\text{ref}}$ , similar to the Newman projection, are used to monitor the dynamically changing Im H-bond structures. They are shown in Figure 3.11. In this case, the line of sight is defined lengthwise down the Im H-bond chain from the  $\text{H}_3\text{PO}_4$  dopant. Based on the assumption that the probability of finding a proton moving in a specific direction is correlated with the probability of the N–H covalent bond formation, the distributions of  $R_{\text{N-H}}$  in H-bond (3) of Im (III) in panel P1 to P4 are constructed and shown in Figure 3.12.

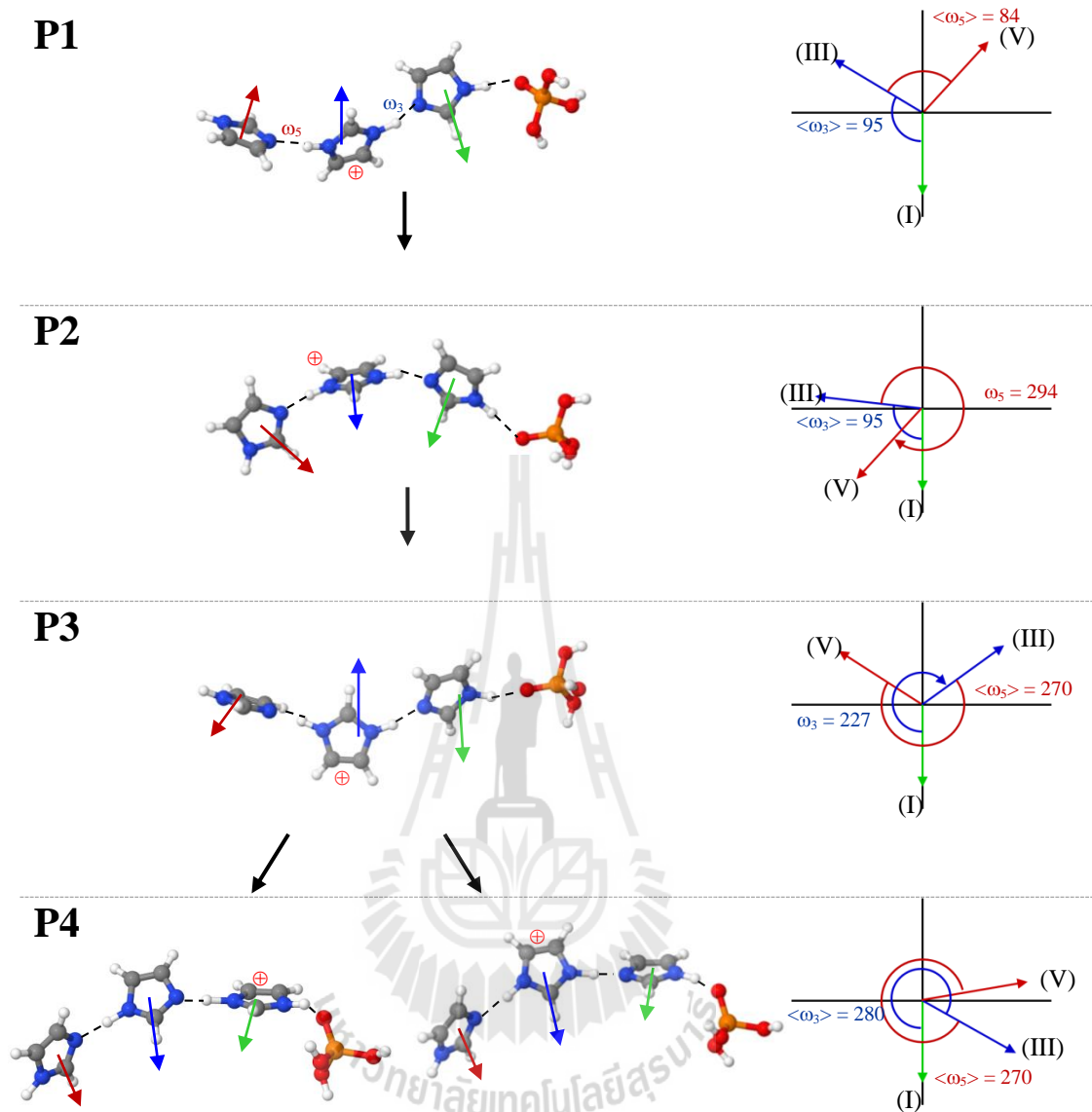


**Figure 3.11** Conformations of structure  $G3-[2]^{(III)}$  sampled from panel **P1** to **P4** and projections of the reference vectors ( $v^{ref}$ ), obtained from the analyses of the time evolutions of  $\omega_3$  and  $\omega_5$  in Figure 3.10. Angles in degree;  $(III) = v^{ref}$  of  $Im(III)$ ;  $(V) = v^{ref}$  of  $Im(V)$ .

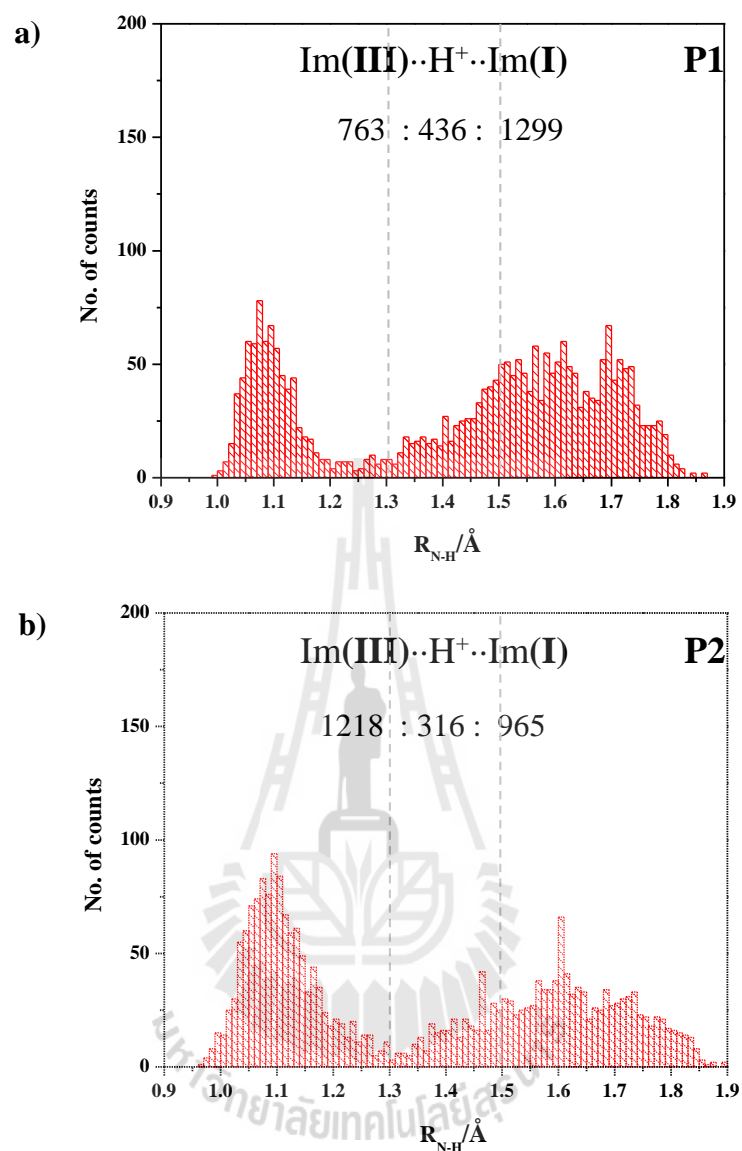


**Figure 3.12** Distributions of the N–H covalent bond distances ( $R_{N-H}$ ) in H-bond (3) of structure  $\text{G3-[2]}^{(\text{III})}$ , obtained from BOMD simulations at 298 K. a) - d) Distributions in panel **P1** to **P4** in Figure 3.10, respectively.

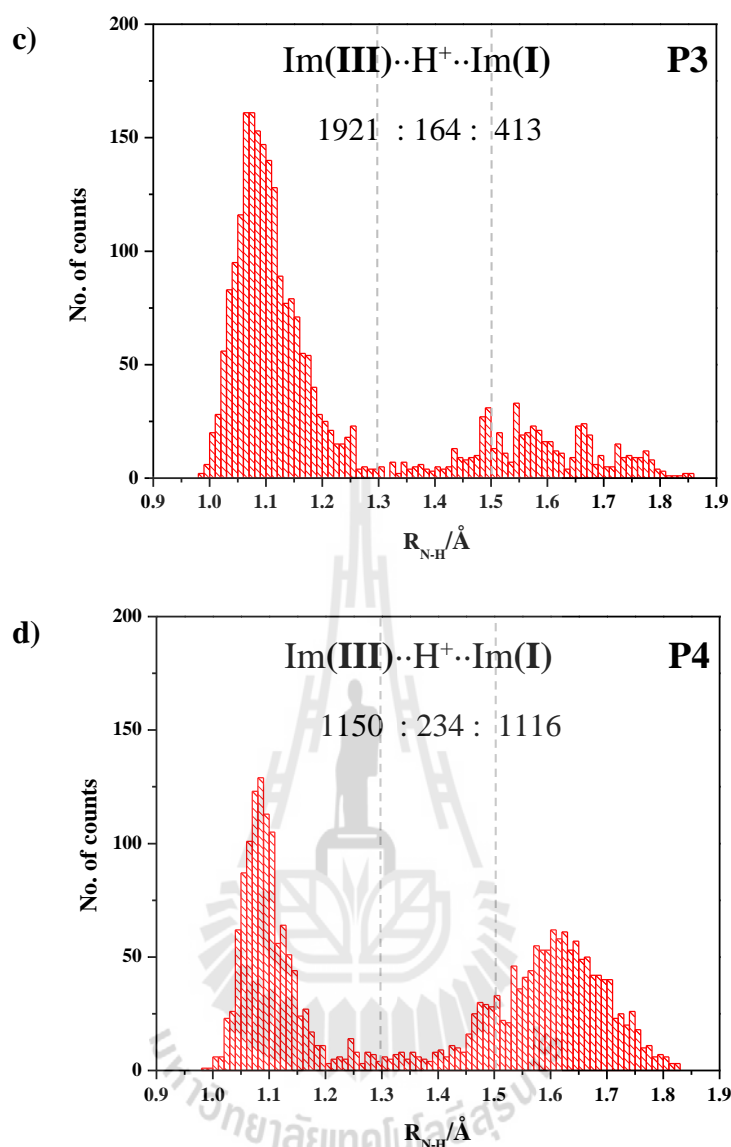


**Figure 3.12** (Continued) Distributions of the N–H covalent bond distances ( $R_{N-H}$ ) in H-bond (3) of structure **G3-[2]<sup>(III)</sup>**, obtained from BOMD simulations at 298 K. a) - d) Distributions in panel **P1** to **P4** in Figure 3.10, respectively.

In the initial state in panel **P1**,  $\omega_3$  and  $\omega_5$  only fluctuate in a narrow range, with average values of  $\langle\omega_3\rangle = 95$  and  $\langle\omega_5\rangle = 84$  degrees. In panel **P2**, the variations in  $\omega_3$  and  $\omega_5$  become unsynchronized; while  $\omega_3$  librates in a narrow range, regarded as a “rotational waiting state”,  $\omega_5$  changes from 84 to 354 degrees, the latter of which can

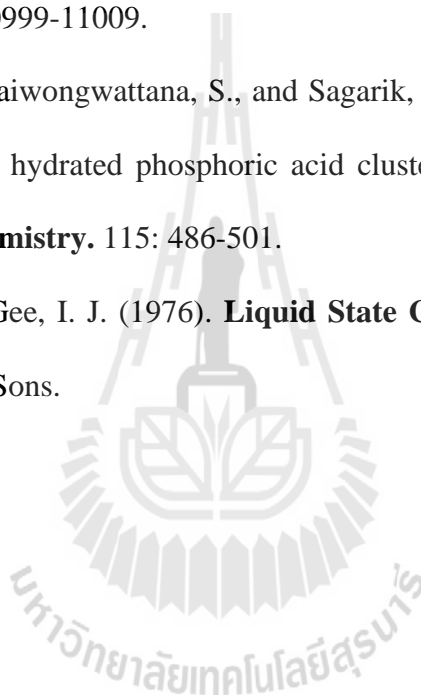
be regarded as a critical angle. In panel **P3**, while  $\omega_5$  is maintained at the critical angle,  $\omega_3$  changes to 282 degrees, in response to the rotation of  $\omega_5$ . Finally, in panel **P4**, both are maintained at  $\langle\omega_3\rangle = 280$  and  $\langle\omega_5\rangle = 270$  degrees. As the torsional rotation of  $\omega_5$  induces the rotation of  $\omega_3$ , with a rotational waiting state of approximately 2500 fs, the rotational motions of  $\omega_5$  and  $\omega_3$  can be collectively regarded as “helical-rotational motion”, which underlies the Im H-bond chain structure reorganization. The Im H-bond chain structure reorganization affects the proton transfer in H-bond (**3**) in such a way that the population of the protons moving away from the dopant is increased from panel **P1** ( $P_{NN} = 0.3$ ) to **P2** ( $P_{NN} = 0.5$ ) and **P3** ( $P_{NN} = 0.8$ ). This finding supports the static results in Figure 3.4a in which the rotation of  $\omega_5$  leads to a modification of the shape of the potential energy curve of H-bond (**3**) in such a way that the lowest minimum of the double-well potential shifts from Im (**I**) to Im (**III**), resulting in a higher probability of finding a proton moving towards Im (**III**), which confirms the effects of the Im H-bond chain structure reorganization suggested by the static results.

### 3.3 References

- Buagern, V. and Sagarik, K. Proton dissociation and transfer in an imidazole cluster. (*in preparation*).
- Chaiwongwattana, S., Phonyiem, M., Vchirawongkwin, V., Prueksaaron, S., and Sagarik, K. (2012). Dynamics and mechanism of structural diffusion in linear hydrogen bond. **Journal of Computational Chemistry**. 33: 175-188.
- Chin, D. T. and Chang, H. H. (1989). On the conductivity of phosphoric acid electrolyte. **Journal of Applied Electrochemistry**. 19: 95-99.

- He, R., Li, Q., Xiao, G., and Bjerrum, N. J. (2003). Proton conductivity of phosphoric acid doped polybenzimidazole and its composites with inorganic proton conductors. **Journal of Membrane Science**. 226: 169-184.
- Koeppe, B., Guo, J., Tolstoy, P. M., Denisov, G. S., and Limbach, H.-H. (2013). Solvent and H/D isotope effects on the proton transfer pathways in heteroconjugated hydrogen-bonded phenol-carboxylic acid anions observed by combined UV-vis and NMR spectroscopy. **Journal of the American Chemical Society**. 135: 7553-7566.
- Lao-ngam, C., Asawakun, P., Wannarat, S., and Sagarik, K. (2011). Proton transfer reactions and dynamics in protonated water clusters. **Physical Chemistry Chemical Physics**. 13: 4562-4575.
- Li, A., Cao, Z., Li, Y., Yan, T., and Shen, P. (2012). Structure and dynamics of proton transfer in liquid imidazole. A molecular dynamics simulation. **The Journal of Physical Chemistry B**. 116: 12793-12800.
- Phonyiem, M., Chaiwongwattana, S., Lao-ngam, C., and Sagarik, K. (2011). Proton transfer reactions and dynamics of sulfonic acid groups of Nafion<sup>®</sup>. **Physical Chemistry Chemical Physics**. 13: 10923.
- Sadeghi, R. R. and Cheng, H.-P. (1999). The dynamics of proton transfer in a water chain. **The Journal of Chemical Physics**. 111: 2086.
- Sagarik, K., Chaiwongwattana, S., Vchirawongkwin, V., and Prueksaaron, S. (2010). Proton transfer reactions and dynamics in CH<sub>3</sub>OH-H<sub>3</sub>O<sup>+</sup>-H<sub>2</sub>O complexes. **Physical Chemistry Chemical Physics**. 12: 918-929.

- Sagarik, K., Phonyiem, M., Lao-Ngam, C., and Chaiwongwattana, S. (2008). Mechanisms of proton transfer in Nafion<sup>®</sup>: Elementary reactions at the sulfonic acid groups. **Physical Chemistry Chemical Physics**. 10: 2098-2112.
- Schmollngruber, M., Schröde, C., and Steinhauser, O. (2014). Dielectric spectra of ionic liquids and their conversion to solvation dynamics: A detailed computational analysis of polarizable systems. **Physical Chemistry Chemical Physics**. 16: 10999-11009.
- Suwannakham, P., Chaiwongwattana, S., and Sagarik, K. (2015). Proton dissociation and transfer in hydrated phosphoric acid clusters. **International Journal of Quantum Chemistry**. 115: 486-501.
- Watts, R. O. and McGee, I. J. (1976). **Liquid State Chemical Physics**. New York: John Wiley & Sons.



## CHAPTER IV

### CONCLUSION

In this work, the dynamics and mechanisms of proton dissociation and transfer in an  $\text{H}_3\text{PO}_4$  doped Im H-bond system were theoretically studied using B3LYP/TZVP calculations and BOMD simulations as model calculations and  $\text{H}^+(\text{H}_3\text{PO}_4)(\text{Im})_n$  ( $n = 1-4$ ) as model systems. The theoretical studies began with choosing appropriate presolvation models for proton dissociation and transfer, represented by embedded and terminal linear H-bond structures, respectively. The structures, energetic and vibrational frequencies of protons in the H-bonds of the presolvation models were studied in low ( $\epsilon = 1$ ) and high local-dielectric ( $\epsilon = 23$ ) environments. The static results confirmed that the excess proton condition is required to promote proton dissociation and transfer, and it must be included in the presolvation model. The 2D-PES and potential energy curves of the proton exchange suggested that the intermediate complexes for proton dissociation and transfer are formed in a low local-dielectric environment, whereas a high local-dielectric environment is required to stabilize the positive charge and prevent a proton from being shared or returning to the original Im molecule, which is in accordance with the localized charge solvent (LCS) concept. The B3LYP/TZVP calculations also revealed that the embedded H-bond structure with  $n = 2$  represents the smallest, most active intermediate complex for proton dissociation, and similarly, the terminal H-bond structure with  $n = 3$  is representative for proton

transfer in the Im H-bond chain. The mechanisms of terminal structure formation and proton transfer in the Im H-bond chain, which involve fluctuations of the H-bond chain lengths and the local-dielectric environment, were proposed based on the static results. Additionally, because the shapes of the potential energy curves are sensitive to the torsional rotations of the H-bonds, the Im H-bond chain structure reorganization is included as an important process in the proton transfer mechanism. A comparison of the threshold frequencies for proton transfer in  $\text{H}^+(\text{H}_3\text{PO}_4)(\text{Im})_n$  ( $n = 1-4$ ) and in the undoped Im H-bond system ( $\text{H}^+(\text{Im})_4$ ) suggested that the strong polarization effects of the dopant lead to a higher probability of finding a delocalized proton and improve proton conduction in the  $\text{H}_3\text{PO}_4$  doped Im system.

Because the static results showed that the embedded H-bond structure with  $n = 2$  and the terminal H-bond structure with  $n = 3$  represent the smallest, most active intermediate complexes for proton dissociation and transfer in a low local-dielectric constant environment, respectively, BOMD simulations were performed on these two H-bond structures. The vibrational spectra obtained from the BOMD simulations suggested three transient vibrational peaks associated with the acid-base proton dissociation, with the activation energy of the proton dissociation in the smallest, most active intermediate complex of 8.7 kJ/mol. It appeared that the extension of the embedded H-bond chain increases the probability of finding the oscillatory shuttling motion and the lifetime of the intermediate complex, resulting in a higher activation energy for proton dissociation from the protonated acid. The comparison of the dynamic results on the  $\text{H}_3\text{PO}_4$  doped Im system with those on  $\text{H}^+(\text{Im})_4$  indicated that the structural diffusion process in the Im H-bond chain of the doped system is almost exclusively through the large-amplitude N–N vibration, without the oscillatory

shuttling motion as the rate-determining process, with an activation energy of only 1.22 kJ/mol. For the undoped Im H-bond system, the proton transfer process is characterized by both the oscillatory shuttling and structural diffusion motions. Analyses of the proton transfer profiles and the time evolutions of the torsional angles revealed coupled torsional motions (helical-rotational motion), which drive the proton away from the dopant and confirm that the Im H-bond chain structure reorganization plays an important role in the proton transfer in the H<sub>3</sub>PO<sub>4</sub> doped Im H-bond system. The results showed for the first time the interplay among the translational, rotational and vibrational motions that underlie the dynamics and mechanisms of proton transfer in the linear H-bond chain. Because the discussion are based on the results on carefully selected presolvation models, the present theoretical study provides new insights into the dynamics and mechanisms of proton exchange processes in doped, weak-polar organic solvent. These pieces of fundamental information are important and can be used as guidelines for further theoretical and experimental investigations on proton transfer processes in aromatic heterocyclic materials, which could eventually lead to an improvement of the proton transfer processes in non-aqueous, high temperature fuel cells.



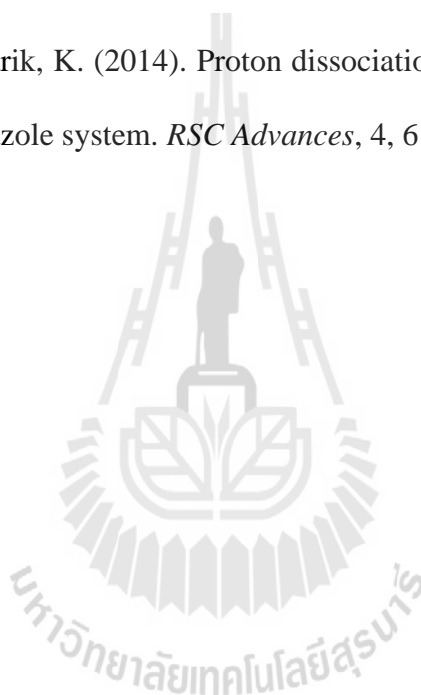
**APPENDICES**

# APPENDIX A

## PUBLICATIONS

### Publication:

Thisuwan, J. and Sagarik, K. (2014). Proton dissociation and transfer in a phosphoric doped imidazole system. *RSC Advances*, 4, 61992-62008.





Cite this: *RSC Adv.*, 2014, 4, 61992

## Proton dissociation and transfer in a phosphoric acid doped imidazole system†

Jittima Thisuwan and Kritsana Sagarik\*

The dynamics and mechanisms of proton exchange in a phosphoric acid ( $\text{H}_3\text{PO}_4$ ) doped imidazole (Im) system were studied using a quantum chemical method at the B3LYP/TZVP level and Born–Oppenheimer molecular dynamics (BOMD) simulations. The theoretical studies began with selecting the appropriate solvation models for proton dissociation and transfer, which were represented by embedded and terminal hydrogen bond (H-bond) structures of  $\text{H}^+(\text{H}_3\text{PO}_4)(\text{Im})_n$  ( $n = 1-4$ ), respectively. B3LYP/TZVP calculations confirmed that excess proton conditions are required to promote proton exchange, and the intermediate complexes are preferentially formed in a low local-dielectric environment. In contrast, a high local-dielectric environment is required to stabilize the positive charge and prevent the proton from returning to the original Im molecule. The static results also revealed that the embedded structure with  $n = 2$  represents the smallest, most active intermediate complex for proton dissociation, whereas the terminal structure with  $n = 3$  favors proton transfer in the Im H-bond chain. BOMD simulations confirmed the static results and further suggested that the fluctuations of the H-bond chain lengths and the local-dielectric environment must be included in the proton dissociation and transfer mechanisms. Analyses of the time evolutions of torsional angles in the Im H-bond chain showed characteristic solvent structure reorganization, regarded as helical-rotational motion, which drives the proton away from the  $\text{H}_3\text{PO}_4$  dopant. The current theoretical results showed in detail for the first time the interplay among the “key molecular motions” that fundamentally underlie the dynamics and mechanisms of proton exchange in the  $\text{H}_3\text{PO}_4$  doped Im H-bond system.

Received 6th August 2014  
Accepted 10th November 2014

DOI: 10.1039/c4ra08198f

www.rsc.org/advances

### Introduction

Proton exchange membrane fuel cells (PEMFCs) have received considerable attention due to their potential as effective power generators.<sup>1–3</sup> Commercially available PEMFCs employ hydrated Nafion® as a polymer electrolyte membrane and therefore have serious limitations on the operating temperature, as Nafion® based fuel cells cannot be operated above the boiling point of water. Over the past decade, attempts have been made to develop electrolyte membranes with high proton conductivity and thermal and mechanical stabilities at elevated temperatures. Aromatic heterocyclic compounds such as benzimidazole (BI), pyrazole (Pz) and imidazole (Im), as well as polymers containing amide functional groups such as poly-(oxodiazole)(POD) and poly(benzimidazole)(PBI), have shown high potential as alternative proton solvents.<sup>4</sup> Due to the auto-protolysis property, a high amphotericity and being a good proton solvent, as well as the ability to form an extensive

H-bond network, these aromatic heterocyclic materials possess high proton conductivities in the condensed phase.<sup>4</sup>

PBI is an aromatic heterocyclic polymer that exhibits excellent thermal, mechanical and chemical stabilities.<sup>4</sup> Although PBI is an intrinsic proton conductor, experiments have revealed that blank PBI is a proton insulator,<sup>5–7</sup> and a sample preparation in which the PBI membrane is dipped into an acid solution represents an essential step for the conductivity measurements.<sup>7,8</sup> Doping a PBI membrane with acids such as  $\text{H}_2\text{SO}_4$ ,  $\text{H}_3\text{PO}_4$  and  $\text{HClO}_4$  can considerably increase the proton conductivity, among which PBI doped with  $\text{H}_3\text{PO}_4$  yields the highest proton conductivity.<sup>7</sup> In the pure state, because all hydrogen atoms are capable of forming extensive H-bonds,  $\text{H}_3\text{PO}_4$  shows the highest intrinsic proton conductivity.<sup>9</sup> However, it was demonstrated that the proton conductivity of  $\text{H}_3\text{PO}_4$  decreases considerably when strong electrolytes such as  $\text{H}_2\text{SO}_4$  were added.<sup>10</sup> In contrast, the conductivity was found to increase significantly with water content. The latter is attributed to the promotion of self-ionization and an increase in the number of protons.<sup>8</sup>

Given the high proton conductivity with respect to the  $c$  crystallographic direction<sup>11,12</sup> and properties as an excellent proton solvent, Im has been frequently employed as a prototypical molecule in the study of proton transfer in aromatic

School of Chemistry, Institute of Science, Suranaree University of Technology, Nakhon Raichasima 30000, Thailand. E-mail: kritsana@sut.ac.th; Fax: +66 44224635; Tel: +66 44224635

† Electronic supplementary information (ESI) available. See DOI: 10.1039/c4ra08198f

heterocyclic materials.<sup>11–16</sup> Experiments have shown that Im can form extensive H-bond chains in the condensed phase, along which protons can be conducted by the Grotthuss mechanism.<sup>11,12</sup> It was suggested that to complete the proton transfer process, the Grotthuss mechanism must be followed by a cooperative ring reorientation (ring-flip) as an important rate-determining step.<sup>16</sup> However, solid-state <sup>15</sup>N NMR experiments demonstrated that for pure Im, the Grotthuss mechanism need not involve the reorientation of the Im ring.<sup>11</sup>

The influence of Im and 1-methyl Im on the conductivity of 99 wt% H<sub>3</sub>PO<sub>4</sub> solutions and H<sub>3</sub>PO<sub>4</sub> doped PBI membranes was studied over the temperature range of 350 to 473 K under various humidity conditions.<sup>17</sup> It appeared that the conductivity of the solutions decreased with an increasing amount of Im and increased with temperature. The former is attributed to a reduction in the number of proton charge carriers as a consequence of the acid–base reaction, and the viscosity of the solutions was suggested to play an important role in the proton conduction, especially at temperatures below 373 K. Because proton conduction in pure H<sub>3</sub>PO<sub>4</sub> is perturbed by the addition of Im,<sup>17</sup> to investigate the mechanism underlying this effect, *ab initio* molecular dynamics (AIMD) simulations on a H<sub>3</sub>PO<sub>4</sub>–Im 2 : 1 system (36 H<sub>3</sub>PO<sub>4</sub> and 18 Im molecules) were performed at 400 K.<sup>18</sup> Due to the acid–base reaction, stable ion-pair complexes between H<sub>2</sub>PO<sub>4</sub><sup>−</sup> and ImH<sup>+</sup> and Zundel-like ions, characterized by proton shuttling between two Im molecules (H<sup>+</sup>(Im)<sub>2</sub>), were observed in AIMD simulations. Analyses of the local structures and energetic and dynamic results suggested that, due to the proton transfer from H<sub>3</sub>PO<sub>4</sub> to Im, the proton density in the H<sub>3</sub>PO<sub>4</sub> phase is reduced and the formation of the ion-pair complexes leads to significantly shorter H-bond chains compared to those in the pure state. These reduce the cooperative effects of the proton transport mechanism and the effectiveness of proton transfer in the Im H-bond chain.<sup>18</sup>

Insights into proton dissociation and transfer in an aqueous solution were obtained in our previous work<sup>19</sup> in which the dynamics and mechanisms of proton exchange in hydrated H<sub>3</sub>PO<sub>4</sub> under excess proton conditions were studied using H<sup>+</sup>(H<sub>3</sub>PO<sub>4</sub>)(H<sub>2</sub>O)<sub>*n*</sub> (*n* = 1–4) as the model system with *ab initio* calculations and Born–Oppenheimer molecular dynamics (BOMD) simulations at the RIMP2/TZVP level as the model calculations. Based on the static results in the gas phase and continuum aqueous solvent, mechanisms of proton dissociation and transfer that involve fluctuations of the number of water molecules in the H-bond chain and the local-dielectric environment were proposed. It was concluded that the smallest, most active intermediate complex for proton dissociation (*n* = 1) is formed in a low local-dielectric environment (*e.g.*,  $\epsilon$  = 1) and that the proton transfer from the first hydration shell is driven by fluctuations in the number of water molecules in a high local-dielectric environment (*e.g.*,  $\epsilon$  = 78) through the Zundel complex, which connects the first and second hydration shells. BOMD simulations over a temperature range of 298 to 430 K confirmed that only the H-bond chains with asymmetric hydration at H<sub>3</sub>PO<sub>4</sub><sup>+</sup> are involved in the proton dissociation and transfer. This finding validated the proposed mechanisms by showing that an agreement between the theoretical and

experimental activation energies can be achieved based on the proposed rate-determining processes.<sup>19</sup>

In the work presented here, the dynamics and mechanisms of proton dissociation and transfer in a H<sub>3</sub>PO<sub>4</sub> doped Im H-bond system were studied using the quantum chemical method at the B3LYP/TZVP level and BOMD simulations. Based on the concept of presolvation<sup>20,21</sup> and the observation that a unit cell of the Im crystal structure is monoclinic with four molecules forming a linear H-bond chain along the *c* crystallographic axis, H<sup>+</sup>(H<sub>3</sub>PO<sub>4</sub>)(Im)<sub>*n*</sub> (*n* = 1–4) were selected as model systems. The characteristic properties of the exchange protons in the intermediate complexes in low and high local-dielectric environments were investigated and analyzed in detail. The elementary steps of proton dissociation and transfer were proposed based on the static results and confirmed by BOMD simulations in the temperature range between 298 and 423 K. The interplay among the key molecular motions that fundamentally underlie the dynamics and mechanisms of proton exchange in the H<sub>3</sub>PO<sub>4</sub> doped Im H-bond system were analyzed and discussed.

## Computational methods

### Presolvation models

Because the proton exchange processes in H-bonds are complicated, care must be exercised in selecting the model systems. In the present case, the model systems for proton dissociation and transfer were chosen based on the concept of presolvation;<sup>20,21</sup> the local energy fluctuations and dynamics in solution lead to the weakening or breaking of some H-bonds in the first and second solvation shells, resulting in a reduction in the solvent coordination number such that the proton-accepting species possesses a solvation structure corresponding to the species into which it will be transformed to complete the structural diffusion process. It was shown in our previous work that the dynamics of the transferring protons can be studied reasonably well because the moderate sizes of the presolvation models help reduce the complexity in the H-bond systems and allow theoretical calculations to be made using quantum chemical methods at higher level of accuracy, provided that an appropriate presolvation model is selected and that all of the important rate-determining processes are included in the model calculations.<sup>22–26</sup>

In the present work, because a unit cell of the Im crystal structure is monoclinic with four Im molecules forming a linear H-bond chain along the *c* crystallographic axis, H<sup>+</sup>(H<sub>3</sub>PO<sub>4</sub>)(Im)<sub>*n*</sub> (*n* = 1–4) were selected as model systems. The cluster size (*n* = 4) is consistent with the average number of Im molecules obtained from MD simulations with excess proton solvated in liquid Im, using a reactive multistate empirical valence bond (MS-EVB) model.<sup>27</sup> Based on the concept of presolvation and some test calculations, the presolvation models for proton dissociation and transfer were proposed and are shown in Fig. 1, regarded hereafter as the “embedded” and “terminal” linear H-bond structures, respectively. Experimental and theoretical studies which support the linear H-bond arrangements in the presolvation models are summarized as follows.

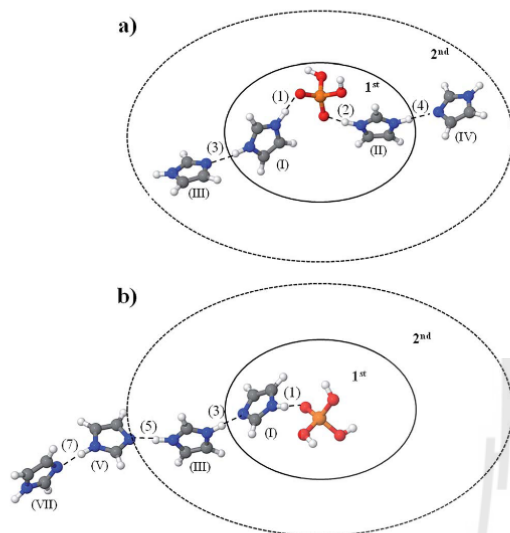


Fig. 1 (a and b) Embedded and terminal presolvation models employed in the studies of proton dissociation and transfer in  $\text{H}^+(\text{H}_3\text{PO}_2)(\text{Im})_n$  ( $n = 1-4$ ), respectively.  $1^{\text{st}}$  = first solvation shell;  $2^{\text{nd}}$  = part of second solvation shell; (1)–(7) = labels of H-bonds; (I)–(VII) = labels of Im molecules.

In condensed phase, due to the amphoteric character, computer simulations<sup>28</sup> and experiments<sup>12</sup> showed that Im molecules form polymeric chains, along which excess proton can be relayed between two Im molecules through the Grotthuss shuttling mechanism. Possessing only one proton donor (N–H) and one proton acceptor (N) in the same molecule, the linear H-bond chains in liquid Im are not as extensive as the H-bond networks in water (two proton donors and two proton acceptors in the same molecule). Because the proton donor and acceptor are used in the H-bond chain formation, the interactions between parallel chains could be the C–H $\cdots\pi$  H-bond and  $\pi\cdots\pi$  interactions, which are considerably weaker than the interactions in the protonated Im H-bond chains; for the benzene dimers, the interaction energies for the C–H $\cdots\pi$  H-bond in the T-shaped structure, and the  $\pi\cdots\pi$  interaction in the sandwich structure, computed at the MP2 level, are only  $-8.8$  and  $-3.6$   $\text{kJ mol}^{-1}$ ,<sup>29</sup> respectively, compared to the interaction energy of the protonated Im dimer of  $-116$   $\text{kJ mol}^{-1}$ .<sup>30</sup>

Our theoretical study on proton transfer in protonated Im H-bond clusters<sup>30</sup> revealed that the intermediate complexes (the H-bond structure with a shared-proton) exist only in the linear H-bond chains (see Table S2†), which is in accordance with the protonic-chain conduction mechanism;<sup>10,31</sup> B3LYP/TZVP geometry optimizations suggested that the linear H-bond arrangements are the global and local minimum energy geometries in the protonated pure,<sup>30</sup> and doped Im systems. It should be noted that, although the globular H-bond structures could possess larger contact area and smaller free energy, based on the characteristic properties of the transferring proton (e.g.,

asymmetric stretching coordinates and vibrational frequencies), the H-bonds in the globular structures are not susceptible to proton transfer.<sup>30</sup> Because we are interested in the dynamics of the transferring protons in the intermediate complexes, linear Im H-bond chains were selected as the presolvation models; the lifetime of the intermediate complex has been shown in many H-bond systems to represent the rate-determining processes in proton transfer mechanisms.

To investigate solvent effects on proton dissociation and transfer, a continuum solvent model was included in the model calculations. To account for the electrostatic effects introduced by the solvent, a conductor-like screening model (COSMO), with the dielectric constant of liquid Im ( $\epsilon = 23$ ), was employed. The application of the continuum solvent model is justified by the following studies.

In liquid phase, analyses of a MS-EVB model revealed that the first solvation shell of the  $\text{ImH}^+$  ion is highly ordered due to the formation of the strong protonated H-bond ( $\text{ImH}^+\cdots\text{Im}$ ), whereas the second solvation shell is highly disordered.<sup>32</sup> These suggest that the interactions connecting the Im molecules in the first and second solvation shells are weak. As the first and second solvation shells are loosely connected, mechanical and chemical interactions between the two solvation shells could be approximately neglected in the model systems, and it is reasonable to incorporate the electrostatic effects introduced by the weak-polar organic solvent by a continuum solvent model.

MD simulations also suggested that the proton transfer in liquid Im can be considered as a “local event”,<sup>16,27</sup> with very short spatial/temporal correlation<sup>27</sup> (involving only Im molecules close to  $\text{ImH}^+$ ) and driven by local rather than long-range cooperative motions (reorientations) of the Im molecules.<sup>16</sup> Based on Car-Parrinello molecular dynamics (CPMD) simulations,<sup>16</sup> the time scale for the long-range cooperative reorientation process is about 30 ps, which is considerably longer than the proton transfer step of about 0.3 ps. Therefore, the effects of the fluctuations of bulk solvent structures on the conformations of the solute ( $\text{ImH}^+\cdots\text{Im}$ ) could be neglected, and the approximation of the electrostatic effects of the local-dielectric environment by a continuum solvent model is reasonable and justifiable.

### Quantum chemical calculations

Three basic steps used in our previous work<sup>21, 26,33,34</sup> were employed: (1) searching for equilibrium structures and intermediate complexes in the proton dissociation and transfer pathways using the Test-particle model (T-model) potentials;<sup>35–39</sup> (2) refining the T-model optimized structures using the quantum chemical method; and (3) performing BOMD simulations on the candidate intermediate complexes using the refined structures as the starting configurations.

It is worth remarking on the quantum chemical method employed in this study. As discussed in the previous work,<sup>24</sup> because of the ability to approximate the effects of electron correlation with reasonable accuracy and computational resources, density functional theory (DFT) methods have been used extensively in studies of interacting systems. However, the

accuracy of the DFT methods depends on the chemical systems under investigation; the DFT methods tend to underestimate the interaction energy ( $\Delta E$ ) for the systems with strong effects of the electron correlation. The T-shaped and parallel-displaced (PD) structures of a phenol-benzene dimer are a typical example in which the interplay between the electrostatic and dispersion interactions was examined in detail;<sup>40</sup> the stability of the former is dominated by the electrostatic interaction and the latter by the dispersion interaction. However, B3LYP/6-311++G(d,p) calculations predicted the PD structure to be unstable, with positive interaction energy ( $\Delta E$ ), whereas  $\Delta E$  of the T-shaped structure with the O-H $\cdots\pi$  interaction is considerably higher than the experimental value,  $-8.4$  kJ mol<sup>-1</sup> and  $-16.7$  kJ mol<sup>-1</sup>,<sup>41</sup> respectively. Because the effects of the electron correlation could play an important role in the present model systems, the applicability and performance of the B3LYP/TZVP calculations were examined by benchmarking with the second-order Møller-Plesset perturbation theory (MP2) method, with the resolution of the identity (RI) approximation and the TZVP basis set, with abbreviated RIMP2/TZVP calculations. The correlations between the key properties, *e.g.*, the H-bond structures, interaction energies and vibrational frequencies, are illustrated in Fig. S1.† The methods were in agreement and obtained correlation coefficient ( $R^2$ ) for  $\Delta d_{\text{DA}}$  of 0.97. Therefore, to ensure reasonable computational efforts, the B3LYP/TZVP calculations were employed in both the static and dynamic calculations. All of the quantum chemical calculations and BOMD simulations were performed using the TURBOMOLE 6.5 software package.<sup>42</sup>

### Static calculations

To obtain the fundamental information for the discussion of the dynamics and mechanisms of proton dissociation and transfer in the H<sub>3</sub>PO<sub>4</sub> doped Im system under an excess proton condition, the structural, energetic and spectroscopic properties of H<sup>+</sup>(H<sub>3</sub>PO<sub>4</sub>)(Im)<sub>*n*</sub> (*n* = 1–4) were computed using B3LYP/TZVP calculations, both in the gas phase and the continuum solvent (COSMO,  $\epsilon = 23$ ). The interaction energies ( $\Delta E$ ) of the H-bond complexes were computed from  $\Delta E = E(\text{H}^+(\text{H}_3\text{PO}_4)(\text{Im})_n) - [E(\text{H}_4\text{PO}_4^+) + nE(\text{Im})]$ ;  $E(\text{H}^+(\text{H}_3\text{PO}_4)(\text{Im})_n)$  is the total energy of the equilibrium structure of H<sup>+</sup>(H<sub>3</sub>PO<sub>4</sub>)(Im)<sub>*n*</sub>;  $E(\text{H}_4\text{PO}_4^+)$  and  $E(\text{Im})$  are the total energies of the isolated species at their equilibrium structures. The solvation energies ( $\Delta E^{\text{sol}}$ ) were approximated from  $\Delta E^{\text{sol}} = E(\text{H}^+(\text{H}_3\text{PO}_4)(\text{Im})_n)^{\text{COSMO}} - E(\text{H}^+(\text{H}_3\text{PO}_4)(\text{Im})_n)$ ;  $E(\text{H}^+(\text{H}_3\text{PO}_4)(\text{Im})_n)^{\text{COSMO}}$  and  $E(\text{H}^+(\text{H}_3\text{PO}_4)(\text{Im})_n)$  are the total energies of the equilibrium structures obtained with and without COSMO, respectively.

The behaviors of proton dissociation and transfer were primarily evaluated from the asymmetric stretching coordinate ( $\Delta d_{\text{DA}}$ ), computed from  $\Delta d_{\text{DA}} = |d_{\text{A-H}} - d_{\text{B}\cdots\text{H}}|$ , where  $d_{\text{A-H}}$  and  $d_{\text{B}\cdots\text{H}}$  are the A-H and B $\cdots$ H distances in the A-H $\cdots$ B H-bond, respectively. The H-bond that is susceptible to proton transfer is represented by a  $\Delta d_{\text{DA}}$  value that is close to zero as for a proton located near or at the center of the H-bond. As an effective probe for the dynamics of proton transfer in the H-bond, this study employed vibrational spectroscopy. The

vibrational frequencies of protons in H<sup>+</sup>(H<sub>3</sub>PO<sub>4</sub>)(Im)<sub>*n*</sub> (*n* = 1–4) were computed using the B3LYP/TZVP method with the harmonic approximation. They were used as guidelines to assign the vibrational modes predicted by the BOMD simulations. As the anharmonicity is neglected, the vibrational frequencies obtained from quantum chemical methods are generally overestimated. A scaling factor of 0.9614 proved to be appropriate for the B3LYP/TZVP calculations<sup>43</sup> and was therefore employed in this work. The dynamics of the proton dissociation and transfer were discussed based on the asymmetric O-H and N-H stretching frequencies,  $\nu^{\text{OH}}$  and  $\nu^{\text{NH}}$ , respectively<sup>24,26,44,45</sup>. Additionally, because the motions of protons moving in single- and double-well potentials are different, H-bonds that are susceptible and not susceptible to transfer were distinguished by the threshold asymmetric N-H stretching frequencies ( $\nu^{\text{NH}^*}$ ) that were calculated from the plots of  $\nu^{\text{NH}}$  and  $\Delta d_{\text{DA}}$ .<sup>33</sup> The relationship between  $\nu^{\text{NH}}$  and  $\Delta d_{\text{DA}}$  is described by a reflected normal distribution function, for which the second derivative is equal to zero at  $\nu^{\text{NH}} = \nu^{\text{NH}^*}$ . The H-bond proton is considered to be susceptible to transfer when  $\nu^{\text{NH}} < \nu^{\text{NH}^*}$ .<sup>33</sup> To provide energetic information for the discussion of the solvent effects, two-dimensional potential energy surfaces (2D-PES) of the transferring protons in the smallest, most active intermediate complexes were constructed in both the gas phase and the continuum solvent by calculating  $\Delta E$  at various R<sub>N-O</sub> and R<sub>N-H</sub> distances. As in our previous studies,<sup>23</sup> equally spaced grid points were generated from  $\Delta E$  and the 2D-PES were plotted as a function of R<sub>N-O</sub> and  $\Delta d_{\text{DA}}$  using the SURFER program.<sup>46</sup> The interaction energy paths connecting the single- and double-well potentials, as well as the path with the highest energy barriers, were identified and discussed in detail.

### Dynamic calculations

The dynamics and mechanisms of proton transfer in H-bonds were successfully studied in our previous work by performing NVT BOMD simulations on the smallest, most active intermediate complexes in the presolvation models.<sup>19,23–26</sup> In the present work, we are interested in the dynamics of the transferring protons (*e.g.*, the oscillatory shuttling and structural diffusion motions) in the intermediate complexes, which occur locally in a very short time scale; according to the MS-EVB MD simulations,<sup>27</sup> these involve linear H-bond chains with few Im molecules. As the intermediate complexes with the shared-proton structures are repeatedly formed and relaxed, and BOMD simulations involve only limited number of Im molecules, the periodic boundary conditions are not necessary in this case; the periodic boundary conditions are generally employed in computer simulations of condensed phase to solve the problem of surface and finite-size effects, and therefore important in the study of the long-range effects in bulk systems.

To study proton dissociation and transfer in H<sup>+</sup>(H<sub>3</sub>PO<sub>4</sub>)(Im)<sub>*n*</sub> (*n* = 1–4), NVT BOMD simulations were performed at the B3LYP/TZVP level. Two thousand steps of 1 fs each were used in the equilibration and 10 000 steps were used in the property calculations, corresponding to 2 and 10 ps, respectively. The NVT ensemble was concluded to be appropriate for the dynamic

processes that take place on relatively short time scales and in the continuum solvent,<sup>47</sup> and the time step proved to be small enough to determine reliable vibrational spectra, activation energies and dynamic properties of the transferring protons.<sup>22–26,48,49</sup>

Because realistic dynamics at constant temperatures are desirable in this work, the BOMD simulation conditions were carefully chosen, especially the temperature control algorithm. The Nosé–Hoover thermostat was selected based on the conclusion that the transport properties and thermodynamic distributions that are statistically indistinguishable from the NVE ensemble can be achieved when globally applied to the system using any coupling strength;<sup>47</sup> the Nosé–Hoover thermostat adjusts velocities by coupling the equations of motion to extended dynamic variables and gives an oscillatory relaxation to the target temperature. To ensure the minimum perturbation on the dynamics of the transferring protons, the energy conservation and stability of the numerical integration in the NVT BOMD simulations were assessed at 323 K, using the smallest, most active intermediate complex as a representative. To test the stability of the numerical integration, a drift in property A ( $\delta_A$ ) over a time interval  $[0, t_{\max}]$  was computed from  $\delta_A = b_A t_{\max} / \sigma_A$ ;<sup>50</sup>  $b_A$  is obtained from a linear least-square fit to the data,  $A(t) = a_A + b_A t + \varepsilon(t)$ , and  $\sigma_A$  is the standard deviation of  $\varepsilon(t)$ . Therefore, for an ideal, isolated-energy conserved system,  $b_A$  is 0, and hence,  $|\delta_A| = 0$ . The drift in property A is significant if  $|\delta_A| \sim 1$  and the result obtained by averaging  $A(t)$  over the simulation time  $t_{\max}$  is considered to be unreliable. Based on this definition, the drifts in energies ( $E^{\text{tot}}$ ,  $E^{\text{pot}}$  and  $E^{\text{kin}}$ ), the H-bond structures ( $R_{\text{N-O}}$ ,  $R_{\text{N-H}}$  and  $R_{\text{O-H}}$ ) and the velocity of the transferring proton ( $v^{\text{H}^+}$ ) were calculated over the integration period of  $t_{\max} = 2$  ps and included in Table S1.† The energy conservation and velocity plots over the entire simulation length (10 ps) are illustrated in Fig. S2.† Additionally, to confirm that the dynamics are not perturbed by the Nosé–Hoover thermostat, the mean-square displacement (MSD) of the transferring proton was computed and included in Fig. S2.† Because the trends of the energy conservation and velocity plots showed no systematic drifts and a general linear relationship was observed for the MSD plot, the dynamic properties computed under the present NVT BOMD simulation conditions, including the Nosé–Hoover thermostat, were determined to be well represented. Additionally, as the energy and velocity drifts are only 0.22, the numerical integration in the NVT BOMD simulations is confirmed to be stable.

The dynamic behaviors of proton dissociation and transfer in the  $\text{H}_3\text{PO}_4$  doped Im system were primarily discussed using proton transfer profiles, with variations of  $R_{\text{A-B}}$ ,  $R_{\text{A-H}}$  and  $R_{\text{B-H}}$  with the simulation time.<sup>49</sup> Proton transfer reactions are generally not concerted and can take place in both the forward and reverse directions, with the oscillatory shuttling motion being the rate-determining process.<sup>49</sup> This is because the transfer reactions involve quasi-dynamic equilibrium between the close-contact  $\text{A-H}\cdots\text{B}$  and the shared-proton  $\text{A}\cdots\text{H}\cdots\text{B}$  H-bonds.<sup>49</sup> It is therefore not straightforward to determine the direction of the proton displacement in the Im H-bond chain. Because a stable covalent bond must be formed in the direction

of the proton displacement to complete proton hopping in a single H-bond, it is reasonable to correlate the probability of finding a proton moving in a specific direction with the probability of covalent bond formation. Hence, to estimate the probability of finding a proton transfer from atom B to A ( $P_{\text{BA}}$ ), the distribution of the A–H covalent bond distance ( $R_{\text{A-H}}$ ) is first computed from the BOMD simulations. Then, based on the criterion for the N–H covalent bond formation ( $R_{\text{N-H}} \leq 1.3 \text{ \AA}$ ),  $P_{\text{BA}}$  is approximated by the number of counts of the N–H covalent bond divided by the total number of samples. In this work, a proton is considered to have favorably transferred from B to A when  $P_{\text{BA}} \geq 0.5$ . Likewise, the probability of finding the intermediate complex with the shared-proton  $\text{A}\cdots\text{H}\cdots\text{B}$  H-bond ( $P_{\text{A}\cdots\text{H}\cdots\text{B}}$ ) can be approximated by the number of counts of  $R_{\text{A-H}}$  in the range between 1.3 and 1.5  $\text{\AA}$ , divided by the total number of samples.

The dynamics and mechanisms of proton dissociation and transfer were finally confirmed using the vibrational spectra obtained from Fourier transformations of the velocity autocorrelation functions (VACF) of the atoms in H-bonds.<sup>24,25</sup> Only the characteristic N–O and N–N vibrational frequencies ( $\nu^{\text{NO,MD}}$  and  $\nu^{\text{NN,MD}}$ , respectively), as well as the asymmetric N–H stretching frequencies ( $\nu^{\text{NH,MD}}$ ), were reported and discussed in detail. The activation energies of the rate-determining processes in the proton dissociation and transfer pathways were determined by performing BOMD simulations over the temperature range of 298 to 423 K. The first-order rate constants ( $k$ ) for proton exchanges were approximated from the exponential relaxation behavior of the envelope of VACF of the N–O and N–N vibrations, which are based on the assumption that the decay process follows the first-order kinetics:  $k = \ln(2)/\tau_{1/2}$ , where  $\tau_{1/2}$  is the half-life of the exponential decay function. The Arrhenius plots were constructed and the activation energies ( $\Delta E^{\ddagger_{\text{Att}}}$ ) of proton dissociation and transfer were approximated from the slopes of the linear relationship between  $\ln(k)$  and  $1000/T$ .<sup>23</sup>

## Results and discussion

### Static results

The equilibrium structures and the interaction ( $\Delta E$ ) and solvation ( $\Delta E^{\text{sol}}$ ) energies obtained from the B3LYP/ITZVP calculations in the gas phase and the continuum solvent are listed in Table S2,† together with the H-bond distances ( $R_{\text{N-N}}$ ,  $R_{\text{N-O}}$  and  $\Delta d_{\text{DA}}$ ) and the asymmetric N–H stretching frequencies ( $\nu^{\text{NH}}$ ). The  $\text{H}_3\text{PO}_4$  doped Im H-bond structures in Table S2† are labelled with a four character code, e.g., **Gn-[m]**<sup>(I–VII)</sup> and **Cn-[m]**<sup>(I–VII)</sup>, where **G** = equilibrium structure in the gas phase; **C** = equilibrium structure in continuum solvent; and **n** = number of Im molecules. Different H-bond structures with the same number of Im molecules are distinguished by **[m]**. Positively charged Im molecules are designated by a Roman numeral in parenthesis, from (I) to (VII). As an example, **G3-[2]**<sup>(I)</sup> and **G3-[2]**<sup>(II)</sup> are the same H-bond structures (**m** = 2 and **n** = 3) with different positively charged Im molecules, at Im (I) and Im (II), respectively.

### Excess proton conditions and tendencies of proton dissociation and transfer

Investigation of the embedded structures and their H-bond properties in Table S2† reveals outstanding acid–base interaction in the  $\text{H}_3\text{PO}_4$  doped Im system, specifically two protons are readily dissociated from  $\text{H}_4\text{PO}_4^+$  and protonate the two neighboring Im molecules (Im (I) and Im (II)), forming the  $\text{ImH}^+ \cdot \text{H}_2\text{PO}_4^- \cdot \text{ImH}^+$  complex, *e.g.*, in the gas phase, structures  $\text{G2-}[1]^{(\text{I,II})}$  and  $\text{G3-}[1]^{(\text{I,II})}$ , and in the continuum solvent, structures  $\text{C2-}[1]^{(\text{I,II})}$  and  $\text{C3-}[1]^{(\text{I,II})}$ . Because the B3LYP/TZVP calculations (not shown here) suggest no proton dissociation from the corresponding unprotonated (neutral) embedded structures, one can conclude that proton dissociation and transfer in the Im system takes place preferentially under excess proton conditions,<sup>8,9</sup> with the  $\text{Im} \cdot \text{H}_4\text{PO}_4^+ \cdot \text{Im}$  complexes as the precursors. This is in agreement with experiments in which dipping the PBI film into a  $\text{H}_3\text{PO}_4$  solution is a necessary step for the conductivity measurement.<sup>8</sup> Therefore, to obtain realistic proton dissociation and transfer mechanisms, excess proton conditions must be included in the presolvation models.<sup>19,24,25,33</sup>

The tendencies of proton dissociation and transfer are primarily discussed using the relationships between  $\nu^{\text{NH}}$  and  $\Delta d_{\text{DA}}$  in Fig. 2. The plot of  $\nu^{\text{NH}}$  and  $\Delta d_{\text{DA}}$  in Fig. 2a suggests that the threshold asymmetric N–H stretching frequency ( $\nu^{\text{NH}*}$ ) for the proton dissociation in the gas phase is at  $\nu^{\text{NH}*} = 2158 \text{ cm}^{-1}$  and  $\Delta d_{\text{DA}} = 0.37 \text{ \AA}$ , approximately  $150 \text{ cm}^{-1}$  lower than in aqueous solution ( $\nu^{\text{OH}*} = 2306 \text{ cm}^{-1}$ ),<sup>19</sup> reflecting a stronger acid–base interaction in the  $\text{H}_3\text{PO}_4$  doped Im system. In the continuum solvent, the  $\nu^{\text{NH}}$  values are all above  $2500 \text{ cm}^{-1}$  without an inflection point ( $\nu^{\text{NH}*}$ ), suggesting that the close-contact  $\text{N-H}\cdots\text{O}$  H-bond with localized positive charge is more favorable than the shared-proton structure ( $\text{N}\cdots\text{H}\cdots\text{O}$ ) with delocalized positive charge in COSMO, which is in accordance with the localized charge solvent (LCS) concept: “a polar solvent solvates species with localized charges more efficiently than species with more delocalized charges”.<sup>31</sup> Similar results were obtained for proton transfer in the Im H-bond chains, for which the plot of  $\nu^{\text{NH}}$  and  $\Delta d_{\text{DA}}$  in Fig. 2b yielded the threshold frequency only in a low local-dielectric environment, in the gas phase at  $\nu^{\text{NH}*} = 1925 \text{ cm}^{-1}$  and  $\Delta d_{\text{DA}} = 0.44 \text{ \AA}$ . The threshold frequency is approximately  $70 \text{ cm}^{-1}$  lower than that of the undoped Im H-bond chains ( $1992 \text{ cm}^{-1}$ ),<sup>30</sup> reflecting the strong polarization effect of the dopant and a higher probability of finding the shared-proton structure and delocalized protons in the  $\text{H}_3\text{PO}_4$  doped Im system; the shared-proton structure is an important intermediate in the proton transfer pathway.

### Two-dimensional potential energy surfaces and solvent effects

The two-dimensional potential energy surfaces (2D-PES) for proton dissociation in the smallest embedded structure in the gas phase and the continuum solvent are shown in Fig. 3. The absolute minimum on the 2D-PES of structure  $\text{G2-}[1]^{(\text{I,II})}$  is represented by an asymmetric single-well potential at  $R_{\text{N-O}} = 2.54 \text{ \AA}$  and  $\Delta d_{\text{DA}} = 0.33 \text{ \AA}$ . At longer  $R_{\text{N-O}}$  distance ( $R_{\text{N-O}} \approx 2.67 \text{ \AA}$ ), a double-well potential emerges. On the 2D-PES, a low-interaction energy, barrier-less path connecting the single-

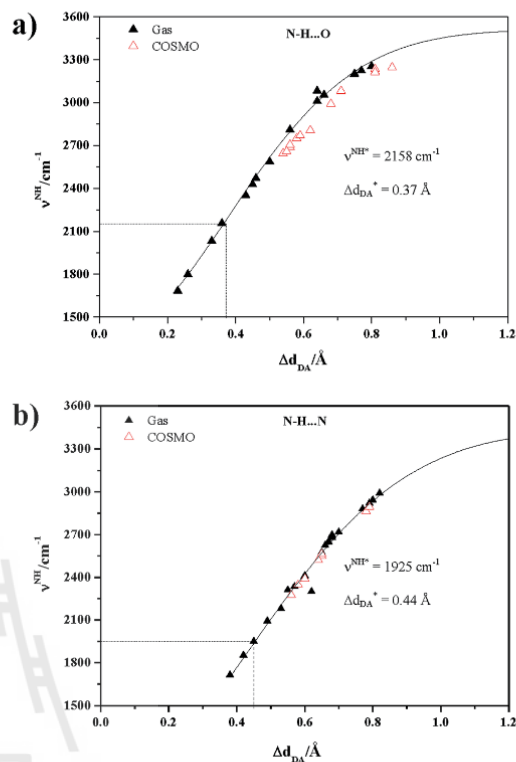


Fig. 2 Plots of asymmetric N–H stretching frequencies ( $\nu^{\text{NH}}$ ) as a function of asymmetric stretching coordinates ( $\Delta d_{\text{DA}}$ ), obtained from B3LYP/TZVP calculations. The dashed lines separate the protons that are susceptible and not susceptible to exchange. (a) N–H...O H-bonds in the first solvation shell. (b) N–H...N H-bonds in Im H-bond chains.

and double-well potentials spans from A to C, regarded hereafter as the “dissociation path” (or path AC), whereas the “association path” spanning from A to B (or path AB) is uphill and therefore unfavorable in this H-bond complex. The shapes of the cross-sectional plots in Fig. 3a suggest at least three N–H stretching modes associated with proton dissociation, namely a vibrational mode associated with a proton moving in the single-well potential and two vibrational modes with a proton moving on the dissociation and association paths. Because conventional quantum chemical calculations on vibrational spectra are based on the harmonic approximation, which requires well-optimized geometry, only the  $\nu^{\text{NH}}$  value of a proton moving in the single-well potential is obtainable from the static calculations; for proton dissociation in structure  $\text{G2-}[1]^{(\text{I,II})}$ ,  $\nu^{\text{NH}} = 2033 \text{ cm}^{-1}$ . Therefore, BOMD simulations must be performed to study the other two characteristic modes that involve H-bond structures distorted from the absolute minimum energy geometry.

A comparison of the cross-sectional plots in Fig. 3a and b reveals the effects of the continuum solvent on the shapes of the

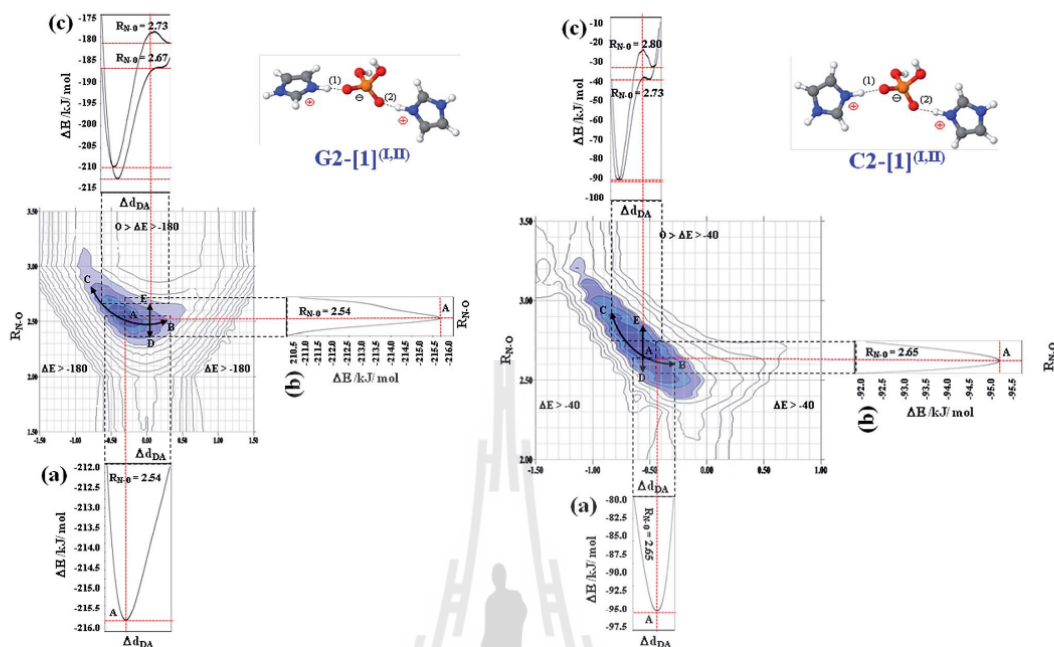


Fig. 3 Two-dimensional potential energy surfaces (2D-PES) of proton dissociation in the gas phase and continuum solvent. (a) Proton dissociation in H-bond (1) of the embedded structure G2-[1]<sup>(I,II)</sup>. (b) Proton dissociation in H-bond (1) of the embedded structure C2-[1]<sup>(I,II)</sup>. (a), (b) and (c) are the cross-sectional plots of the single- and double-well potentials, respectively.

2D-PES, namely the single- and double-well potentials are shifted closer to the Im molecules, suggesting stronger N-H covalent bonds and weaker N-H $\cdots$ O H-bonds in structure C2-[1]<sup>(I,II)</sup>. In other words, due to the partial neutralization of positive charges by the continuum solvent, protons are localized nearer to the nitrogen atoms, resulting in a lower probability of finding the shared-proton structure and the oscillatory shuttling motion. These findings confirm that the intermediate complexes of proton dissociation and transfer in the H<sub>3</sub>PO<sub>4</sub> doped Im system are favorably formed in a low local-dielectric environment and that a high local-dielectric environment is required to stabilize the transferred proton before the successive transfer.

#### Mechanisms of proton transfer in the Im H-bond chains

Apart from the excess proton condition and the effects of the local-dielectric environment, to propose the elementary steps of proton transfer in the H<sub>3</sub>PO<sub>4</sub> doped Im system, the effects of fluctuations of the H-bond chain lengths are discussed in detail. In this case,  $\Delta d_{DA}$  of the embedded structures G2-[1]<sup>(I,II)</sup>, G3-[1]<sup>(I,II)</sup> and G4-[2]<sup>(I,II)</sup> are analyzed and the effects of the H-bond chain extension are shown schematically in Fig. 4a. Starting from the smallest, most active embedded structure G2-[1]<sup>(I,II)</sup>, an extension of the Im H-bond chain at Im (II) leads to structure G3-[1]<sup>(I,II)</sup>, with a decrease in  $\Delta d_{DA}$  of H-bond (1) from 0.33 to 0.26 Å and an increase in  $\Delta d_{DA}$  of the H-bond (2) from 0.36 to 0.46 Å. These

findings suggest that an increase in the Im H-bond chain length at one side of the embedded structure results in a stronger N-H $\cdots$ O H-bond on the other side. Further extension of the Im H-bond chain at Im (IV) of structure G3-[1]<sup>(I,II)</sup> yields structure G4-[2]<sup>(I,II)</sup>, with a decrease in the  $\Delta d_{DA}$  of H-bond (1) from 0.26 to 0.23 Å and an increase in the  $\Delta d_{DA}$  of H-bond (2) from 0.46 to 0.50 Å. Because the two N-H $\cdots$ O H-bonds in the embedded structures are simultaneously stabilized and destabilized by the H-bond chain extension, it is reasonable to anticipate that terminal structures, which are precursors for proton transfer in the Im H-bond chain, can be formed in a low local-dielectric environment. In a high local-dielectric environment, a comparison of the  $\Delta d_{DA}$  of H-bonds (1) and (2) in structures C2-[1]<sup>(I,II)</sup>, C3-[1]<sup>(I,II)</sup> and C4-[1]<sup>(I,II)</sup> reveals different results. Because the protonated H-bonds are weakened in a continuum solvent, the  $\Delta d_{DA}$  values are not sensitive to the H-bond chain extension as in the gas phase. Therefore, the successive addition of Im molecules does not lead to significant changes in the  $\Delta d_{DA}$ . However, structures C2-[2]<sup>(I,II)</sup>, C3-[2]<sup>(V)</sup> and C4-[3]<sup>(VII)</sup> in Table S2† suggest that the outstanding effect of the continuum solvent is to stabilize the positive charge at the end of the Im H-bond chains.

Because the intermediate complexes (strong H-bonds with shared-proton structures) are favorably formed in a low local-dielectric environment and a high local-dielectric environment is required to stabilize the positive charge and drive protons in the Im H-bond chain, the fluctuations of the local-dielectric



an acid, proton transfer takes place in the opposite direction, from the proton donor ( $\text{H}_3\text{PO}_4^+$ ) to the end of the Im H-bond chains, as shown in Fig. 4b.

It should be noted that due to the thermal energy fluctuations and dynamics, as well as the local geometrical requirements, H-bonds in liquids can be considered as “forming” and “breaking”.<sup>53</sup> For liquid Im in excess proton conditions, MD simulations based on an MS-EVB model suggested continuous forming and breaking of protonated H-bond chains in which the average H-bond cluster size is approximately four ( $\text{H}^+(\text{Im})_4$ ). The proton transfer in the Im H-bond chain is therefore considered to be a local event, characterized by the fluctuations of the H-bond chain lengths between the Eigen-like ( $n = 3$ ) and Zundel-like ( $n = 2$ ) complexes.<sup>27</sup> Because the fluctuations of the Im H-bond chain lengths and the structure reorganization lead to fluctuations of the local polarization that determine the local-dielectric environment, and because the dielectric spectra of imidazolium compounds suggested that the dipolar relaxation times can be quite short<sup>54</sup> and could synchronize with the lifetimes of the intermediate complexes in the proton transfer pathways, it is justifiable to include the effects of the local-dielectric environment in the proton dissociation and transfer mechanisms.

#### Effects of Im H-bond chain structure reorganization

To discuss the effects of Im H-bond chain structure reorganization, the relative energy diagrams and potential energy curves for proton displacement in  $\text{H}^+(\text{H}_3\text{PO}_4)(\text{Im})_4$  are constructed and shown in Fig. 5a. The relative energy diagram shows that structures  $\text{G4-}[3]^{(I)}$ ,  $\text{G4-}[3]^{(III)}$  and  $\text{G4-}[3]^{(V)}$  are close in energy and are accessible through the Im H-bond chain structure reorganization, *e.g.*, through the rotations of the dihedral angles  $\omega_3$  and  $\omega_5$ . It appears that in a low local-dielectric environment ( $\epsilon = 1$ ), the orientations of the Im molecules, especially Im (III) and Im (V), determine the relative stabilities and the shapes of the potential energy curves that define the energy barriers for proton displacement; *e.g.*, to convert structure  $\text{G4-}[3]^{(I)}$  to  $\text{G4-}[3]^{(III)}$ ,  $\omega_5$  decreases from 107 to 93 degrees. The rotation of  $\omega_5$  results in the modification of the shape of the potential energy curve of H-bond (3) in such a way that the lowest minimum of the double-well potential shifts from Im (I) to Im (III). As a consequence, the positive charge (the proton in H-bond (3)) displaces from Im (I) to Im (III). Similarly, to further drive the proton away from the  $\text{H}_3\text{PO}_4$  dopant (from Im (III) to Im (V)), structure  $\text{G4-}[3]^{(III)}$  must be changed to structure  $\text{G4-}[3]^{(V)}$  by the rotation of  $\omega_3$  from 87 to 101 degrees. It should be recognized that in a low local-dielectric environment, although the rotations of  $\omega_5$  and  $\omega_3$  modify the shapes of the potential energy curves, the energy barriers ( $\Delta E^\ddagger$ ) in the double-well potentials are not high enough to prohibit protons from returning to the original Im molecules, *e.g.*, in H-bond (5),  $\Delta E^\ddagger$  is only approximately  $3.3 \text{ kJ mol}^{-1}$ , compared with the thermal energy fluctuation at room temperature of approximately  $2.5 \text{ kJ mol}^{-1}$ . To visualize the roles played by the continuum solvent, the relative energy diagram and potential energy curves for proton displacement in structures  $\text{C4-}[3]^{(I)}$ ,  $\text{C4-}[3]^{(III)}$ ,

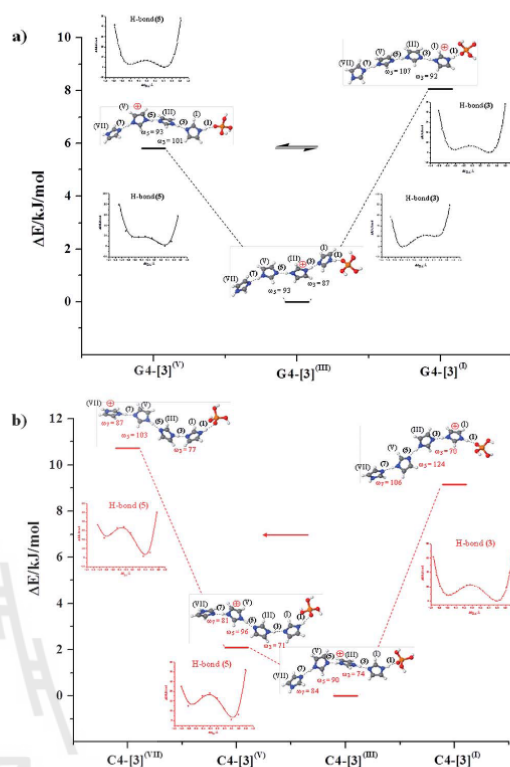


Fig. 5 Effects of Im H-bond chain structure reorganization on the energetics of proton transfer. Potential energy curves of proton displacement in H-bonds (3) and (5) are included. (a) Proton displacement in  $\text{H}^+(\text{H}_3\text{PO}_4)(\text{Im})_4$  in low local-dielectric environment ( $\epsilon = 1$ ). (b) Proton displacement in  $\text{H}^+(\text{H}_3\text{PO}_4)(\text{Im})_4$  in high local-dielectric environment (COSMO,  $\epsilon = 23$ ).

$\text{C4-}[3]^{(V)}$  and  $\text{C4-}[3]^{(III)}$ , which are shown in Fig. 5b, are discussed. It appears that in general, in a high local-dielectric environment (when COSMO is switched on), the energy barriers are substantially higher than in the gas phase. It is therefore reasonable to conclude that a high local-dielectric environment stabilizes the positive charge and prohibits protons from shuttling back to the original Im molecule.

#### Dynamic results

BOMD simulations on the presolvation models reveal that in the continuum solvent (COSMO,  $\epsilon = 23$ ), a proton spends the majority of the time at the bottom of the double-well potential (a close-contact  $\text{A-H}\cdots\text{B}$  H-bond structure) and there is no intermediate complex with the oscillatory shuttling motion (the shared-proton  $\text{A}\cdots\text{H}\cdots\text{B}$  H-bond structure) observed at any temperature. This is in accordance with the static results and confirms that the intermediate complexes are effectively formed in a low local-dielectric environment. Because the quasi-dynamic equilibrium between the oscillatory shuttling and

structural diffusion motions has been shown in our previous studies to be a rate-determining process,<sup>24,26,44,45,49</sup> the dynamics of proton dissociation and transfer are discussed based only on the BOMD results on the intermediate complexes in a low local-dielectric environment ( $\epsilon = 1$ ).

### Dynamics of proton dissociation

To verify the elementary steps of proton dissociation and transfer suggested by the static calculations, the BOMD results on structures G2-[1]<sup>(I,II)</sup>, G3-[1]<sup>(I,II)</sup> and G3-[2]<sup>(III)</sup> at 353 K are analyzed in detail. Structures G2-[1]<sup>(I,II)</sup> and G3-[2]<sup>(III)</sup> are, according to  $\nu^{\text{NH}}$  ( $\nu^{\text{NH}} < \nu^{\text{NH}^*}$ ), intermediate complexes for the proton transfer in the embedded and terminal presolvation models, respectively. Because H-bonds (1) and (2) in structure G2-[1]<sup>(I,II)</sup> are equivalent, only the dynamics in H-bond (1) are discussed. The proton transfer profile (variations of the  $R_{\text{N-O}}$ ,  $R_{\text{N-H}}$  and  $R_{\text{O-H}}$  distances) in Fig. 6a is dominated by a close-contact N-H...O H-bond, with an occasional shared-proton N...H...O H-bond, examples of which are shown in panels P1 and P2. Due to the strong acid-base interaction, a stable

$\text{Im}^+\text{-H}_2\text{PO}_4^-\text{-Im}^+$  structure is formed, evident from the probability of proton transfer from O to N,  $P_{\text{ON}} = 0.87$ , computed from the distribution of the N-H covalent bond distance ( $R_{\text{N-H}}$ ) in Fig. S3a.†

Investigation of the proton transfer profile in panel P1 of Fig. 6b reveals two characteristic N-O vibrations associated with proton dissociation, namely small (S) and large (L) amplitude vibrations. In our previous study, these two characteristic modes were shown to underlie the oscillatory shuttling and structural diffusion motions of protons in H-bonds, respectively.<sup>49</sup> For structure G2-[1]<sup>(I,II)</sup>, the Fourier transformation of VACF of the atoms in panel P1 (between 3500 and 4200 fs) yields the vibrational spectra in Fig. 6c in which the N-O vibrational frequency ( $\nu^{\text{NO,MD}}$ ) is outstanding at 894  $\text{cm}^{-1}$ , with strong interferences of torsional oscillations at frequencies below 500  $\text{cm}^{-1}$  and bending motions in the range between 1000 and 1550  $\text{cm}^{-1}$ .<sup>30</sup> According to the static results in Table S2,† peak B at 2177  $\text{cm}^{-1}$  and peak C at 2322  $\text{cm}^{-1}$  are characteristic asymmetric N-H stretching frequencies ( $\nu^{\text{NH,MD}}$ ) of protons moving on the dissociation and association paths (see Fig. 3),

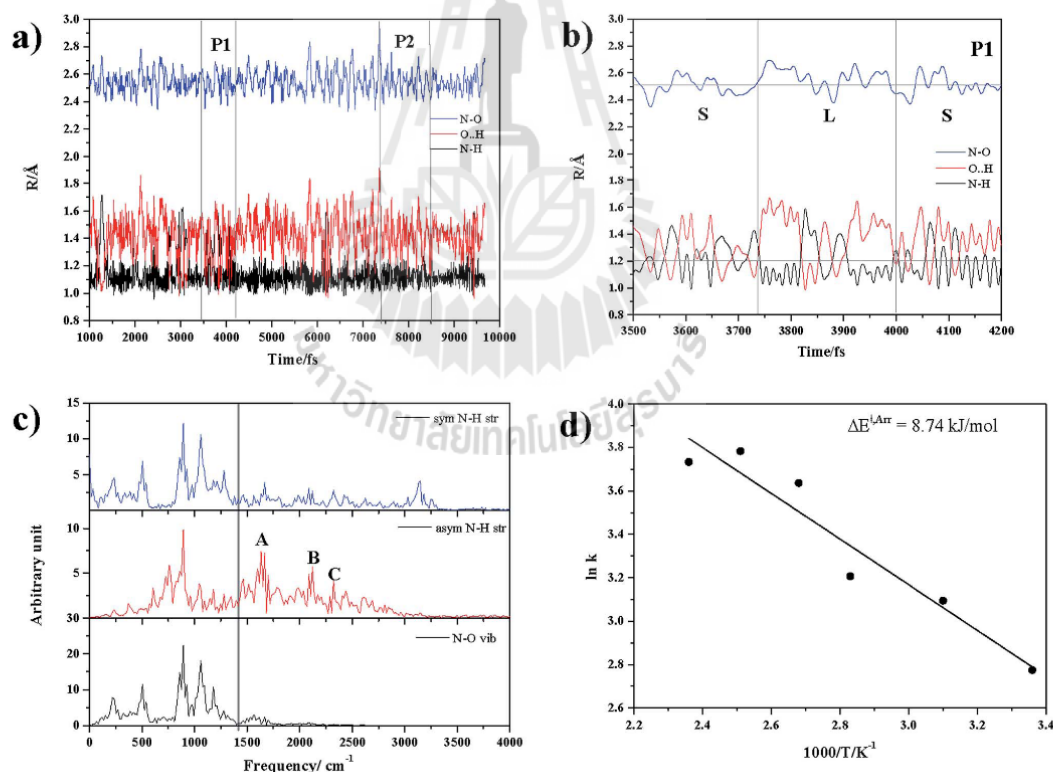


Fig. 6 (a and b) Variations of the  $R_{\text{N-O}}$  and  $R_{\text{N-H}}$  distances in H-bond (1) of structure G2-[1]<sup>(I,II)</sup>, obtained from BOMD simulations at 353 K. (c) Characteristic vibrational spectra of proton dissociation in H-bond (1) of structure G2-[1]<sup>(I,II)</sup>, obtained from BOMD simulations at 353 K. (d) Arrhenius plot of proton dissociation in H-bond (1) of structure G2-[1]<sup>(I,II)</sup>, obtained from BOMD simulations over the temperature range of 298 to 423 K. S and L – small- and large-amplitude N-O vibrations, respectively.  $\Delta E^{\ddagger, \text{Arr}}$  – Arrhenius activation energy of proton dissociation.

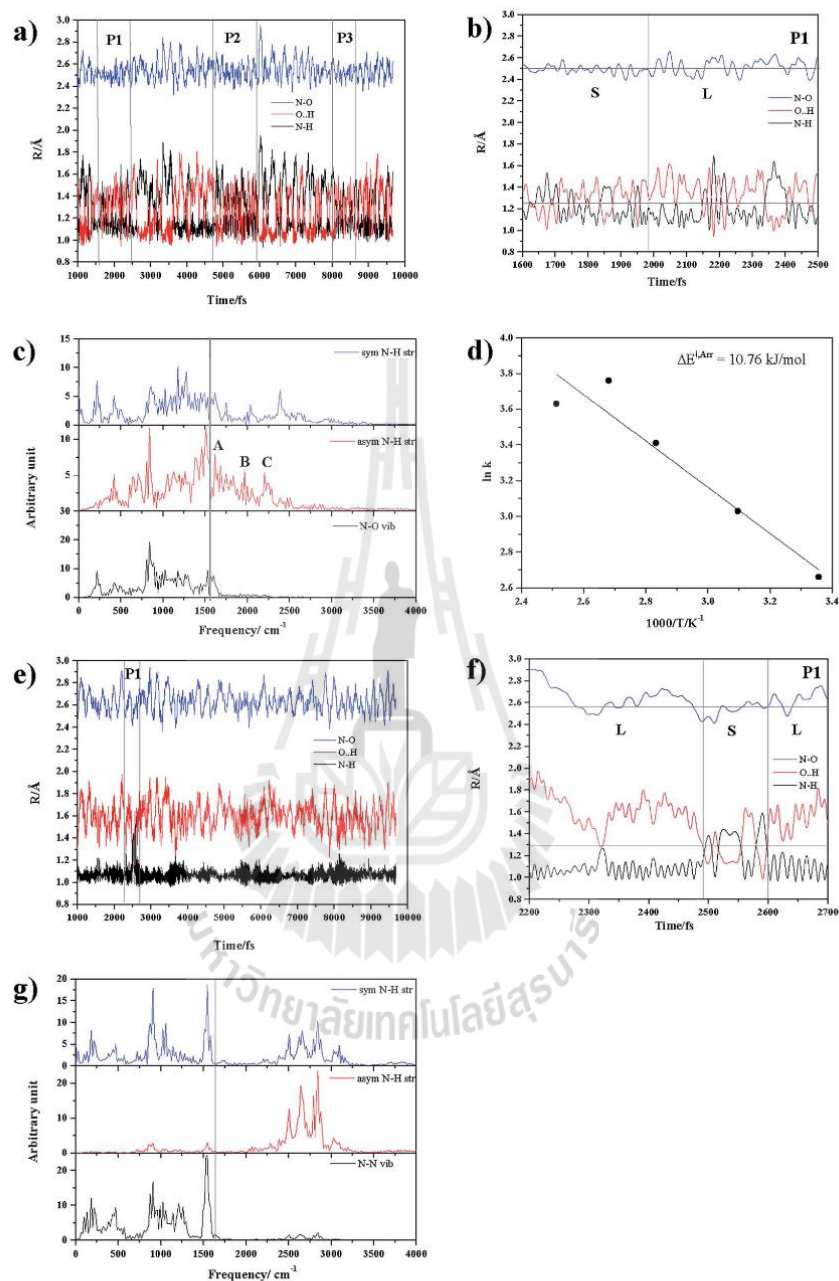


Fig. 7 (a and b) Variations of the  $R_{N-O}$  and  $R_{N-H}$  distances in H-bond (1) of structure  $G3-[1]^{(0,0)}$ , obtained from BOMD simulations at 353 K. (c) Characteristic vibrational spectra of proton dissociation in H-bond (1) of structure  $G3-[1]^{(0,0)}$ , obtained from BOMD simulations at 353 K. (d) Arrhenius plot of proton dissociation in H-bond (1) of structure  $G3-[1]^{(0,0)}$ , obtained from BOMD simulations over the temperature range of 298 to 423 K. (e and f) Variations of the  $R_{N-O}$  and  $R_{N-H}$  distances in H-bond (2) of structure  $G3-[1]^{(0,0)}$ , obtained from BOMD simulations at 353 K. (g) Characteristic vibrational spectra of H-bond (2) of structure  $G3-[1]^{(0,0)}$ , obtained from BOMD simulations at 353 K. S and L = small- and large-amplitude N–O vibrations, respectively.  $\Delta E^{\ddagger,Arr}$  = Arrhenius activation energy of proton dissociation.

respectively, whereas peak A at  $1633\text{ cm}^{-1}$  is the vibrational signature of the shared-proton in the  $\text{N}\cdots\text{H}\cdots\text{O}$  H-bond, which is a proton moving in single-well potential. These transient vibrational frequencies can be used to monitor the acid-base proton dissociation in experiments. The Arrhenius plot in Fig. 6d yields the activation energy of proton dissociation ( $\Delta E^{\ddagger,\text{Arr}}$ ) in H-bond (1) in structure  $\text{G2-}[1]^{(\text{I,II})}$  to be  $8.7\text{ kJ mol}^{-1}$ , which is considerably lower than that in an aqueous solution,  $\Delta E^{\ddagger,\text{Arr}} = 13.1\text{ kJ mol}^{-1}$ .<sup>19</sup>

To confirm the effects of the Im H-bond chain extension suggested by the static results, the proton transfer profiles, distributions of the N-H covalent bond distances ( $R_{\text{N-H}}$ ) and vibrational spectra of protons in H-bonds (1) and (2) of structures  $\text{G2-}[1]^{(\text{I,II})}$  and  $\text{G3-}[1]^{(\text{I,II})}$  are discussed. Extension of the Im H-bond chain at Im (II) of structure  $\text{G2-}[1]^{(\text{I,II})}$  leads to structure  $\text{G3-}[1]^{(\text{I,II})}$ . The analyses of the proton transfer profiles in Fig. 6a, 7a and e and the distributions of  $R_{\text{N-H}}$  in Fig. S3<sup>†</sup> confirm that H-bond (1) is stabilized and H-bond (2) is destabilized upon the Im H-bond chain extension. The former is evident from a significant increase in the probability of finding the shared-proton structure ( $R_{\text{N-H}}$  between 1.3 and 1.5 Å) in H-bond (1),

from  $P_{\text{N}\cdots\text{H}\cdots\text{O}} = 0.10$  in structure  $\text{G2-}[1]^{(\text{I,II})}$  to 0.22 in structure  $\text{G3-}[1]^{(\text{I,II})}$  (see Fig. S3a and S3b<sup>†</sup>), whereas in H-bond (2),  $P_{\text{N}\cdots\text{H}\cdots\text{O}}$  decreases from 0.10 to 0.01 (see Fig. S3a and S3c<sup>†</sup> where H-bond (1) and H-bond (2) in structure  $\text{G2-}[1]^{(\text{I,II})}$  are equivalent). Because the shared-proton structure of H-bond (1) is more stable, the activation energy ( $\Delta E^{\ddagger,\text{Arr}}$ ) for proton dissociation in structure  $\text{G3-}[1]^{(\text{I,II})}$  is higher; the Arrhenius plot in Fig. 7d yields  $\Delta E^{\ddagger,\text{Arr}} = 10.8\text{ kJ mol}^{-1}$ , compared with  $8.7\text{ kJ mol}^{-1}$  in structure  $\text{G2-}[1]^{(\text{I,II})}$ . The stabilization effect of H-bond (1) in structure  $\text{G3-}[1]^{(\text{I,II})}$  is also indicated by the red-shifts of  $\nu^{\text{NH,MD}}$  of peaks A, B and C in Fig. 7c compared with those of structure  $\text{G2-}[1]^{(\text{I,II})}$  in Fig. 6c. The destabilization effect of H-bond (2) is manifested by the very rare proton exchange event observed in Fig. 7e and the disappearance of the three characteristic peaks in Fig. 7g. Additionally, in Fig. 7c, as the relative intensity of peak A is higher than peaks B and C, the extension of the Im H-bond chain is confirmed to increase the probability of finding the oscillatory shuttling motion, leading to a longer lifetime of the rate-determining process in H-bond (1) and a higher  $\Delta E^{\ddagger,\text{Arr}}$  in structure  $\text{G3-}[1]^{(\text{I,II})}$  compared with structure  $\text{G2-}[1]^{(\text{I,II})}$ .

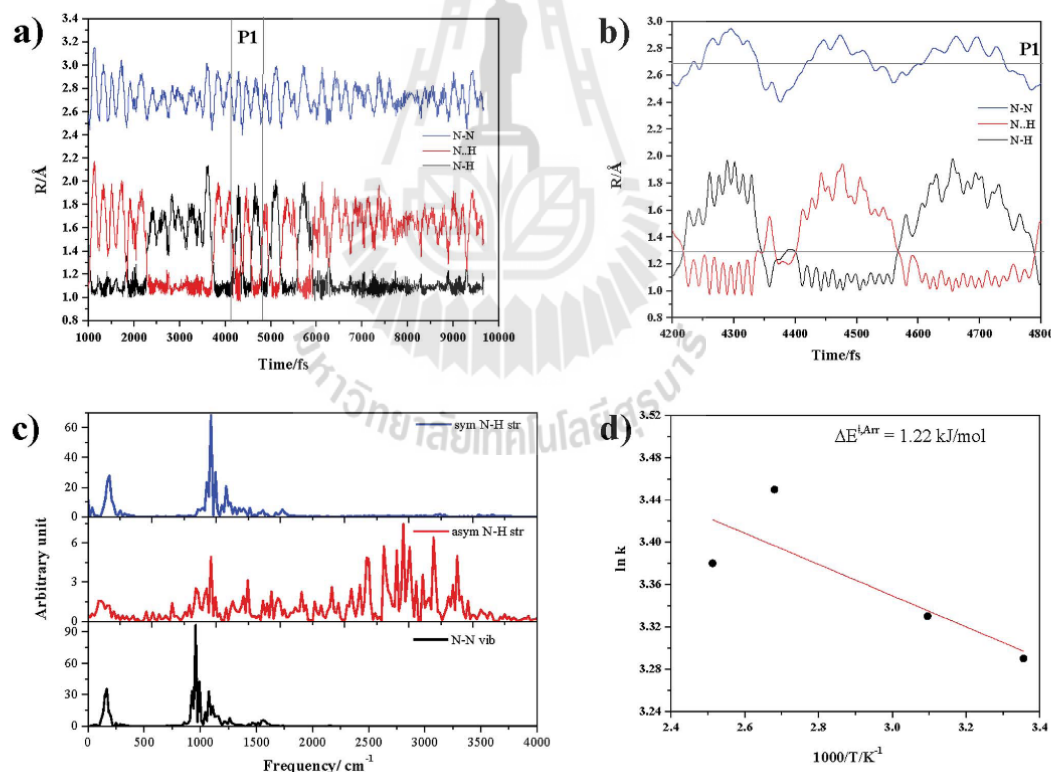


Fig. 8 (a and b) Variations of the  $R_{\text{N-N}}$  and  $R_{\text{N-H}}$  distances in H-bond (3) of structure  $\text{G3-}[2]^{(\text{III})}$ , obtained from BOMD simulations at 353 K. (c) Characteristic vibrational spectra of proton transfer in H-bond (3) of structure  $\text{G3-}[2]^{(\text{III})}$ , obtained from BOMD simulations at 353 K. (d) Arrhenius plot of proton transfer in H-bond (3) of structure  $\text{G3-}[2]^{(\text{III})}$ , obtained from BOMD simulations over the temperature range of 298 to 423 K.  $\Delta E^{\ddagger,\text{Arr}} = 1.22\text{ kJ mol}^{-1}$  – Arrhenius activation energy of proton transfer.

### The effects of doping on the dynamics of proton transfer

The effects of doping are verified by comparing the proton transfer profiles and vibrational spectra of a proton in H-bond (3) of structure G3-[2]<sup>(III)</sup> with those in H<sup>+</sup>(Im)<sub>4</sub>.<sup>30</sup> The proton transfer profile in panel P1 of Fig. 8a and b is dominated by a large-amplitude N-N vibration in which R<sub>N-N</sub> varies over a very wide range, between 2.4 and 2.9 Å. It is shown in panel P1 that the proton exchange in H-bond (3) takes place almost exclusively through the structural diffusion mechanism, without the oscillatory shuttling motion as the rate-determining process.<sup>49</sup> In contrast, in the undoped Im H-bond system (H<sup>+</sup>(Im)<sub>4</sub>), the proton transfer profile in Fig. S4a† is characterized by both large- and small-amplitude N-N vibrations, labeled L and S, respectively, in panel P1 of Fig. S4b.† Due to the interference between various modes of vibrations, especially below 2500 cm<sup>-1</sup>, the oscillatory shuttling and structural diffusion frequencies of a proton in H-bond (3) cannot be precisely determined from the vibrational spectra in Fig. 8c. However, based on the static results in Table S2,† the two vibrational frequencies associated with the proton exchange in H-bond (3) can be estimated: peaks B and C at 1901 and 2345 cm<sup>-1</sup>, respectively. For H<sup>+</sup>(Im)<sub>4</sub>,<sup>30</sup> the oscillatory shuttling and structural diffusion frequencies can be easily assigned from the vibrational spectra in Fig. S4c,† for peaks A, B and C at 1195 cm<sup>-1</sup>, 2205 and 2508 cm<sup>-1</sup>, respectively. The red shifts of peaks B and C in structure G3-[2]<sup>(III)</sup>, compared with those in H<sup>+</sup>(Im)<sub>4</sub>, confirm that H<sub>3</sub>PO<sub>4</sub> helps promote the structural diffusion process by strengthening the Im H-bond chain and enhancing the large-amplitude N-N vibration in the H<sub>3</sub>PO<sub>4</sub> doped Im H-bond system. This results in a lower activation energy ( $\Delta E^{\ddagger, \text{Arr}}$ )

and a higher rate of proton transfer in H-bond (3) of the doped system; the Arrhenius plot in Fig. 8d yields  $\Delta E^{\ddagger, \text{Arr}}$  of 1.22 kJ mol<sup>-1</sup>, compared with  $\Delta E^{\ddagger, \text{Arr}} = 3.28$  kJ mol<sup>-1</sup> in H<sup>+</sup>(Im)<sub>4</sub> (see Fig. S4d†).<sup>30</sup>

It should be noted that  $\Delta E^{\ddagger, \text{Arr}}$  is computed during the proton exchange process, *e.g.*, in panel P1 of Fig. 8a and b, which involves the quasi-dynamic equilibrium between the oscillatory shuttling and structural diffusion motions. Therefore,  $\Delta E^{\ddagger, \text{Arr}}$  might not be directly measurable in an experiment in which different experimental techniques generally yield different activation energies and where other effects could play important roles. As the proton transfer profile in Fig. 8a shows both the shared-proton and close-contact structures, the actual proton transfer is expected to take place not very often and a frequency factor must be included in the model calculations to obtain a more accurate first-order rate constant for the proton displacement in the Im H-bond chain. It should be added that although our presolvation models do not take into account a continuous H-bond network, because proton transfer in the Im H-bond system can be considered a local process with a short spatial, temporal correlation,<sup>27</sup> it is reasonable to investigate only the rate-determining process (the dynamic behavior of the intermediate complex), which, in this case, is the quasi-dynamic equilibrium between the oscillatory shuttling and structural diffusion motions (the close-contact N-H...O and shared-proton N...H...O H-bonds).

### Dynamics of the Im H-bond chain structure reorganization

Because the static results suggest that the shapes of the potential energy curves for proton displacement are sensitive to

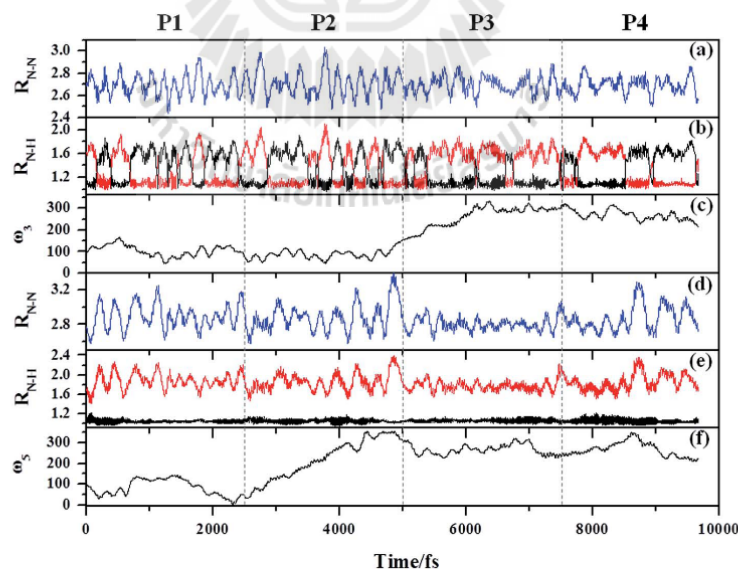


Fig. 9 Proton transfer profiles of H-bonds (3) and (5), and time evolutions of  $\omega_3$  and  $\omega_5$  in the terminal structure G3-[2]<sup>(III)</sup>, obtained from BOMD simulations at 298 K. (a–c) – H-bond (3); (d–f) – H-bond (5).

the Im H-bond chain structure reorganization (see Fig. 5), the effects of a conformation change on the dynamics of proton transfer are discussed using the proton transfer profiles of structure G3-[2]<sup>(III)</sup>, which were obtained from the BOMD simulations at 298 K. Variations of  $R_{N-N}$  and  $R_{N-H}$  in H-bonds (3) and (5), as well as the time evolutions of  $\omega_3$  and  $\omega_5$ , as shown in Fig. 9, confirm that the Im H-bond chain structure reorganization does affect the dynamics of proton transfer. Investigation of the time evolutions of the torsional angles suggests division of the proton transfer profiles into four panels of 2500 fs each (P1 to P4).

To visualize the effects of the conformation change on the proton displacement in H-bond (3), a reference vector ( $v^{\text{ref}}$ ) coinciding with the  $C_2$  axis of  $\text{ImH}^+$  is defined, and projections of  $v^{\text{ref}}$ , similar to the Newman projection, are used to monitor the dynamically changing Im H-bond structures. They are shown in Fig. 10. In this case, the line of sight is defined lengthwise down the Im H-bond chain from the  $\text{H}_3\text{PO}_4$  dopant. Based on the assumption that the probability of finding a proton moving in a specific direction is correlated with the

probability of the N-H covalent bond formation, the distributions of  $R_{N-H}$  in H-bond (3) of Im (III) in panel P1 to P4 are constructed and shown in Fig. 11.

In the initial state in panel P1,  $\omega_3$  and  $\omega_5$  only fluctuate in a narrow range, with average values of  $\langle\omega_3\rangle = 95$  and  $\langle\omega_5\rangle = 84$  degrees. In panel P2, the variations in  $\omega_3$  and  $\omega_5$  become unsynchronized; while  $\omega_3$  librates in a narrow range, regarded as a “rotational waiting state”,  $\omega_5$  changes from 84 to 354 degrees, the latter of which can be regarded as a critical angle. In panel P3, while  $\omega_5$  is maintained at the critical angle,  $\omega_3$  changes to 282 degrees, in response to the rotation of  $\omega_5$ . Finally, in panel P4, both are maintained at  $\langle\omega_3\rangle = 280$  and  $\langle\omega_5\rangle = 270$  degrees. As the torsional rotation of  $\omega_5$  induces the rotation of  $\omega_3$ , with a rotational waiting state of approximately 2500 fs, the rotational motions of  $\omega_5$  and  $\omega_3$  can be collectively regarded as “helical-rotational motion”, which underlies the Im H-bond chain structure reorganization. The Im H-bond chain structure reorganization affects the proton transfer in H-bond (3) in such a way that the population of the protons moving away from the dopant is increased from panel P1 ( $P_{N-N} = 0.3$ ) to

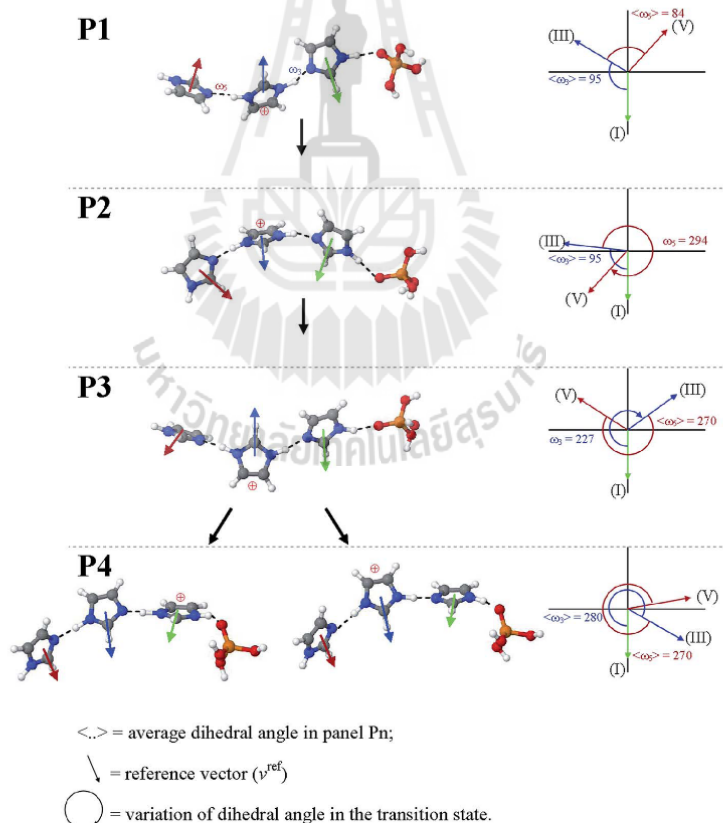


Fig. 10 Conformations of structure G3-[2]<sup>(III)</sup> sampled from panel P1 to P4 and projections of the reference vectors ( $v^{\text{ref}}$ ), obtained from the analyses of the time evolutions of  $\omega_3$  and  $\omega_5$  in Fig. 9. Angles in degree; (III) –  $v^{\text{ref}}$  of Im (III); (V) –  $v^{\text{ref}}$  of Im (V).

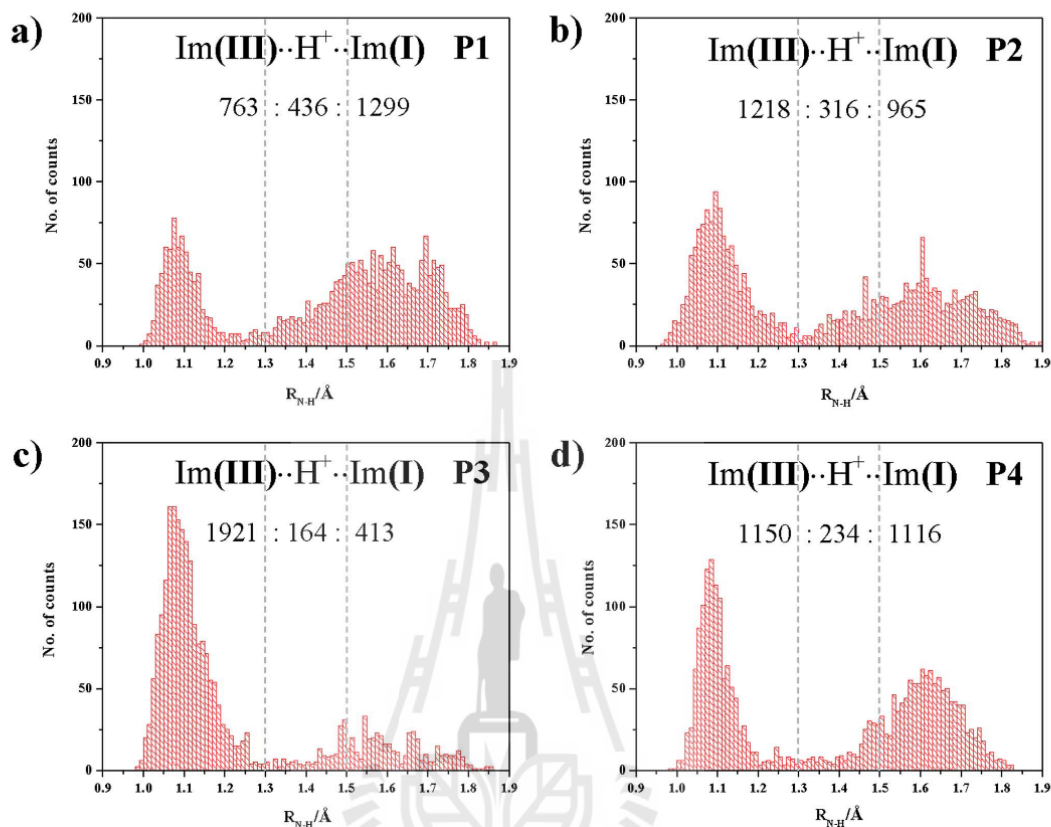


Fig. 11 Distributions of the N–H covalent bond distances ( $R_{\text{NH}}$ ) in H-bond (3) of structure G3-[2]<sup>000</sup>, obtained from BOMD simulations at 298 K. (a–d) Distributions in panel P1 to P4 in Fig. 9, respectively.

P2 ( $P_{\text{NN}} = 0.5$ ) and P3 ( $P_{\text{NN}} = 0.8$ ). This finding supports the static results in Fig. 5a in which the rotation of  $\omega_5$  leads to a modification of the shape of the potential energy curve of H-bond (3) in such a way that the lowest minimum of the double-well potential shifts from Im (I) to Im (III), resulting in a higher probability of finding a proton moving towards Im (III), which confirms the effects of the Im H-bond chain structure reorganization suggested by the static results.

## Conclusion

In this work, the dynamics and mechanisms of proton dissociation and transfer in an  $\text{H}_3\text{PO}_4$  doped Im H-bond system were theoretically studied using B3LYP/TZVP calculations and BOMD simulations as model calculations and  $\text{H}^+(\text{H}_3\text{PO}_4)_n(\text{Im})_n$  ( $n = 1-4$ ) as model systems. The theoretical studies began with choosing appropriate presolvation models for proton dissociation and transfer, represented by embedded and terminal linear H-bond structures, respectively. The structures, energetic and vibrational frequencies of protons in the H-bonds of the presolvation

models were studied in low ( $\epsilon = 1$ ) and high local-dielectric ( $\epsilon = 23$ ) environments. The static results confirmed that the excess proton condition is required to promote proton dissociation and transfer, and it must be included in the presolvation model. The 2D-PES and potential energy curves of the proton exchange suggested that the intermediate complexes for proton dissociation and transfer are formed in a low local-dielectric environment, whereas a high local-dielectric environment is required to stabilize the positive charge and prevent a proton from being shared or returning to the original Im molecule, which is in accordance with the localized charge solvent (LCS) concept. The B3LYP/TZVP calculations also revealed that the embedded H-bond structure with  $n = 2$  represents the smallest, most active intermediate complex for proton dissociation, and similarly, the terminal H-bond structure with  $n = 3$  is representative for proton transfer in the Im H-bond chain. The mechanisms of terminal structure formation and proton transfer in the Im H-bond chain, which involve fluctuations of the H-bond chain lengths and the local-dielectric environment, were proposed based on the static results. Additionally, because

the shapes of the potential energy curves are sensitive to the torsional rotations of the H-bonds, the Im H-bond chain structure reorganization is included as an important process in the proton transfer mechanism. A comparison of the threshold frequencies for proton transfer in  $\text{H}^+(\text{H}_3\text{PO}_4)(\text{Im})_n$  ( $n = 1-4$ ) and in the undoped Im H-bond system ( $\text{H}^+(\text{Im})_4$ ) suggested that the strong polarization effects of the dopant lead to a higher probability of finding a delocalized proton and improve proton conduction in the  $\text{H}_3\text{PO}_4$  doped Im system.

Because the static results showed that the embedded H-bond structure with  $n = 2$  and the terminal H-bond structure with  $n = 3$  represent the smallest, most active intermediate complexes for proton dissociation and transfer in a low local-dielectric constant environment, respectively, BOMD simulations were performed on these two H-bond structures. The vibrational spectra obtained from the BOMD simulations suggested three transient vibrational peaks associated with the acid-base proton dissociation, with the activation energy of the proton dissociation in the smallest, most active intermediate complex of  $8.7 \text{ kJ mol}^{-1}$ . It appeared that the extension of the embedded H-bond chain increases the probability of finding the oscillatory shuttling motion and the lifetime of the intermediate complex, resulting in a higher activation energy for proton dissociation from the protonated acid. The comparison of the dynamic results on the  $\text{H}_3\text{PO}_4$  doped Im system with those on  $\text{H}^+(\text{Im})_4$  indicated that the structural diffusion process in the Im H-bond chain of the doped system is almost exclusively through the large-amplitude N-N vibration, without the oscillatory shuttling motion as the rate-determining process, with an activation energy of only  $1.22 \text{ kJ mol}^{-1}$ . For the undoped Im H-bond system, the proton transfer process is characterized by both the oscillatory shuttling and structural diffusion motions. Analyses of the proton transfer profiles and the time evolutions of the torsional angles revealed coupled torsional motions (helical-rotational motion), which drive the proton away from the dopant and confirm that the Im H-bond chain structure reorganization plays an important role in the proton transfer in the  $\text{H}_3\text{PO}_4$  doped Im H-bond system. The results showed for the first time the interplay among the translational, rotational and vibrational motions that underlie the dynamics and mechanisms of proton transfer in the linear H-bond chain. Because the discussion are based on the results on carefully selected presolvation models, the present theoretical study provides new insights into the dynamics and mechanisms of proton exchange processes in doped, weak-polar organic solvent. These pieces of fundamental information are important and can be used as guidelines for further theoretical and experimental investigations on proton transfer processes in aromatic heterocyclic materials, which could eventually lead to an improvement of the proton transfer processes in non-aqueous, high temperature fuel cells.

## Acknowledgements

The authors would like to acknowledge the financial supports provided by Suranaree University of Technology through the SUT-Ph.D. program (SUT-Ph.D./05/2554). This work was

supported in part by the Higher Education Research Promotion and National Research University Project (HERB-NRU), the Office of the Higher Education Commission (OHEC), Thailand. Prof. Kritsana Sagarik received financial supports from the Thailand Research Fund (TRF), the Advanced Research Scholarship (BRG-5580011). Super- and high-performance computer facilities provided by the following organizations are gratefully acknowledged; School of Mathematics and School of Chemistry, SUT; National Electronics and Computer Technology Center (NECTEC), National Science and Technology Development Agency (NSTDA); the Thai National Grid Center (THAIGRID), Ministry of Information and Communication Technology (MICT).

## References

- 1 T. Koppel, *Powering the Future: The Ballard fuel cell and the race to change the world*, John Wiley & Sons Ltd., New York, 1999.
- 2 J. Larminie and A. Dicks, *Fuel Cell Systems*, John Wiley & Sons Ltd., Chichester, 2001.
- 3 S. R. Narayanan, S. P. Yen, L. Liu and S. G. Greenbaum, *J. Phys. Chem. B*, 2006, **110**, 3942-3948.
- 4 M. F. H. Schuster and W. Meyer, *Annu. Rev. Mater. Res.*, 2003, **33**, 233-261.
- 5 H. A. Pohl and R. P. Chartoff, *J. Polym. Sci., Polym. Chem. Ed.*, 1964, **2**, 2787-2806.
- 6 X. Glipta, B. Bonnet, B. Mula, D. J. Jones and J. RozieÁre, *J. Mater. Chem.*, 1999, **9**, 3045-3049.
- 7 B. Xing and O. Savadogo, *J. New Mater. Electrochem. Syst.*, 1999, **2**, 95-101.
- 8 R. He, Q. Li, G. Xiao and N. J. Bjerrum, *J. Membr. Sci.*, 2003, **226**, 169-184.
- 9 D. T. Chin and H. H. Chang, *J. Appl. Electrochem.*, 1989, **19**, 95-99.
- 10 R. A. Munson and M. E. Lazarus, *J. Phys. Chem.*, 1967, **71**, 3245-3248.
- 11 B. S. Hickman, M. Mascal, J. J. Titman and I. G. Wood, *J. Am. Chem. Soc.*, 1999, **121**, 11486-11490.
- 12 A. Kawada, A. R. McGhie and M. M. Labes, *J. Chem. Phys.*, 1970, **52**, 3121-3125.
- 13 I. Fischbach, H. W. Spiess, K. Saalwächter and G. R. Goward, *J. Phys. Chem. B*, 2004, **108**, 18500-18508.
- 14 M. Iannuzzi and M. Parrinello, *Phys. Rev. Lett.*, 2004, **93**, 025901.
- 15 K. D. Kreuer, A. Fuchs, M. Ise, M. Spaeth and J. Maier, *Electrochim. Acta*, 1998, **43**, 1281-1288.
- 16 W. Münch, K. D. Kreuer, W. Silvestri, J. Maier and G. Seifert, *Solid State Ionics*, 2001, **145**, 437-443.
- 17 A. Schechter and R. F. Savinell, *Solid State Ionics*, 2002, **147**, 181-187.
- 18 L. Vilciauskas, M. E. Tuckerman, J. P. Melchior, G. Bester and K. D. Kreuer, *Solid State Ionics*, 2013, **252**, 34-39.
- 19 P. Suwannakum and K. Sagarik, submitted.
- 20 T. C. Berkelbach, H.-S. Lee and M. E. Tuckerman, *Phys. Rev. Lett.*, 2009, **103**, 238302.

- 21 D. Marx, A. Chandra and M. E. Tuckerman, *Chem. Rev.*, 2010, **110**, 2174–2216.
- 22 C. Lao-ngam, P. Asawakun, S. Wannarat and K. Sagarik, *Phys. Chem. Chem. Phys.*, 2011, **13**, 4562.
- 23 C. Lao-ngam, M. Phonyiem, S. Chaiwongwattana, Y. Kawazoe and K. Sagarik, *Chem. Phys.*, 2013, **420**, 50–61.
- 24 M. Phonyiem, S. Chaiwongwattana, C. Lao-ngam and K. Sagarik, *Phys. Chem. Chem. Phys.*, 2011, **13**, 10923.
- 25 S. Chaiwongwattana, M. Phonyiem, V. Vchirawongkwin, S. Prueksaaron and K. Sagarik, *J. Comput. Chem.*, 2012, **33**, 175–188.
- 26 K. Sagarik, S. Chaiwongwattana, V. Vchirawongkwin and S. Prueksaaron, *Phys. Chem. Chem. Phys.*, 2010, **12**, 918.
- 27 A. Li, Z. Cao, Y. Li, T. Yan and P. Shen, *J. Phys. Chem. B*, 2012, **116**, 12793–12800.
- 28 M. Iannuzzi, *J. Chem. Phys.*, 2006, **124**, 204710.
- 29 P. Hobza, H. L. Selzle and E. W. Schlag, *Chem. Rev.*, 1994, **94**, 1767.
- 30 V. Buagern and K. Sagarik, in preparation.
- 31 N. N. Greenwood and A. Thompson, *J. Chem. Soc.*, 1959, 3485.
- 32 H. Chen, T. Yan and G. A. Voth, *J. Phys. Chem. A*, 2009, **113**, 4507–4517.
- 33 C. Lao-ngam, P. Asawakun, S. Wannarat and K. Sagarik, *Phys. Chem. Chem. Phys.*, 2011, **13**, 4562–4575.
- 34 C. Lao-ngam, M. Phonyiem, S. Chaiwongwattana, Y. Kawazoe and K. Sagarik, *Chem. Phys.*, 2013, **420**, 50–61.
- 35 K. P. Sagarik and R. Ahlrichs, *J. Chem. Phys.*, 1987, **86**, 5117.
- 36 K. P. Sagarik and P. Asawakun, *Chem. Phys.*, 1997, **219**, 173.
- 37 K. P. Sagarik, S. Chaiwongwattana and P. Sisot, *Chem. Phys.*, 2004, **1**.
- 38 K. P. Sagarik and S. Dokmaisrijan, *J. Mol. Struct.*, 2005, **718**, 31.
- 39 K. P. Sagarik, V. Pongpituk, S. Chiyapongs and P. Sisot, *Chem. Phys.*, 1991, **156**, 439.
- 40 K. Kwac, C. Lee, Y. Jung and J. Han, *J. Chem. Phys.*, 2006, **125**, 244508.
- 41 J. L. Knee, L. R. Knundkar and A. H. Zewail, *J. Chem. Phys.*, 1985, **82**, 4715.
- 42 S. J. Paddison, *J. New Mater. Electrochem. Syst.*, 2001, **4**, 197–207.
- 43 A. P. Scott and L. Radom, *J. Phys. Chem.*, 1996, **100**, 16502.
- 44 S. Chaiwongwattana, M. Phonyiem, V. Vchirawongkwin, S. Prueksaaron and K. Sagarik, *J. Comput. Chem.*, 2012, **33**, 175–188.
- 45 C. Lao-ngam, P. Asawakun, S. Wannarat and K. Sagarik, *Phys. Chem. Chem. Phys.*, 2011, **13**, 4562.
- 46 *SURFER for Window*, Golden Software Inc., USA, 6.04 edn, 1997.
- 47 J. E. Basconi and M. R. Shirts, *J. Chem. Theory Comput.*, 2013, **9**, 2887–2899.
- 48 S. Chaiwongwattana, C. Lao-ngam, M. Phonyiem, V. Vchirawongkwin and K. Sagarik, submitted.
- 49 K. Sagarik, M. Phonyiem, C. Lao-Ngam and S. Chaiwongwattana, *Phys. Chem. Chem. Phys.*, 2008, **10**, 2098.
- 50 R. L. Davidchack, *J. Comput. Phys.*, 2010, **229**, 9323–9346.
- 51 B. Koeppe, J. Guo, P. M. Tolstoy, G. S. Denisov and H.-H. Limbach, *J. Am. Chem. Soc.*, 2013, **135**, 7553–7566.
- 52 R. R. Sadeghi and H.-P. Cheng, *J. Chem. Phys.*, 1999, **111**, 2086.
- 53 R. O. Watts and I. J. McGee, *Liquid State Chemical Physics*, John Wiley & Sons, New York, 1976.
- 54 M. Schmollngruber, C. Schröde and O. Steinhauser, *Phys. Chem. Chem. Phys.*, 2014, **16**, 10999–11009.

## APPENDIX B

### LIST OF ABSTRACTS

#### Abstracts

**Thisuwan, J.** and Sagarik, K. Structural diffusion in protonated phosphoric acid-imidazole clusters. *The 7<sup>th</sup> Conference of the Asian Consortium on Computational Materials Science (ACCMS7)*. 23-28 July 2013. Surasammanakhan, Suranaree University of Technology, Nakhon Ratchasima, Thailand.

**Thisuwan, J.** and Sagarik, K. Mechanism of proton exchange in phosphoric acid-imidazole H-bond chain. *51<sup>st</sup> Symposium on Theoretical Chemistry*. 20-24 September 2015. University of Potsdam, Campus Griebnitzsee. Potsdam, Germany.



# CURRICULUM VITAE

**Name** Miss Jittima Thisuwan

**Date of Birth** April 2, 1985

## **Education**

2007 Bachelor of Science (Chemistry), 2<sup>nd</sup> Class Honors, Valaya Alongkorn Rajabhat University, Pathumthani, Thailand.

2010 Master of Science (Chemistry), Suranaree University of Technology, Thailand.

## **Research and Academic Experiences**

2007-2010 Teaching assistant, School of Chemistry, Institute of Science, Suranaree University of Technology, Thailand.

2014–present Research assistant, Computational Chemistry Research Laboratory (CCRL), School of Chemistry, Institute of Science, Suranaree University of Technology, Thailand.

02-07/2015 Visiting researcher, Department of Physical Chemistry, Ruđer Bošković Institute, Croatia.

## **Fellowship**

2009 Research at Molecular Technology Research Unit, School of Science, Walailak University, Thailand.

2011 SUT-Ph.D. research scholarship from Institute of Research and Development (IRD), Suranaree University of Technology, Thailand.